



UNIVERSITY OF
LIVERPOOL

**Millimetre-Wave Components Based on
Groove Gap Waveguide Technology:
Design and Development**

By

Bahaa Jasim Mousa

A thesis submitted in accordance with the requirements for the
award of the degree of Doctor of Philosophy of the University
of Liverpool

January 2022

To my dear parents, wife and sons, sisters and brothers.

Thank you for everything.

Copyright

Copyright © 2021 Bahaa Al-Juboori, all rights reserved.

The copyright of this thesis rests with the author. Copies (by any means) either in full, or of extracts, may not be made without prior written consent from the author.

Acknowledgements

First, I thank GOD ALMIGHTY Who has given me the mental and physical strength and confidence to do this work.

I would like to dedicate my deepest and sincerest gratitude to my supervisor Dr Zhou Jiafeng for the invaluable comments and advice on my research. This thesis would have not seen the light without the support and guidance of him. I have learned so much from him both academically and personally. I would also like to thank Professor Huang Yi for his valuable support and advice along the period of my study.

Special thanks are paid to my parents and family. You have always supported me with no expectation of a reward. Your continuous help and understanding have made my life full of love and I am grateful for everything you have done. Finally, thanks to my beloved wife and my sons for their invaluable support. This journey would not have been possible without their love and prayers.

I would also like to thank my brilliant and lovely colleagues and friends; in particular to Dr Muayad Kod, Dr Muaad Hussein, Dr Ahmed Alieldin, Dr Manoj Stanley, Dr Chaoyun Song, Dr Anqi Chen, Dr Yuan Zhuang, Dr. Abed Pour Sohrab, Dr. Ahmed Al-Tahmeesschi, Dr Zhouxiang Fei, Dr. Tianyuan Jia, Dr. Sumin Joseph and Miss Wenzhang Zhang for their valuable advice, fruitful discussions and enjoyable moments during the whole PhD life.

Particular thanks should also be paid to, Mark Norman and Gareth Blacoe from the Electrical Workshop for always being very kind to me and fabricating my components very quickly and beautifully.

Table of Contents

Table of Contents	v
Abstract	1
List of Publications.....	3
Acronyms	5
Chapter 1. Introduction.....	8
1.1. Millimetre-Wave Frequency Band	8
1.2. Guiding Structures in the mmWave Frequency Band	9
1.3. Gap Waveguide Technology.....	10
1.4. Motivation and Objectives	10
1.5. Organisation of the Thesis.....	12
References	14
Chapter 2. Overview of Millimetre-Wave Components and Gap Waveguide Technology	16
2.1. Introduction	16
2.2. Transmission Line Challenges at Millimetre-Wave	16
2.2.1. Planar Technologies.....	16
2.2.2. Waveguide Technologies.....	18
2.3. The Concept of Gap Waveguide.....	21
2.3.1. The Origin of Gap Waveguide.....	21
2.3.2. Electromagnetic Bandgaps.....	23
2.3.3. Gap Waveguide Types.....	24
2.3.4. Pin forms in Gap Waveguide Technology	26
2.3.5. Millimetre-Wave Applications.....	29
2.3.6. Millimetre-Wave Components Fabrication.....	36
2.4. Summary	39
References	40
Chapter 3. Filters and Filtering Antennas Network Theory	51
3.1. Introduction	51
3.2. Filter Network	51
3.2.1. Filter Design by the Insertion Loss Method.....	52
3.2.2. Bandpass Filter Design Example	57

3.2.3.	Coupling Matrix Synthesis.....	63
3.2.4.	Resonators Coupling.....	64
3.3.	Waveguide Cavity Resonator	68
3.4.	Antenna Theory.....	70
3.4.1.	Overview of Antennas	70
3.4.2.	Filtering Antenna	71
3.5.	Summary	73
	References	74
Chapter 4. Millimetre-Wave Bandpass Filter Design Based on Gap Waveguide		77
.....		77
4.1.	Introduction	77
4.2.	Gap Waveguide-Based Bandpass Filter Design.....	79
4.2.1.	Filter Specifications and Synthesis	79
4.2.2.	Coupling Matrix and Design Procedure.....	80
4.3.	Simulations and Measurements.....	88
4.3.1.	Filter Specifications and Synthesis	88
4.3.2.	Fabrication Process and Measurements	88
4.4.	Summary	94
	References	95
Chapter 5. A Novel Gap Waveguide Structure: Analysis and Investigation ...		99
5.1.	Introduction	99
5.2.	The Proposed Unit-Cell Geometry.....	100
5.3.	S-parameters Investigation.....	101
5.4.	Summary	118
	References	119
Chapter 6. A Cavity-Backed Slot Antenna and Filtering Antenna Based on Gap Waveguide Using Novel Sidewalls		121
6.1.	Cavity-Backed Slot Antenna (CBSA).....	121
6.1.1.	Concept of CBSA.....	121
6.1.2.	The Proposed CBSA Structure	122
6.1.3.	Simulations and Measurements	125
6.2.	Cavity-Backed Slot Filtering Antenna (CBSFA)	129
6.2.1.	A Brief Concept of CBSFA	129
6.2.2.	CBSFA Design.....	130

6.2.3. CBSFA Results	135
6.3. Summary	142
References	143
Chapter 7. Conclusions and Future Work.....	145
7.1. Conclusions	145
7.2. Key Contributions	148
7.3. Future Work.....	149
References	150
Appendices	151
Appendix A.....	151

Abstract

Millimetre-wave (mmWave) passive devices have been a pivotal research topic for the last decades. Low loss, low mass and ease of manufacture for passive components operating at mmWave frequency bands and beyond are of high importance for aerospace and satellite applications. A vast number of mmWave components using various design technologies have been reported. For high-frequency applications, designers prefer conventional waveguides due to their low loss and high power-handling capabilities. However, the poor contact between the joined waveguide parts is one of the drawbacks. Gap waveguide technology has been introduced as a promising and an alternative solution to the conventional waveguides, at mmWave frequency bands and beyond. A gap waveguide consists of two parallel plates, one acts as a perfect electrical conducting, while the other has a periodic structure of metal pins to act as an artificial magnetic conductor.

The work of this thesis can be divided into three major parts: (i) A comprehensive review of the design technologies of mmWave passive devices is accomplished, exhibiting the advantages and features of using the metamaterial-based gap waveguide technology. (ii) A mmWave bandpass filter is designed and fabricated using two different manufacturing technologies (computer numerical control machining and high-resolution metalised polymer jetting 3D printing) showing the difference between the two fabricated counterparts in terms of performance and mass. The metalised 3D printed BPF exhibits lower mass and better performance. Such low mass and low loss for BPFs are of high importance for aerospace applications. (iii) A novel periodic pin-form of gap waveguide structures is proposed to overcome the limitations of the traditional forms of pins. Instead of only full-height pins in a conventional gap waveguide, a combination of wall and pins constitutes the new pin-form.

Four advantages can be achieved by using the proposed pin-form. First, the wave shielding will be much more effective at the operating band compared to the traditional full-height pins. Second, the bandwidth of the passband can be enhanced by moving the

upper edge of the passband towards higher frequencies due to the use of shorter pins instead of full-height pins, with the same width and height of the groove. Third, a good matching between a groove gap waveguide structure and a standard waveguide port can be achieved without the need for a transition. The fourth advantage is the solid wall can be exploited to make a horizontal slot to be used for wave radiation. This is the first time that the sidewalls of gap waveguides can be used for slot radiation. Based on the proposed structure, two components, a cavity-backed slot antenna and a cavity-backed slot filtering antenna, are designed and experimentally tested to yield excellent results with the simulations.

List of Publications

- [1] **B. Al-Juboori**, J. Zhou, Y. Huang, M. Hussein, A. Alieldin, W. Otter, D. Klugmann, S. Lucyszyn, "Lightweight and Low-Loss 3-D Printed Millimetre-Wave Bandpass Filter Based on Gap-Waveguide," in *IEEE Access*, vol. 7, pp. 2624-2632, 2019.
- [2] **B. Al-Juboori**, J. Zhou and Y. Huang and S. D. Joseph, "Cavity-Backed Slot Filtering Antenna Based on Gap Waveguide Using Novel Sidewall Structures," [submitted to] *IEEE Transactions on Microwave Theory and Techniques*.
- [3] **B. Al-Juboori**, Y. Huang, D. Klugmann, M. Hussein and J. Zhou, "Millimetre wave cross-coupled bandpass filter based on groove gap waveguide technology" *10th UK-Europe-China Workshop on Millimetre Waves and Terahertz Technologies (UCMMT)*, Liverpool, UK, 2017.
- [4] **B. Al-Juboori**, J. Zhou, Y. Huang, A. Alieldin, T. Jia, "Cavity Backed Slot Antenna Fed by New Groove Gap Waveguide Structure," *Proceedings of UK-Europe-China Workshop on Millimetre Waves and Terahertz Technologies (UCMMT)*, Tianjin, China, 2020. (*Best Student Paper Second Prize*).
- [5] **B. Al-Juboori**, J. Zhou, Y. Huang, "A Slot Filtenna Based on Gap Waveguide Using Novel Sidewalls," *IEEE MTT-S International Microwave Filter Workshop (IMFW)*, Perugia, Italy, 2021, pp. 162-164.
- [6] A. Alieldin, Y. Huang, S. J. Boyes, M. Stanley, S. D. Joseph and **B. Al-Juboori**, "A Dual-Broadband Dual-Polarised Fylfot-Shaped Antenna for Mobile Base Stations Using MIMO Over-Lapped Antenna Subarrays," in *IEEE Access*, vol. 6, pp. 50260-50271, 2018.

-
- [7] M. Hussein, J. Zhou, Y. Huang and **B. Al-Juboori**, "A Low-Profile Miniaturised Second-Order Bandpass Frequency Selective Surface," in *IEEE Antennas and Wireless Propagation Letters*, vol. 16, pp. 2791-2794, 2017.
- [8] M. Hussein, Y. Huang, **B. Al-Juboori** and J. Zhou, "A multi-band high selectivity frequency selective surface for ka-band applications," *IEEE 10th Global Symposium on Millimeter-Waves*, Hong Kong, 2017, pp. 63-65,
- [9] A. Chen, **B. Al-Juboori**, Y. Zhuang, Y. Huang and J. Zhou, "Compact Ka-band substrate-integrated waveguide filter with spurlines for satellite communication systems," *IEEE 9th UK-Europe-China Workshop on Millimetre Waves and Terahertz Technologies (UCMMT)*, Qingdao, China, 2016.

Acronyms

2D	2-Dimensional
3D	3-Dimensional
ADS	Advanced Design System
AMC	Artificial Magnetic Conductor
BPF	Bandpass Filter
BW	Bandwidth
CAD	Computer-Aided Design
CBSA	Cavity-Backed Slot Antenna
CBSFA	Cavity-Backed Slot Filtering Antenna
CM	Coupling Matrix
CNC	Computer Numerical Control
CPW	Coplanar Waveguide
CST-MWS	Computer Simulation Technology Microwave Studio
DUT	Device under Test
EBG	Electromagnetic Bandgap
EHF	Extremely High Frequency
EM	Electromagnetic
ESIW	Empty Substrate Integrated Waveguide
FBW	Fractional Bandwidth
FDM	Fused Deposition Modelling
GGW	Groove Gap Waveguide

GW	Gap Waveguide
LTCC	Low-Temperature Co-fired Ceramic
MIMC	Monolithic Microwave Integrated Circuit
mmWave	Millimetre-Wave
MW	Microwave
PCB	Printed Circuit Boards
PEC	Perfect Electric Conductor
PIM	Passive Intermodulation
PMC	Perfect Magnetic Conductor
PolyJet	Polymer Jetting
PRGW	Printed Ridge Gap Waveguide
RF	Radio Frequency
RGW	Ridge Gap Waveguide
RWG	Rectangular Waveguide
Rx	Receiver
SIW	Substrate Integrated Waveguide
SLA	Stereolithographic Apparatus
SLM	Selective Laser Melting
S-Parameters	Scattering Parameters
TE	Transverse Electric
TEM	Transverse Electromagnetic
TM	Transverse Magnetic
TRL	Thru-Reflect-Line
Tx	Transmitter

TZ	Transmission Zero
UV	Ultraviolet
VNA	Vector Network Analyzer
WG	Waveguide

Chapter 1. Introduction

1.1. Millimetre-Wave Frequency Band

The millimetre-wave (mmWave) frequency band of the electromagnetic spectrum include frequencies from 30 GHz to 300 GHz. It is sometimes called the extremely high frequency (EHF) range, with wavelengths between 10 mm and 1 mm, which is the so-called mmWave region as shown in Fig. 1.1.

The growth in the demand for a spectrum to meet the global communication needs has never ceased. Recently, mmWave frequency band and beyond have become quite interesting for wireless applications compared to the conventional microwave frequency band. Two main reasons are behind the orientation towards the mmWave frequency band [1]: First, higher frequency leads to higher data transfer rate and hence real-time applications. Second, because of the small wavelength, mmWave components will have tiny dimensions and consequently a compact overall size. These advantages imply the use of the mmWave systems to satisfy several demands, e.g., from satellite communications to security systems, and more. However, as the frequency increases, the loss increases and the propagation suffers from the high attenuation problem.

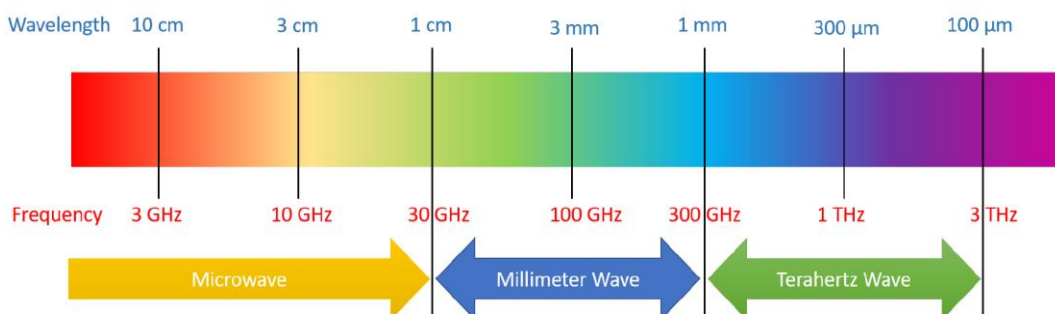


Fig. 1.1. Frequency spectrum showing the mmWave frequency band [2].

1.2. Guiding Structures in the mmWave Frequency Band

One of the most exciting and challenging parameters in RF systems is the hosting guiding mechanisms. At the lower frequency range, transmission lines are mostly used where waves travel in the form of transverse electromagnetic (TEM) mode, which is neither electric nor magnetic field in the direction of propagation. As the frequency increases, the attenuation increases, which is proportional to the square of the frequency [3]. Hollow waveguides are low loss guiding structures with a high power-handling capability. Circular waveguides and rectangular waveguides are the most popular air-filled waveguides used for high-frequency applications. Particularly, the rectangular waveguide is the most common guiding structure for devices operating at high frequencies, and the loss is low compared to most other guiding structures because of its high Q-factor. The rectangular waveguide has a hollow tube inside where the wave travels. At the mmWave band, it is challenging to construct a rectangular waveguide with a proper electrical contact between its parts. With the increase in frequency, the dimensions become smaller; as a result, conventional machining becomes more complex and less accurate.

Planar technologies, such as strip lines and microstrip lines, are suitable for low-frequency applications. As they are printed on a dielectric substrate, they suffer from high dielectric losses at high frequencies [4]. Besides, microstrip lines suffer from high cavity modes and surface waves at higher frequencies which leads to unwanted radiation. These drawbacks significantly affect the suitability of microstrip lines in the mmWave band. The co-planar waveguide, which is also preferable for low-frequency application, is another type of planar waveguides constructed on a dielectric substrate,

In the last decades, lots of work had been done to propose and analyse different guiding structures suitable for mmWave applications, such as substrate integrated waveguide (SIW) and the packaged microstrip line. The operating mode of SIW is similar to the conventional rectangular waveguide, which makes it a reasonable extension of the rectangular waveguide. In SIW, the field travels in the substrate between two rows of

via holes replacing the sidewalls of a rectangular waveguide. This type of structures is low-profile and can be integrated more easily with other system parts on a single board. However, SIW suffers from dielectric loss and dispersive propagation. Therefore, the need for a new guiding technology that can fill the gap between the great performance of hollow waveguides and the cost-effectiveness of printed boards is present in today's research and industrial environment.

1.3. Gap Waveguide Technology

Gap waveguide technology is a modified parallel-plate waveguide where the metal plate at the bottom is replaced by a textured surface of a periodic structure, typically metal pins. The main concept of gap waveguides is based on confining and directing the electromagnetic waves inside a parallel-plate waveguide towards a specific direction. This can be done by electromagnetic bandgap (EBG) structures where they are a special type of periodic structures that prevent the propagation of modes at a specific frequency band. EBG surfaces have a very high surface impedance that synthesises the magnetic conductor features at normal incidences of waves. This feature can be invoked in microwave circuits and antennas for performance improvement of the device. Indeed, this concept is inspired by soft and hard surfaces where soft surfaces prevent waves from propagating, whereas hard surfaces allow propagating waves. In 1988, Kildal introduced the idea of soft and hard surfaces to the electro-magnetic community [5], [6].

1.4. Motivation and Objectives

With the significant growth of telecommunication applications that utilising high data transfer rates, high-frequency bands particularly the mmWave frequency band, have become highly demanded. The mmWave frequency band that extend from 30 to 300 GHz with a corresponding wavelength of 1-10 mm, has many advantages over the lower bands, such as larger available bandwidth, less interference, more compact component size, etc. A high data transfer rate can be more easily achieved in the

mmWave frequency band. Potential high-frequency wireless applications include point to multipoint services, satellite communications, automotive radars, radiometers, imaging and security systems [7]-[14]. Significant research and efforts have been going on the mmWave frequency range (or even higher) to validate different RF system aspects.

The most common technologies for radio frequency (RF) devices are hollow waveguides (rectangular and cylindrical waveguide) and planar transmission lines (stripline, microstrip line, slotline and coplanar waveguide), both of which have inevitable problems in high-frequency bands. On the one hand, planar transmission lines usually consist of one or two layers of metallisation with a solid dielectric substrate. The main features for such transmission lines are compact in size, low in cost and can be easily incorporated with other active circuit devices to form microwave integrated circuits. However, planar-based components operating at mmWave frequency band suffer from the high loss and low-quality factor due to the presence of substrate materials. Another problem that could be noticed in microstrip structures is the existence of radiation loss [3], [4].

On the other hand, hollow waveguides play an important role, especially in very high-frequency systems, for their low loss and high power-handling capability. In terms of loss, unlike planar-based structures, waveguides exhibit a noticeable improvement. This improvement is attributed to the non-use of a dielectric substrate in the hollow waveguide structures. Waveguide structures are usually manufactured in two parts that are joined together, but then there are mechanical complexities. Ensuring good electrical contact in the joints is difficult and expensive at high-frequency bands. Therefore, even though hollow waveguide devices have excellent performance in the millimetre and sub-millimetre bands, tiny dimensions require very high accurate manufacturing technologies.

Gap waveguides, as modified parallel-plate waveguides, are regarded as a compromise solution for mmWave components. Unlike planar and SIW technologies, gap waveguides are characterised by their high Q-factor and, thus, low losses at mmWave frequency band. The motivation for this research is triggered by the demand to design

mmWave components with low loss, high power-handling and easy manufacturing. In recent years, with the rapid development of wireless communication systems, a lot of research and studies have been dedicated to improving the overall performance of mmWave passive components. The main objectives of this work are:

- To present the main geometries/forms of pins of the periodic structures in the gap waveguide technology and to address the pros and cons of each category.
- To realise a compact groove gap waveguide bandpass filter (BPF) operating at the mmWave frequency band with a high-selectivity response by introducing transmission zeros around the passband. Design of low mass, low loss and high-selective BPFs operating at mmWave frequencies are of high importance for aerospace (unmanned drone, manned aircraft, satellite and interplanetary mission) applications.
- To obtain an efficient guiding structure that can be applied to design passive components/devices operating at mmWave frequency band with low loss, an enhanced bandwidth and ease of manufacture. That leads to the proposal of a novel gap waveguide structure with a new pin-form that can overcome the drawbacks of the conventional gap waveguide structures.
- To adopt and compare different manufacturing technologies in the fabrication of mmWave components in terms of performance and mass.

1.5. Organisation of the Thesis

The contents of this thesis are organised in the following manner:

Chapter 2 presents the literature review of previous work on the design and fabrication of mmWave-based components. Transmission lines challenges at the mmWave are listed first. Then, gap waveguide technology is introduced.

Chapter 3 presents a brief introduction to filters and their types in terms of attenuation characteristics, amplitude responses, bandwidth and design technology. Filters and filtering antennas design steps and methodology with a filter design example are presented. All components in the next chapters will be designed based on the procedure and formulas mentioned in this chapter.

Chapter 4 presents a comprehensive study and design of a groove gap waveguide BPF at Ka-band. The filter is fabricated using two technologies: computer numerical control (CNC) machining technology and high-resolution metalised polymer jetting (PolyJet) 3-D printing technology. The metalised PolyJet 3D printed filter exhibits lower loss, lighter weight and more cost-effective when compared to the solid metal case.

Chapter 5 introduces a novel pin-form in gap waveguide technology. With the new form, the effect of wave shielding will be much stronger at the operating band. Also, the bandwidth of the operating passband can be enhanced. A good matching between a with the standard waveguide ports can also be achieved without the need for a transition. In addition, the sidewalls can also be exploited for wave radiation.

Chapter 6 presents the design of a cavity-backed slot antenna (CBSA) and a 3rd-order cavity-backed slot filtering antenna (CBSFA) based on the new gap waveguide structure proposed in Chapter 5. The CBSA operates at X-band while the CBSFA operates at Ka-band. Both antennas are fabricated using CNC machining technology and tested.

Chapter 7 concludes the work. The main contributions of the work are reviewed and highlighted. Moreover, the potential extensions of the work and several future research topics are presented.

References

- [1] Z. Pi and F. Khan, “An Introduction to Millimeter-Wave Mobile Broadband Systems,” *IEEE Commun. Mag.*, no. June, pp. 101–107, 2011.
- [2] R. Chataut and R. Akl. “Massive MIMO Systems for 5G and Beyond Networks- Overview, Recent Trends, Challenges, and Future Research Direction.” *Sensors (Basel, Switzerland)* vol. 20(10), 2753, May 2020.
- [3] Ali Zaidi, Fredrik Athley, Jonas Medbo, Ulf Gustavsson, Giuseppe Durisi, Xiaoming Chen, 5G Physical Layer, Academic Press, 2018.
- [4] R. E. Amaya, A. Momciu and I. Haroun, "High-Performance, Compact Quasi-Elliptic Band Pass Filters for V-Band High Data Rate Radios," in *IEEE Transactions on Components, Packaging and Manufacturing Technology*, vol. 3, no. 3, pp. 411-416, March 2013.
- [5] P. S. Kildal, “Definition of artificially soft and hard surfaces for electromagnetic waves,” *Electronics Letters*, vol. 24, no. 3, pp. 168–170, 1988.
- [6] P. S. Kildal, “Artificially soft and hard surfaces in electromagnetics,” *IEEE Transactions on Antennas and Propagation*, vol. 38, no. 10, pp. 1537–1544, 1990.
- [7] Lockie and D. Peck, “High-data-rate millimeter-wave radios,” *IEEE Microwave Mag.*, vol. 10, no. 5, pp. 75–83, Aug. 2009.
- [8] J. Wells, “Faster than fiber: The future of multi-G/s wireless,” *IEEE Microwave Mag.*, vol. 10, no. 3, pp. 104–112, May 2009.
- [9] J. Hasch, E. Topak, R. Schnabel, T. Zwick, R. Weigel, and C. Waldschmidt, “Millimeterwave technology for automotive radar sensors in the 77 GHz frequency band,” *IEEE Trans. Microw. Theory Tech.*, vol. 60, no. 3, pp. 845–860, Mar. 2012.
- [10] Y.-C. Ou and G. M. Rebeiz, “On-chip slot-ring and high-gain horn antennas for millimeter-wave wafer-scale silicon systems,” *IEEE Trans. Microw. Theory Tech.*, vol. 59, no. 11, pp. 1963–1972, Aug. 2011.
- [11] H. Kaouach, L. Dussopt, J.Lantéri, T. Koleck, R.Sauleau, “Wideband Low-Loss Linear and Circular Polarisation Transmit-Arrays in V-Band,” *IEEE Trans. on Antennas and Propag.*, vol: 59, no.7, pp. 2513 - 2523, July 2011.

-
- [12] Joe W. Waters, Lucien Froidevaux, Robert S. Harwood, Robert F. Jarnot, “The Earth Observing System Microwave Limb Sounder (EOS MLS) on the Aura satellite,” *IEEE Trans. Geosci. Remote Sens.*, vol. 44, no. 5, pp. 1075–1092, May 2006.
- [13] K. B. Cooper, R. J. Dengler, N. Llombart, T. Bryllent, G. Chattopadhyay, E. Schlecht, J. Gill, C. Lee, A. Skalare, I. Mehdi, and P. H. Siegel, “Penetrating 3D imaging at 4- and 25-m range using a submillimeter- wave rader,” *IEEE Trans. Microw. Theory Tech.*, vol. 56, no. 12, pp. 2771–2778, Dec. 2008.
- [14] K. Wu, Y. J. Cheng, T. Djerafi, and W. Hong, “Substrate-integrated millimeter-wave and terahertz antenna technology,” *Proc. IEEE*, vol. 100, no. 7, pp. 2219–2232, Jul. 2012.

Chapter 2. Overview of Millimetre-Wave Components and Gap Waveguide Technology

2.1. Introduction

In this chapter, the state-of-the-art millimetre-wave (mmWave) components design based on different technologies are presented. Transmission line challenges at mmWave bands are also discussed. The merits and drawbacks of each technology are addressed. Then, an overview of gap waveguide technology is introduced. The definition, origin and types of gap waveguides are presented. Finally, main manufacturing techniques of mmWave components are addressed.

2.2. Transmission Line Challenges at Millimetre-Wave

Various technologies have been used to design components operating at the mmWave band for different applications. Two main technologies will be discussed in the following sections, planar technologies and waveguide technologies.

2.2.1. Planar Technologies

One of the most commonly used transmission lines is the planar-based type which can be constructed using a low-cost printed circuit board (PCB) in the form of striplines, microstrip lines, slotlines, coplanar waveguides (CPW) and several other types. These transmission lines usually consist of one or two layers of metallisation with a solid dielectric substrate. The main features for such transmission lines are compact in size, low in cost and can be easily incorporated with other active circuit devices to form

microwave integrated circuits. Two types of planar technologies will be discussed in this subsection.

A- Microstrip Line

Microstrip transmission line technology has become the most widely used for radio frequency and microwave front ends. This widespread use is attributed to its planar design, ease of manufacturing using different methods, easy integration with solid-state products, good heat sinking and good mechanical processing. Recently, various mmWave components are designed based on microstrip line technology, such as a coupler [1], an antenna [2], [3] and a filter [4]-[7]. However, all the above microstrip-based components suffer from high loss and low-quality factor due to the presence of substrate materials.

B- Coplanar Waveguide

Coplanar Waveguides are alternative to stripline and microstrip technologies. Simply, a CPW comprises of one conducting strip in the middle of two ground conductors, one to either side of the middle conducting strip. Because of using conductor layers on only one surface of the substrate and also eliminating via-holes, the fabrication process of CPW is easier than other planar technologies. Also, compared to microstrip line, coplanar waveguide structures have many preferences such as less sensitivity to the substrate thickness and low dispersion effect in the design of microwave and mmWave circuits. This leads to the dispense of post-fabrication tuning of filters. On the other hand, CPW-based components still have a lack in terms of quality factor (Q-factors) and insertion loss when compared to waveguide-based components. In addition, planar structures suffer from the existence of radiation loss. CPW has been adopted to design many mmWave devices for power divider/combiner applications [8], filters [9], [10] and antennas [11].

2.2.2. Waveguide Technologies

Waveguides are one of the earliest types of transmission lines that used to transmit microwave signals. For high-power systems, mmWave applications, radar applications, satellite systems, etc., waveguides are considered the best choice. A large variety of components such as couplers, detectors, isolators, attenuators and slotted lines are commercially available for various standard waveguide bands. Three types of waveguide filters are discussed next: rectangular waveguide, circular waveguide and substrate integrated waveguide (SIW).

A- Rectangular Waveguide

Rectangular waveguides are the earliest form of waveguides. They are used in many applications, especially high selectivity devices for their high Q-factors. It is well known that transmission lines based on planar forms are most widely used in monolithic microwave integrated circuits due to the simplicity of fabrication and integration easiness. However, rectangular waveguides still play an important role, especially in very high-frequency systems. Unlike stripline, microstrip and CPW structures, hollow waveguides exhibit a noticeable improvement in terms of loss due to the absence radiation loss.

A conventional rectangular waveguide window has a broad dimension a and a short dimension b (in the most standard cases $a = 2b$) as shown in Fig. 2.1. The dimensions a and b of the window in a rectangular waveguide determine the cut-off frequencies of the waveguide modes. Choosing b to be half of a is based on the concept that the lower the value of b the higher cut-off frequency of higher modes, but at the same time reducing b increases waveguide loss. The TE_{10} mode has the lowest cut-off frequency and is the dominant mode. All other modes have higher cut-off frequencies. Waveguides are usually designed so that at the frequency of operation only the dominant mode is propagating, while all higher-order modes are cut-off.

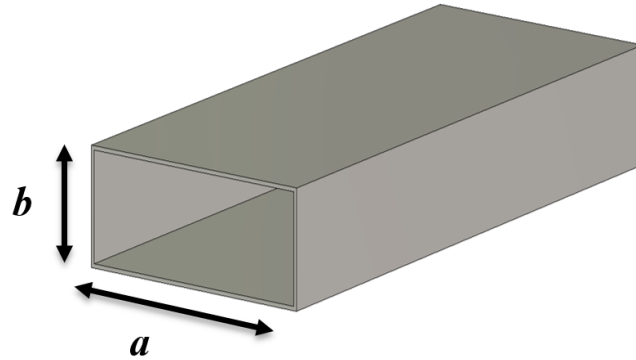


Fig. 2.1. A conventional rectangular waveguide.

The cut-off frequencies of rectangular waveguide modes can be calculated as

$$f_{c_{mn}} = \frac{1}{2\sqrt{\mu\epsilon}} \sqrt{\left(\frac{m}{a}\right)^2 + \left(\frac{n}{b}\right)^2} \quad (2.1)$$

where ϵ and μ are the permittivity and permeability of the medium, the indices m and n indicate the mode number.

A hybrid folded rectangular waveguide is proposed to design bandpass filters providing multiple TZs below the passband. A fifth-order filter composed of two trisections providing four TZs is designed and tested in [12]. A very good performance has been recorded in this work, but this is in X- or Ku-band (12.6 GHz) not in mmWave bands. An iris waveguide filter for mmWave applications is presented [13]. The proposed filter has a centre frequency of 35.75 GHz. The measured insertion loss is lower than 0.8 dB. When the spectrum shifts to extremely high frequencies, the drawbacks of this technology start to appear such as the physical connection between the plates.

B- Circular Waveguide

In addition to the rectangular waveguide, the circular waveguide is another type of conventional waveguides. From the name, it is obvious that the cross-section of this type of waveguides is simply a circle. Circular waveguides are used thoroughly to design microwave and mmWave components [14]-[17]. A wideband circularly polarised dielectric rod waveguide antenna for mmWave applications is presented in

[14]. Dual-mode filters based on circular waveguide technology are proposed in [15]. A wideband and mode converter from a rectangular waveguide to a circular waveguide is designed [16]. Also, a compact circularly polarised horn antenna is presented. By cutting a slot along the 45° direction at the end of the circular waveguide, the proposed antenna achieves a wideband circularly polarised radiation [17].

C- Substrate Integrated Waveguide

Substrate integrated waveguide (SIW) technology provides an effective solution for the low-cost and high-performance integrating and packaging of microwave and mmWave systems [18]. A filter with a centre frequency of 35 GHz is presented. Compared to the dominant mode of SIW cavity filters, the high-mode can provide good performance in the higher frequency with the same size. This property enables designers to implement higher frequency components with a normal PCB process [19]. The measured centre frequency shifts down to 35.8GHz and the insertion loss is about 3 dB. This shifting and high loss are probably due to the dielectric constant shift and high dielectric loss at a high frequency. A Ka-band 5-pole micromachined filter with a fractional bandwidth of 6.5% at a centre frequency of 30.9 GHz on a silicon substrate is presented in [20]. It is based on the SIW design and MEMS fabrication process. The filter is fed by CPW transmission-lines through current probes. Inductively coupled plasma deep etching is used to form the via-holes of SIW cavities. The measured IL is 0.5 dB. The unloaded Q-factor of SIW resonators is calculated to be 341. This monolithic silicon micromachined filter results in small size, low cost, high performance and easy integration with planar circuits.

SIW platform is adopted to realise BPFs having asymmetric frequency response operating at Ka-band. For high rejection between neighbouring transmitting and receiving channels in diplexers, these kinds of filters are highly recommended. Also, the self-packaging feature is available in these types of filters because of using conductor-backed coplanar waveguide [18]. A filter with a centre frequency of 35 GHz and a fractional bandwidth of 3.7% was realised on a single layer Rogers RT/ Duroid 6002 substrate with 0.508 mm thickness that has stable dielectric and mechanical properties. Only 0.8% or less frequency shift is noticed due to fabrication error such

as via-hole radius and substrate permittivity. The obtained in-band insertion loss of the filters is better than 1.25 dB, while the measured return loss is better than 14 dB. The proposed filters have shown a very good single-side stopband attenuation, low insertion loss and compact-sized geometry for microwave and mmWave planar diplexer applications. Besides, self-packaged SIW filters can be directly used in the development of advanced packaging systems.

Two low-loss BPFs based on air-filled SIW are suggested in [21] and produced using a low-cost multilayer PCB. To achieve a very lightweight, high efficiency, low cost and self-packaged mmWave integrated system, the top and bottom layers should use an incredibly low-cost standard substrate such as FR-4 on which base-band or digital circuits can be constructed. Comparing with its dielectric-filled counterparts, the proposed air-filled SIW filter exhibits lower loss, higher Q-factor and increased average power-handling capability. The fabricated filter is anticipated to be utilised in the microwave and mmWave applications.

2.3. The Concept of Gap Waveguide

2.3.1. The Origin of Gap Waveguide

The gap waveguide is based on the concept of hard and soft surfaces [22], [23]. Soft and hard surfaces are metamaterials that do not exist in nature. Metamaterials are artificial surfaces that possess unique and desirable electromagnetic properties that are not present in nature. For instance, a magnetic conductor is one of the most desirable property but it does not exist in nature. Therefore, massive work has been done in the last years to the creation of metamaterial surfaces that could artificially generate magnetic conductivity, so-called artificial magnetic conductors, or ideally a perfect magnetic conductor (PMC).

Artificially, a soft surface can be realised by corrugating a surface transversely, as shown in Fig. 2.2(a). When the depth of the corrugations is a quarter wavelength at the

operating frequency, the short circuit is transformed to an open circuit at the aperture of the corrugation and the surface impedance will be infinite, having a rejection of propagation for all the waves along the direction of propagation. Typically, soft surfaces are employed to prevent undesirable radiation along a certain surface in a specific direction, for example, to minimise the side lobes of the microstrip and aperture antennas in the E-plane [24], [25] and with horn antennas [26].

The hard surfaces, which allow waves to travel along the direction of propagation, can be obtained by filling longitudinal corrugations with dielectric content, as shown in Fig. 2.2(b). Kishk and Kildal [27] realised perfect electric conductors (PECs) and PMCs in terms of hard and soft surfaces. When the strips are created longitudinally in the same direction of wave propagation, they represent a hard surface that allows the wave to propagate. However, when the strips are created transversally in the normal direction of wave propagation, they represent a soft surface that prohibits the wave to propagate as shown in Fig. 2.2(c).

The concept of gap waveguide technology is based on confining and directing electromagnetic waves inside two not physically contacted parallel-plates. On the one hand, if both of these plates are metal or PEC, electromagnetic waves will be allowed to propagate regardless of the distance between the two plates. On the other hand, if one of these plates is an EBG structure or a PMC and the distance between the plates is less than $\lambda/4$, no electromagnetic waves are allowed to travel as shown in Fig. 2.3(a). Having this concept, Fig. 2.3(b) shows that one of the parallel-plates is spaced by less than $\lambda/4$ of the other plate and constitutes a PEC sheet in the centre surrounded by PMCs on both sides, which will allow the electromagnetic waves to propagate following the PEC sheet while the propagation is prohibited on both sides.

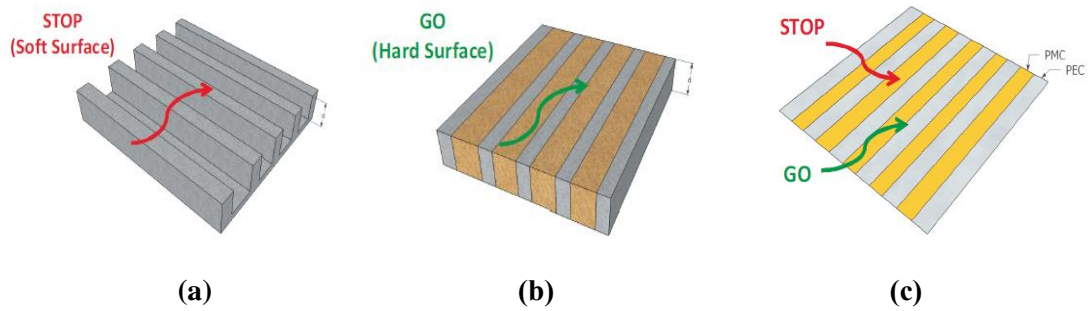


Fig. 2.2. (a) Soft surface realised with transverse corrugations. (b) Hard surface realised with longitudinal dielectric-filled corrugations. (c) Soft-hard surface ideally realised with PEC/PMC strips [27].

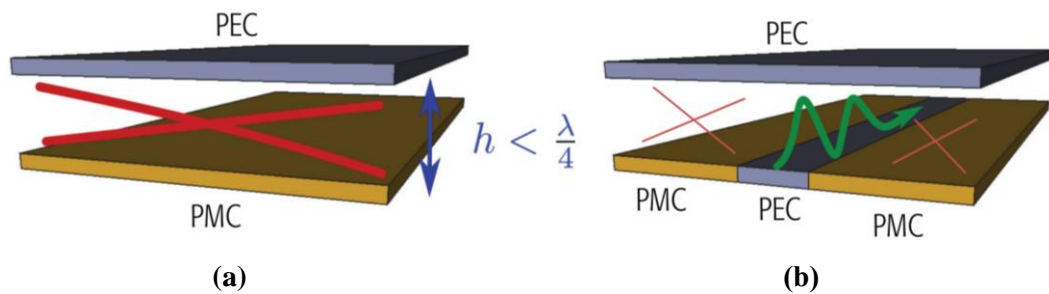


Fig. 2.3. The concept of gap waveguide technology. (a) PEC-PMC parallel-plates. (b) PEC-PEC with the existence of PMC on one plate. The green arrow means propagation is allowed while the red crosses mean propagation is forbidden. The distance between the parallel-plates is less than $\lambda/4$ [28].

2.3.2. Electromagnetic Bandgaps

In the last two decades, researchers have put great efforts to innovate and develop new electromagnetic materials with specific electromagnetic characteristics, which cannot be observed in nature, to be utilised for high-performance applications. These materials are called "metamaterial". Metamaterials can be broadly defined as "artificially structured materials that are designed to interact with and control electromagnetic waves" [29]. Various designations are given to metamaterials in the literature [30], depending on the exhibited electromagnetic properties, such as soft and hard surfaces, high-impedance surfaces, artificial magnetic conductors, etc.

Electromagnetic Bandgap surfaces are high impedance surfaces [31], which prevent waves from propagating in all directions within a frequency range due to their isotropic

characteristics. The most common EBG realisation in gap waveguides is a textured surface made of periodic metal pins, which is known as a “bed of nails” [32] and mushrooms-type EBG textures proposed in [31]. The stopband characteristics of these parallel-plate structures are presented in [33]. The metal bed of nails can be easily realised with milling techniques. It is made of only metal or realised with one of the additive manufacturing techniques followed by a metal plating process if required, being suitable for high-frequency applications. The bed of nails or pins work as a high impedance surface within a stopband defined by a lower and an upper cut-off frequency. The mushroom-type EBG surface is realised with PCB technology and metal patches on the top of the substrate connected to the ground via holes. For this reason, this structure can be made compactly, thus being suitable also for low-frequency applications.

2.3.3. Gap Waveguide Types

According to the channel geometry utilised for wave propagation in gap waveguide technology, four different realisations are represented as shown in Fig. 2.4. These four types are named ridge, groove, inverted-microstrip and microstrip-ridge gap waveguides. The operating modes in the different gap waveguide geometries are different as shown in Fig. 2.5. The advantages and disadvantages of each version are related to the manufacturing simplicity, compactness and power-handling capability [34].

A- Ridge Gap Waveguide

To obtain a ridge gap waveguide structure, a ridge along the propagation channel is located among the sided pins as shown in Fig. 2.4(a). The ridge gap waveguide geometry allows a quasi-TEM mode within the stopband created by the periodic structure. This configuration of gap waveguide is usually proposed to obtain wider bandwidth due to the presence of the ridge.

B- Groove Gap Waveguide

A Groove gap waveguide structure is equivalent to a conventional rectangular waveguide and consequently supports propagation of transverse electric (TE) and transverse magnetic (TM) modes depending on the dimensions of its cross-section of the groove, although in most cases the TE₁₀ mode is preferred. As shown in Fig. 2.4(b), among the sided pins, a groove is created by removing a set of pins in the centre. The dimensions of this groove, width and height, are equal to that in the conventional rectangular waveguide for the same operating frequency. The groove gap waveguide structure has the lowest loss compared to the other gap waveguide configurations.

C- Inverted Microstrip Gap Waveguide

From its name, inverted microstrip gap waveguide, shown in Fig. 2.4(c), is similar to the conventional microstrip line in planar technology, but replacing the ground plane with a PMC ground plane made of periodic pins, and the circuit is printed on a thin dielectric material located on the PMC plane. Similar to ridge gap waveguide, inverted microstrip gap waveguide geometry allows a quasi-TEM mode within the stopband created by the periodic structures.

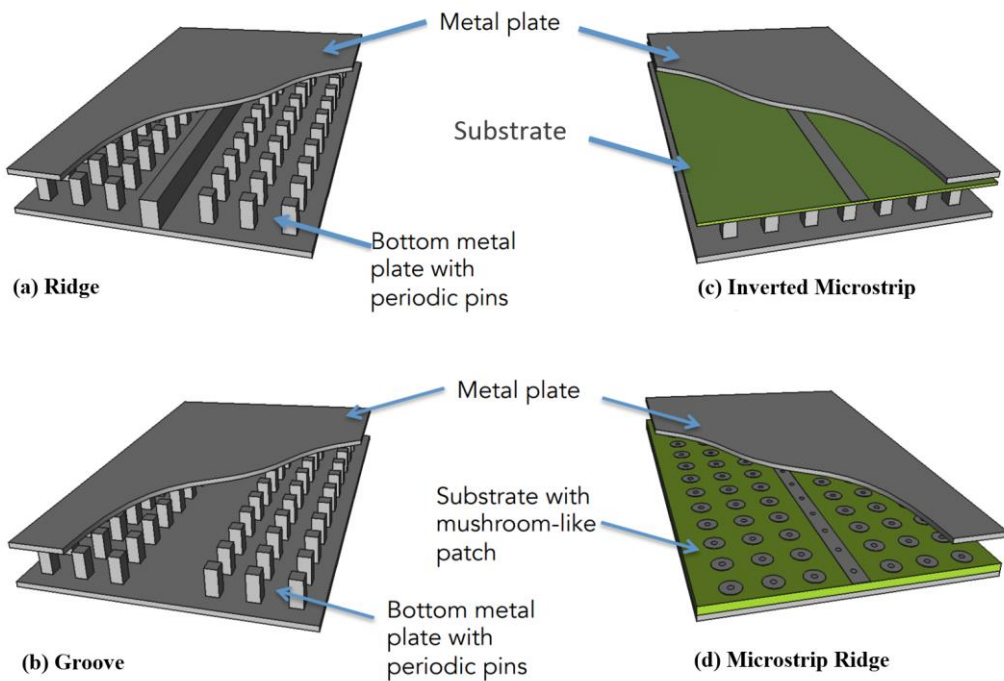


Fig. 2.4. The main types of gap waveguide technology [28].

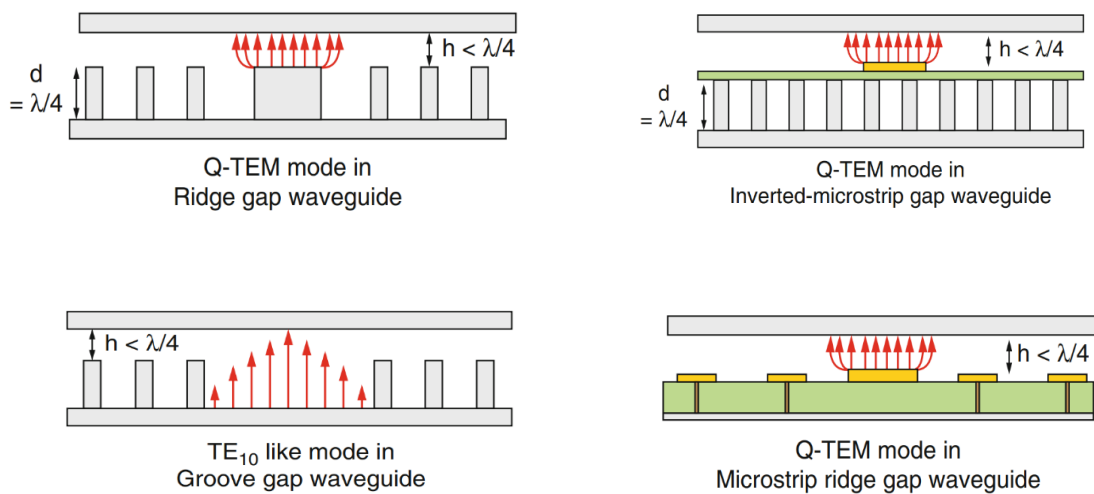


Fig. 2.5. A cross-sectional view shows the localisation of the propagating field in different gap waveguide geometries [34].

D- Microstrip-Ridge Gap Waveguide

Fig. 2.4(d) depicts the geometry of the microstrip-ridge gap waveguide structure. As can be seen, between the two parallel plates, the metal strip on the surface of the dielectric material is connected to the lower plate (ground plane) through a bed of periodic via-holes. Similar to the concept of periodic pins in earlier types, these via-holes establish a forbidden region on both sides of the middle ridge so the waves stop propagating through the gap between the top of via-holes and the upper metal plate. The only propagation direction, that the waves will follow, is the middle microstrip-ridge in the form of a quasi-TEM mode.

2.3.4. Pin forms in Gap Waveguide Technology

As mentioned earlier, gap waveguide technology is a modified parallel-plate waveguide where the metal plate at the bottom is replaced by a textured surface of a periodic structure, typically metal pins. These pins act as a high impedance surface within a stopband defined by a lower and an upper cut-off frequency. Since the emergence of gap waveguide technology [35], different pin geometries/forms have

been proposed. In this section, three main categories of pin forms will be addressed, and under each category, different shapes will be discussed. To be more specific, the unit cell of each pin form will be analysed.

A. Traditional pins

The traditional form of pins in gap waveguides is a full-length pin mounted on one plate while the other plate is kept flat. Different traditional gap waveguide pin-forms are reported in the review, square pins shown in Fig. 2.6(a) [35], circular pins [33], inverted pyramid-shaped pins [36] and double cone pins [37] are the main geometries of the conventional gap waveguide pins. The former two geometries are proposed as the very basic forms that are used to realise the EBG structure in gap waveguide technology while the latter two were proposed for wideband performance enhancement in gap waveguides. All the proposed pin-shapes in this category are based on a full-length pin-form. That means the pins will be thin and long, approximately $\lambda/4$, at mmWaves, which poses a difficulty for low-cost manufacturing.

B. Half-height pins

The half-height-pin form, shown in Fig. 2.6(b), is firstly proposed in [38] to reduce the fabrication cost of gap waveguide structures. In this form, the full-height conventional pins on one of the parallel plates are divided into two half-height pins located on both plate. The Q-factor and insertion loss analysis were carried out using half-height pins in ridge gap waveguides in [39]. It is noticed that, with the increase of the air gap between the half-height pins, the unloaded Q-factor increases while the insertion loss was not affected as rapidly as the Q-factor value. In [40], a planar slot array antenna with a corporate power divider based on half-height pin gap-waveguide technology operating at V-band was reported.

The stopband of the unit-cell of the half-height-pin form is investigated and compared with that in the full-height pin form in [41]. It is confirmed that the air gap between the upper and lower pins is the main factor to define the stopband width, where the relationship between them is the inverse. Other unit-cell parameters such as pin width,

height and period are studied. Pin height determines the centre frequency of the stopband, pin period has a significant influence on the stopband width, while pin width does not affect the stopband significantly for the half-height pins but does for the full-height pins. Also, the effect of alignment between the upper and the lower pins on the performance is studied in the same work. Accordingly, the tolerance for the misalignment between the upper and the lower pins should be smaller than 20% of the width of the pins.

C. Interdigital pins

An interdigital-pins bed has been proposed in [42]. In this form, the metal pins are allocated to the two plates alternatively, where each pin on a plate is surrounded by four pins of the other plate, as depicted in Fig. 2.6(c). The advantage of the interdigital-pin lattice is that a minimum pin gap could be achieved, without reducing the diameter of the milling cutter. This makes it possible to manufacture EBG structures operating at higher frequencies using the same machining centre. However, in this configuration, the pin shape is similar to that in the traditional form, i.e. quite long and thin.

D. Glide-Symmetric Holes

A glide-symmetric structure is an EBG periodic structure constructed through a translation and a mirroring of holes. Its unit cell is shown in Fig. 2.6(d). Although a glide-symmetric structure does not contain pins (hole instead), it is included here as a type of gap waveguide periodic structure. These structures, in their 1-D configuration, were extensively studied in the 1960s through the generalised Floquet theorem [43]. The 2D glide-symmetric holey metasurfaces were introduced for the first time in [44]. It is noticed that a very narrow stopband is achieved when the holes made on only one plate. But using glide-symmetric structures on both parallel plates leads to widening the stopband much further. In [45], hollow straight waveguides and double 90° bent waveguide lines with glide-symmetric holey EBG at the location of the junction are investigated. A wideband phase shifter in mmWave based on glide-symmetric in groove gap waveguide technology is presented in [46] as a good solution to be integrated with antenna feed structures. In [47], a waveguide flange for fast and

contactless measurement and also beneficial in repetitive measurements at high frequencies is proposed. The holey glide-symmetric surface machined around the waveguide opening significantly reduces the leakage in the case of an air gap between the flange joints. In [48], a fully metallic glide-symmetric waveguide filter with transmission in the Ka-band and attenuation at its second harmonic is proposed.

2.3.5. Millimetre-Wave Applications

A- Filters

Low loss and low mass for BPFs operating at mmWave frequencies are of high importance for aerospace (unmanned drone, manned aircraft, satellite and interplanetary mission) applications. A large number of mmWave BPFs using various design and fabrication technologies have been reported over the past few decades. A conventional filter design based on planar technology and manufactured using PCB technology is presented in [49]. SIW technology is used to implement BPFs at mmWave frequencies [50]. A high-Q narrow bandwidth BPF based on empty SIW (empty denotes that there is no dielectric substrate) has been proposed in [51]. Recently, many BPFs have been reported based on gap waveguide (also known as waffle-iron) technology at X-band [52], [53], Ku-band [54], Ka-band (26.5-40 GHz) [55]-[57], Q-band (33-50 GHz) [58] and V-band (50-75 GHz) [59].

B- Cavity-Backed Slot Antennas (CBSAs)

Over the past few decades, many efforts have been made to develop cavity-backed slot antennas (CBSAs). As an early attempt, a wide slot antenna supported by a cavity is suggested using a simple short end waveguide [60]. Then, in [61], a cavity-backed annular slot antenna with one shortened point is studied. Due to its desirable advantages including low-profile, light-weight and ease of integration, planar CBSA has gained considerable attention and has been widely used in satellite and radar communications systems.

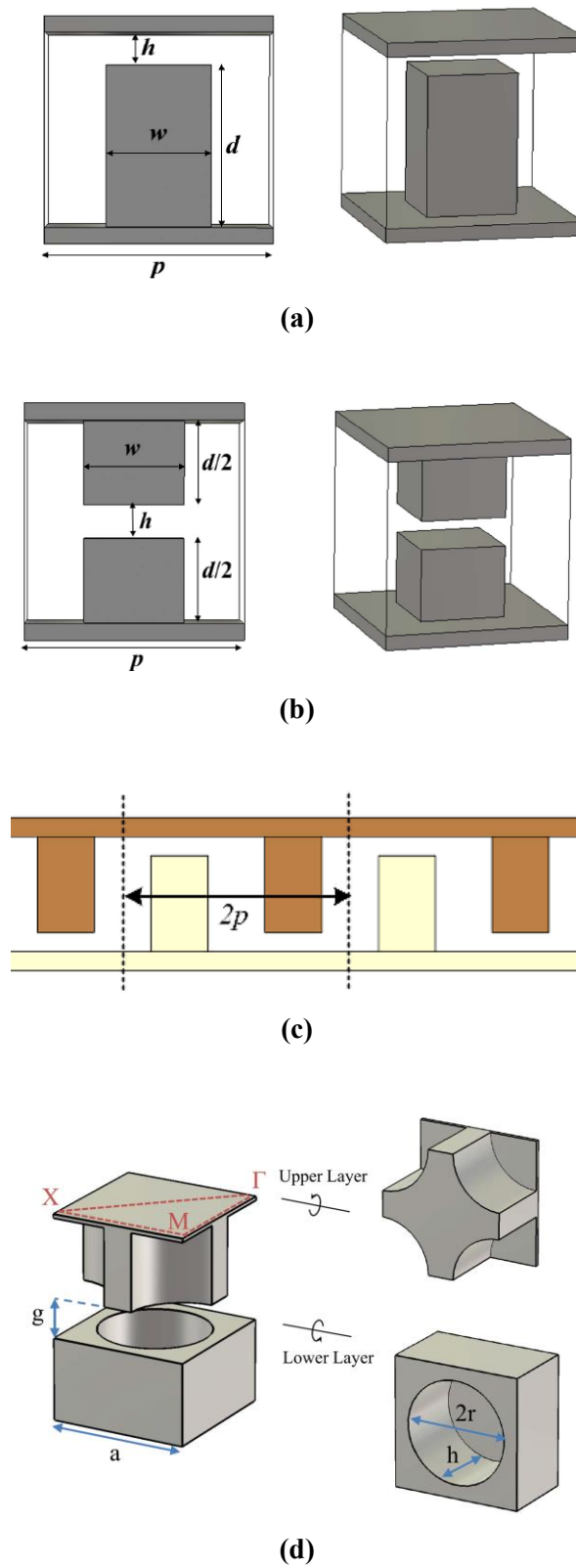


Fig. 2.6. Some pin forms for gap waveguide technology. (a) Full-height pin. (b) Half-height pin. (c) Interdigital pins. (d) Glide-symmetric holes.

Recently, based on SIW technology, CBSA is extensively proposed [62]–[65]. A SIW short backfire antenna operating in the mmWave band is presented in [62]. The excitation of the proposed antenna is done by a high-gain quad-slot cavity-backed feed as shown in Fig. 2.7. This type of feeding performs a lower cross-polarisation level compared to the conventional cavity-backed feed. As the proposed antenna can be fully integrated into a multilayer PCB structure, it is suitable for in-package front-end mmWave planar systems.

A low-profile SIW dual-band CBSA with circular polarisation operating at the mmWave band is reported in [63]. To achieve circular polarisation radiations at two designated bands, two similar structure of annular exponential slots working at two different modes were investigated as shown in Fig. 2.8. In [64], the conventional narrow rectangular slot is replaced by a bow-tie shaped slot fed by a SIW cavity-backed. A broadband response compared with that of the conventional SIW CBSA is achieved as depicted in Fig. 2.9. A low-profile cavity-backed planar slot antenna realised for linearly polarised application is presented in [65]. Using a triangle substrate constructed by metalised via-hole, all antenna elements including the feeding, the cavity and the radiating slot, are realised. Compared with conventional rectangular and circular SIW cavities in the same area, the utilised triangle resonator has a more compact structure and higher radiation efficiency.

C- Filtering Antennas

Filters and antennas are key components in each wireless communication transceivers. They are mostly designed individually and connected by transmission lines which increases interconnection loss [67] and circuit size. Filtering antenna (filtenna) terminology is an expression of a combination of a filter and an antenna into a single component. This combination exhibits miniaturisation and a low profile as well as a low loss of such a component. As well known, antennas are used for receiving and transmitting signals, while filters act as band selective devices. Filtennas can provide both the desired filtering and radiating performances. Since both antennas and filters are mostly arranged at the very front-end of wireless communication transceivers, the integration of these two components contributes to enhancing the overall performance

and miniaturizing the overall circuit size. Moreover, transmitted/received signals in a transceiver will no longer be interfered with by noise in unwanted bands.

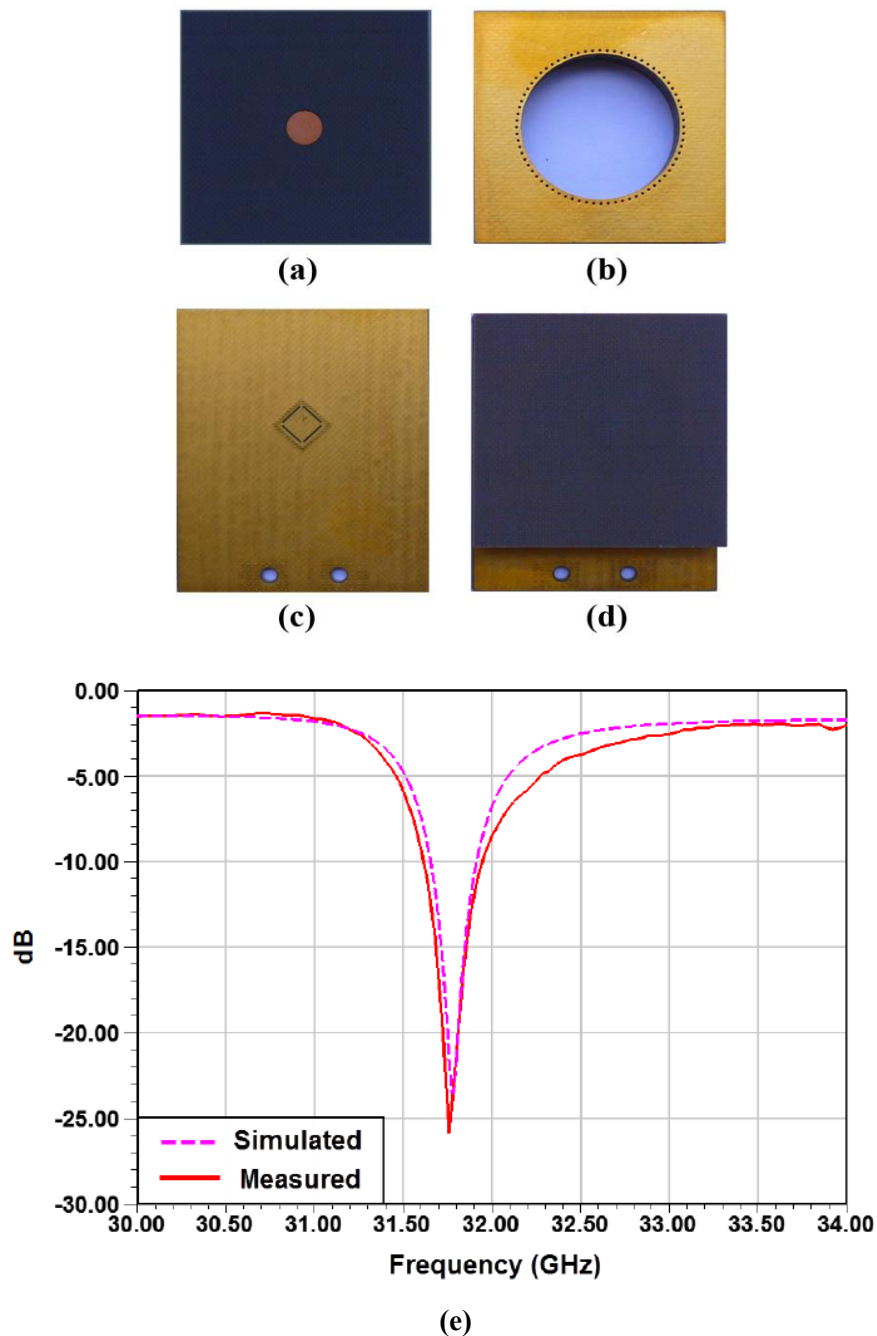


Fig. 2.7. Photograph of the fabricated antenna [62]. (a) Subreflector. (b) Leaky cavity. (c) Quad-slot feed. (d) Top view of the whole antenna. (e) Simulated and measured $|S_{11}|$ for the proposed antenna.

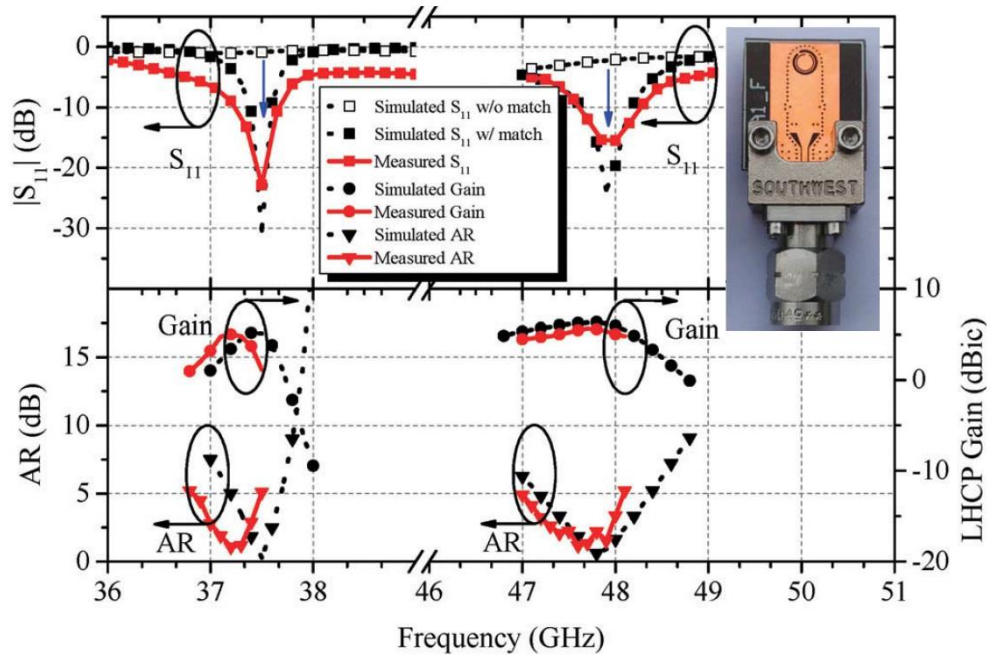
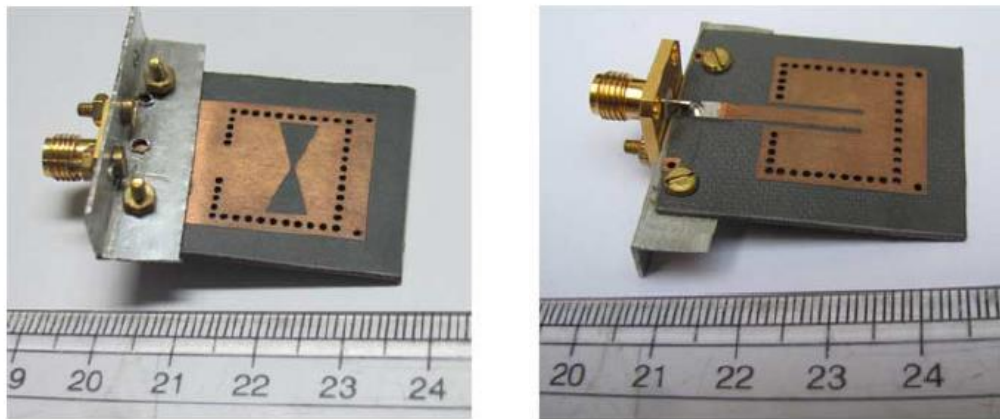


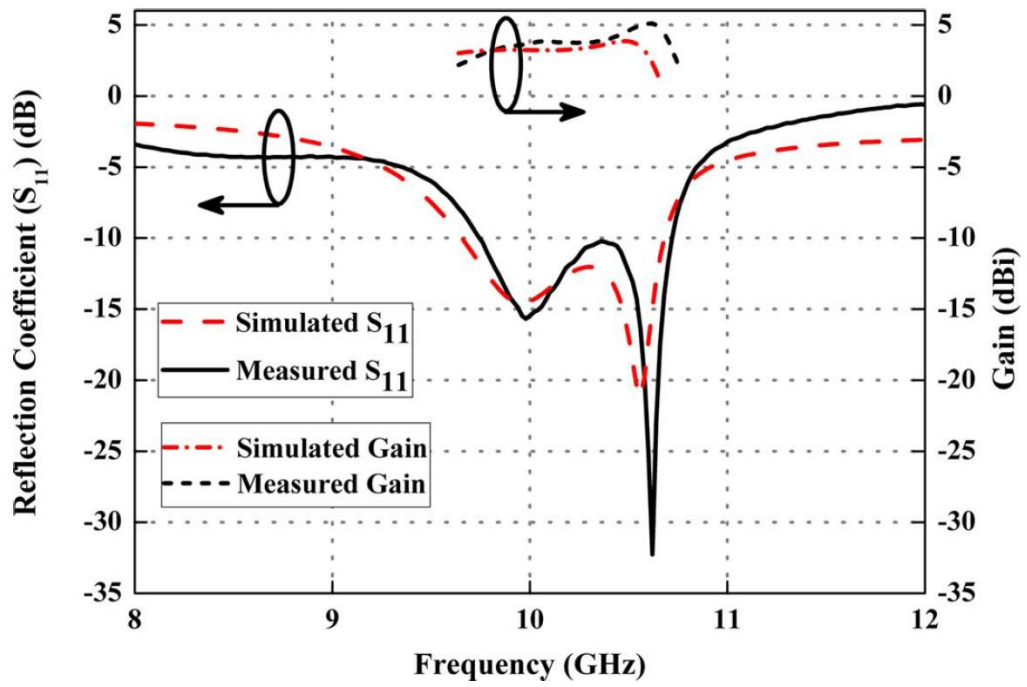
Fig. 2.8. Simulated and measured results of the proposed antenna [63].

An extensive investigation of filtering antennas operating at the mmWaves is conducted in [68]–[77]. The development of a mechanically tunable horn filtenna is proposed in [68]. This waveguide-based filtenna represents the integration of a horn antenna and a mechanically tunable BPF filter based on dual-post resonators. Planar filtenna is proposed in [69] and [70]. A compact mmWave tunable filtenna with defected ground-plane structure resonators was introduced. Substrate integrated waveguide is also adopted to design filtenna [71]–[74]. In [72], a 2×2 dual-polarised antenna subarray with filtering responses is proposed. The top view and the bottom view of the fabricated filtering antenna is shown in Fig. 2.10a. The measured S-parameters of the proposed dual-polarised filtering antenna subarray is shown in Fig. 2.10b. A mmWave filtering patch antenna array fed by an SIW four-way anti-phase filtering power divider is proposed in [74]. Fig. 2.11 shows the simulated and measured broadside gain curves and $|S_{11}|$ responses of the proposed filtering 1×4 patch antenna array. Moreover, based on gap waveguide technology, a slotted array antenna integrated with a BPF is presented in [75], [76], and filter-horn-antenna [77].



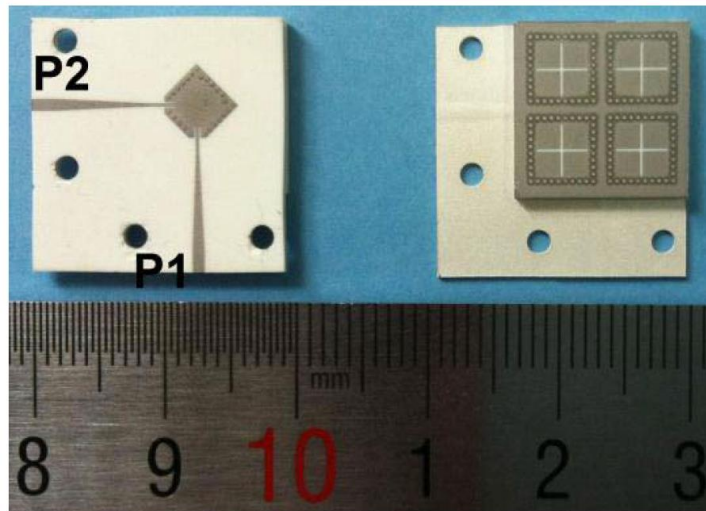
(a)

(b)

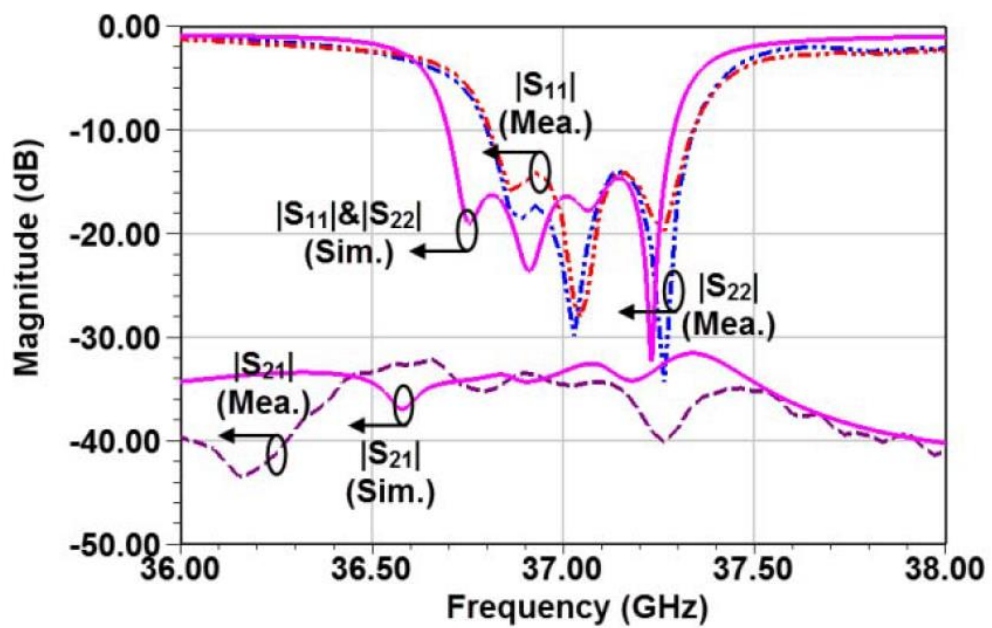


(c)

Fig. 2.9. Comparative study between simulated and measured reflection coefficient and gain of the antenna [64].



(a)



(b)

Fig. 2.10. (a) Top view and bottom view of the fabricated filtering antenna. (b) Simulated and measured reflection coefficients and isolation of the proposed filtering antenna.

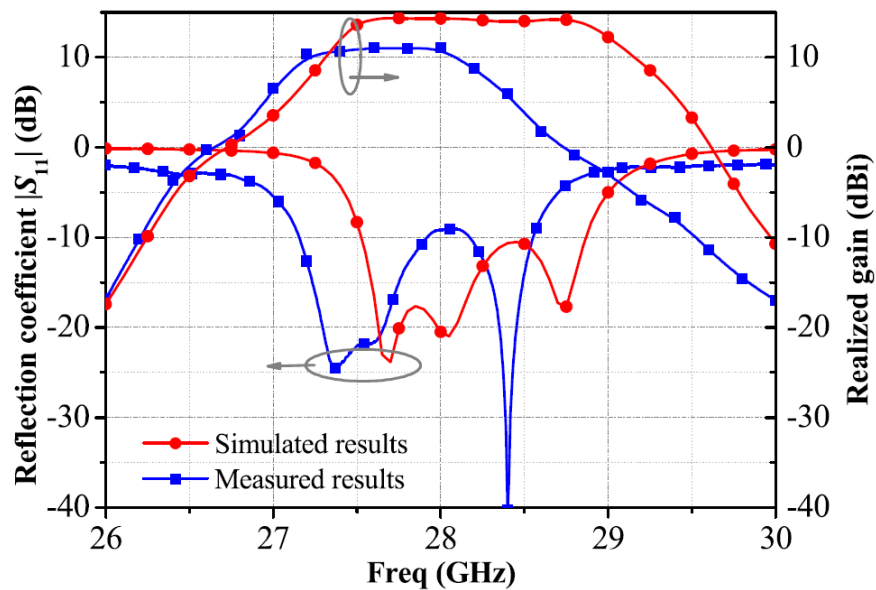


Fig. 2.11. Comparison of the measured and simulated gain curves and $|S_{11}|$ responses of the proposed 1×4 filtering patch antenna array.

2.3.6. Millimetre-Wave Components Fabrication

Manufacturing microwave components to higher levels of accuracy than those found at longer wavelengths becomes increasingly more difficult as frequency increases. Different technologies can be adopted for the manufacture of components operating at mmWave frequencies. The choice of manufacturing technology, to some extent, depends on the technology on which the component is designed. For example, with conventional filter designs based on planar technology, PCB or micromachining technology is adopted for manufacturing; while machining technology is used to fabricate waveguide or gap waveguide-based components. The merits and challenges of the four main manufacturing technologies that can be utilised to fabricate mmWave BPFs will be briefly discussed in this section.

A- Co-Fired Ceramic

For harsh environments, including high humidity and high-temperatures, co-fired ceramic technology can be a good choice for component fabrication. Low temperature co-fired ceramic (LTCC) technology, with sintering below $1,000^{\circ}\text{C}$, is used to produce

compact multilayer circuits. LTCC has been used to implement different mmWave BPFs; for example, a planar-based filter of 60 GHz [78], [79] and SIW-based filter at 40 GHz [53], 140 GHz [80] and [81] and 174 GHz [82]. LTCC technology has many advantages for the manufacture of microwave BPFs. For example, ceramic materials provide highly robust performance under stringent environmental and mechanical conditions. Furthermore, unlike micromachining, 3D structures having complex designs can be realised with a cost-effective fabrication technique, especially for medium and high volumes of manufacture. Having said this, LTCC-based mmWave BPFs suffer from notably high insertion loss, when compared to some other fabrication technologies, such as machining and 3D printing. Therefore, it is not desirable for the fabrication of high Q-factor and low-loss components.

B- Micromachining

Both bulk or surface micromachining technologies can be used to implement BPFs at (sub-) mmWave frequencies [83]. Two waveguide filters, one operating in the WR-3 band (220-325 GHz) and the other in the WR-1.5 band (500-750 GHz), were fabricated using SU-8. A comparative manufacturing study of sub-THz bandpass frequency selective surface (FSS) filters has been reported [84]. Photolithography facilitates batch processing when compared to the other methods. However, the need for cleanroom microfabrication processing increases complexity, time to manufacture and ultimately cost.

C- Machining

Machining technology is mainly used for metal-based component fabrication. For high Q-factor and low-loss BPFs, air-filled metal-pipe rectangular waveguide or gap waveguide technologies can be adopted. In recent years, many waveguide- and gap waveguide-based mmWave BPFs have been fabricated using machining technology, by milling out or drilling into metal structures [58]-[60] and [85]-[87]. Machining technology is preferred for high-Q and low-loss components within the mmWave band. However, the small dimensions of their structures (e.g., pin arrays in gap waveguide) increase the complexity of the milling or drilling process in machining technology and,

hence, also the time and cost of fabrication. Additionally, with aerospace and satellite applications, excess mass is also an important factor.

In gap waveguide structures, the periodic structure parameters play an important role to determine the complexity of the fabrication process. One of these parameters is the height of pins, where shorter pins, i.e. less depth, reduces the manufacturing time and facilitate the process. Another parameter is the periodicity of the periodic structure (the distance between the pins). Although reducing the distance between pins improve the performance of gap waveguide structures, it makes the machining process more complicated where more precise tools will be required leading to costly fabrication.

D- 3D Printing

3D printing technology is emerging for the fabrication of lightweight and low-loss components, as well as complex structured components operating at mmWave frequencies [88] - [91]. 3D printing technology can be mainly classified as either metal-based or polymer-based (with additional metal plating) 3D printing. With the former, binder jetting/sintering and selective laser melting (SLM) can be adopted to construct metal-pipe rectangular waveguides, with Cu-15Sn powder melted layer by layer [92]. With the latter, metal-pipe rectangular waveguides have been demonstrated using fused deposition modelling (FDM), stereolithographic apparatus (SLA) [90] and polymer-jetting (Polyjet) [93]. A variety of groove gap waveguide-based prototypes operating at the Ka-band and manufactured by metallised 3D printing technique have been presented [94]. Their work proved the potential of using 3D printing technology to fabricate groove gap waveguide structures at high frequencies. Furthermore, 3D printing and metallisation technology is adopted to fabricate a novel leaky-wave antenna based on gap waveguide technology [95]. In the work reported here, Polyjet 3D printing of a groove gap waveguide BPF is demonstrated.

2.4. Summary

This chapter has presented and discussed the state-of-the-art mmWave components design based on different technologies. The merits and drawbacks of the transmission lines technologies, such as planar and waveguide technologies, especially at mmWave band have been presented. On the one hand, although planar circuits have good features, such as low cost and easy compact integration, they suffer from high loss and low-quality factor due to the presence of substrate materials. On the other hand, conventional waveguides exhibit a noticeable improvement in terms of loss. This improvement is attributed to the absence of dielectric substrates in their structures. However, a perfect contact between the waveguide parts is required. Therefore, gap waveguide technology has been proposed as a compromise solution.

An overview of gap waveguide technology and its application have then been presented. According to the channel geometry utilised for wave propagation in gap waveguide structures, four different types have been discussed. The main categories of pin forms with different shapes have been discussed. The unit cell of each form has been analysed showing the features and limitations of each form. Finally, the main manufacturing techniques of mmWave components have been addressed.

References

- [1] I. Haroun, C. Plett, Y. Hsu and D. Chang, "Compact 60-GHz IPD-Based Branch-Line Coupler for System-on-Package V-Band Radios," in *IEEE Transactions on Components, Packaging and Manufacturing Technology*, vol. 2, no. 7, pp. 1070-1074, July 2012.
- [2] W. Yang, K. Ma, K. S. Yeo and W. M. Lim, "A Compact High-Performance Patch Antenna Array for 60-GHz Applications," in *IEEE Antennas and Wireless Propagation Letters*, vol. 15, pp. 313-316, 2016.
- [3] A. Bondarik, T. Forsberg, D. Sjöberg, H. Sjöland and M. Törmänen, "A Bond Wire Connection Implementation at mmWave Active Microstrip Antenna," in *IEEE Microwave and Wireless Components Letters*, vol. 29, no. 6, pp. 427-429, June 2019.
- [4] D. L. Cuenca, G. Alavi and J. Hesselbarth, "On-chip mmWave spherical dielectric resonator bandpass filter," *2017 IEEE MTT-S International Microwave Symposium (IMS)*, Honolulu, HI, 2017, pp. 1460-1463.
- [5] M. T. Craton, J. Sorocki, I. Piekarz, S. Gruszczynski, K. Wincza and J. Papapolymerou, "Realisation of Fully 3D Printed W-Band Bandpass Filters Using Aerosol Jet Printing Technology," *2018 48th European Microwave Conference (EuMC)*, Madrid, 2018, pp. 1013-1016.
- [6] S. Yang, S. Zhen and A. Shamim, "Fully Inkjet Printed 85GHz Band Pass Filter on Flexible Substrate," *2018 48th European Microwave Conference (EuMC)*, Madrid, 2018, pp. 652-654.
- [7] E. González-Carvajal and G. Mumcu, "Frequency and Bandwidth Tunable mmWave Hairpin Bandpass Filters Using Microfluidic Reconfiguration With Integrated Actuation," in *IEEE Transactions on Microwave Theory and Techniques*, vol. 68, no. 9, pp. 3756-3768, Sept. 2020.
- [8] A. S. Abd El-Hameed, A. Barakat, A. B. Abdel-Rahman, A. Allam and R. k. Pokharel, "Design of Low-Loss Coplanar Transmission Lines Using Distributed Loading for Millimeter-Wave Power Divider/Combiner Applications in 0.18- μm CMOS Technology," in *IEEE Transactions on Microwave Theory and Techniques*, vol. 66, no. 12, pp. 5221-5229, Dec. 2018.

- [9] A. Franc, E. Pistono, D. Gloria and P. Ferrari, "High-Performance Shielded Coplanar Waveguides for the Design of CMOS 60-GHz Bandpass Filters," in *IEEE Transactions on Electron Devices*, vol. 59, no. 5, pp. 1219-1226, May 2012.
- [10] K. Hettak, T. Ross, R. James and A. Momciu, "Low-cost mmWave coplanar waveguide bandpass filter using inkjet printing of silver nano-particles on flexible plastic substrate," *2015 IEEE MTT-S International Microwave Symposium*, Phoenix, AZ, 2015, pp. 1-3.
- [11] W. Zhang, E. Kasper and J. Schulze, "An 82-GHz 14.6-mW Output Power Silicon Impact Ionisation Avalanche Transit Time Transmitter With Monolithically Integrated Coplanar Waveguide Patch Antenna," in *IEEE Transactions on Microwave Theory and Techniques*, vol. 67, no. 1, pp. 308-317, Jan. 2019.
- [12] C. Carceller, P. Soto, V. E. Boria and M. Guglielmi, "Design of Hybrid Folded Rectangular Waveguide Filters with Transmission Zeros Below The Passband," in *IEEE Transactions on Microwave Theory and Techniques*, vol. 64, no. 2, pp. 475-485, Feb. 2016.
- [13] Y. Zhai, Q. Wang, Z. Wang, and X. G. Xiu, "The design of an iris waveguide filter at 35.75 GHz," *2008 Glob. Symp. Millim. Waves, Proceeding, GSMM 2008*, pp. 8-10, 2008.
- [14] Z. Ji, K. X. Wang and H. Wong, "Circularly Polarised Dielectric Rod Waveguide Antenna for Millimeter-Wave Applications," in *IEEE Transactions on Antennas and Propagation*, vol. 66, no. 10, pp. 5080-5087, Oct. 2018.
- [15] Santiago Cogollos, Maria Brumos, Vicente E. Boria, Carlos Vicente, Jordi Gil, Benito Gimeno, Marco Guglielmi, "A Systematic Design Procedure of Classical Dual-Mode Circular Waveguide Filters Using an Equivalent Distributed Model," in *IEEE Transactions on Microwave Theory and Techniques*, vol. 60, no. 4, pp. 1006-1017, April 2012.
- [16] Yong Xu, Tinghui Peng, Miao Sun, Yong Luo, Jianxun Wang, Wei Jiang, Guo Liu, Zewei Wu, "Design and Test of Broadband Rectangular Waveguide TE₁₀ to Circular Waveguide TE₂₁ and TE₀₁ Mode Converters," in *IEEE Transactions on Electron Devices*, vol. 66, no. 8, pp. 3573-3579, Aug. 2019.

- [17] H. Yu, J. Yu, Y. Yao, X. Liu and X. Chen, "Wideband Circularly Polarised Horn Antenna Exploiting Open Slotted End Structure," in *IEEE Antennas and Wireless Propagation Letters*, vol. 19, no. 2, pp. 267-271, Feb. 2020.
- [18] X. Chen and K. Wu, "Self-Packaged Millimeter-Wave Substrate Integrated Waveguide Filter With Asymmetric Frequency Response," in *IEEE Transactions on Components, Packaging and Manufacturing Technology*, vol. 2, no. 5, pp. 775-782, May 2012.
- [19] Y. Tao, W. Hong and H. Tang, "Design of A Ka-Band Bandpass Filter Based on High Order Mode SIW Resonator," *7th International Symposium on Antennas, Propagation & EM Theory*, Guilin, 2006.
- [20] Y. Yu, Y. Zhang and J. Zhu, "Monolithic silicon micromachined Ka-band filters," *2008 International Conference on Microwave and Millimeter Wave Technology*, Nanjing, 2008, pp. 1397-1400.
- [21] F. Parment, A. Ghiotto, T. Vuong, J. Duchamp and K. Wu, "Air-Filled Substrate Integrated Waveguide for Low-Loss and High Power-Handling Millimeter-Wave Substrate Integrated Circuits," in *IEEE Transactions on Microwave Theory and Techniques*, vol. 63, no. 4, pp. 1228-1238, April 2015.
- [22] P. S. Kildal, "Definition of artificially soft and hard surfaces for electromagnetic waves," *Electronics Letters*, vol. 24, no. 3, pp. 168–170, 1988.
- [23] P. S. Kildal, "Artificially soft and hard surfaces in electromagnetics," *IEEE Transactions on Antennas and Propagation*, vol. 38, no. 10, pp. 1537–1544, 1990.
- [24] Y. Zhang, J. von Hagen, and W. Wiesbeck, "Patch array as artificial magnetic conductors for antenna gain improvement," *Microwave and Optical Technology Letters*, vol. 35, no. 3, pp. 172–175, 2002.
- [25] D. Sievenpiper, J. Schaffner, and J. Navarro, "Axial ratio improvement in aperture antennas using high-impedance ground plane," *Electronics Letters*, vol. 38, no. 23, pp. 1411–1412, 2002.
- [26] D. J. Salomonsson, J. Hirokawa, P. S. Kildal, and A. Tengs, "Corrugated soft sector horn with different beam properties in the two principal planes," *IEEE Proceedings Microwaves, Antennas and Propagation*, vol. 144, no. 1, pp. 13–19, 1997.

- [27] A. A. Kishk and P. S. Kildal, "Modelling of soft and hard surfaces using ideal perfect electric conducting/perfect magnetic conducting strip grids," *IET Microwaves, Antennas & Propagation*, vol. 3, no. 2, pp. 296–302, 2009.
- [28] E. Rajo-Iglesias, M. Ferrando-Rocher and A. U. Zaman, "Gap Waveguide Technology for Millimeter-Wave Antenna Systems," in *IEEE Communications Magazine*, vol. 56, no. 7, pp. 14-20, July 2018.
- [29] D. R. Smith, W. J. Padilla, D. C. Vier, S. C. Nemat-Nasser, and S. Schultz, "Composite medium with simultaneously negative permeability and permittivity," *Physical Review Letters*, vol. 84, no. 18, pp. 4184–4187, 2000.
- [30] F. Yang and Y. Rahmat-Samii, *Electromagnetic Band Gap Structures in Antenna Engineering*, Cambridge University Press, Cambridge, UK, 2009.
- [31] D. Sievenpiper, Z. Lijun, R. F. J. Broas, N. G. Alexopolous, and E. Yablonovitch, "High-impedance electromagnetic surfaces with a forbidden frequency band," *IEEE Transactions on Microwave Theory and Techniques*, vol. 47, no. 11, pp. 2059–2074, 1999.
- [32] M. G. Silveirinha, C. A. Fernandes, and J. R. Costa, "Electromagnetic characterisation of textured surfaces formed by metallic pins," *IEEE Transactions on Antennas and Propagation*, vol. 56, no. 2, pp. 405–415, 2008.
- [33] E. Rajo-Iglesias and P. S. Kildal, "Numerical studies of bandwidth of parallel-plate cut-off realised by a bed of nails, corrugations and mushroom-type electromagnetic bandgap for use in gap waveguides," *IET Microwaves, Antennas & Propagation*, vol. 5, no. 3, pp. 282–289, 2011.
- [34] A. U. Zaman and P.-S. Kildal, "GAP Waveguides," *Handbook of Antenna Technologies*, Springer, 2016, pp. 3273–74.
- [35] P.-S. Kildal, E. Alfonso, A. Valero-Nogueira, and E. Rajo-Iglesias, "Local metamaterial-based waveguides in gaps between parallel metal plates," *IEEE Antennas Wireless Propag. Lett.*, vol. 8, no. 4, pp. 84–87, Apr. 2009.
- [36] A. U. Zaman, V. Vassilev, P.-S. Kildal, and A. Kishk, "Increasing parallel plate stop-band in gap waveguides using inverted pyramid-shaped nails for slot array application above 60 GHz," in *Proc. 5th Eur. Conf. Antennas Propag. (EuCAP)*, Rome, Italy, Apr. 2011, pp. 2254–2257.

- [37] S. I. Shams and A. A. Kishk, "Double cone ultra wide band unit cell in ridge gap waveguides," in *Proc. IEEE Antennas Propag. Soc. Int. Symp. (APSURSI)*, Jul. 2014, pp. 1768–1769.
- [38] F. Fan, J. Yang and P. Kildal, "Half-height pins - a new pin form in gap waveguide for easy manufacturing," *10th European Conference on Antennas and Propagation (EuCAP)*, Davos, 2016.
- [39] F. Fan, J. Yang, Z. Yan and Y. Liu, "Q factor and insertion loss analysis of half-height pin ridge gap waveguide," *International Conference on Electromagnetics in Advanced Applications (ICEAA)*, Cairns, QLD, 2016.
- [40] P. Taghikhani, J. Yang and A. Vosoogh, "High gain V-band planar array antenna using half-height pin gap waveguide," *2017 11th European Conference on Antennas and Propagation (EUCAP)*, Paris, 2017, pp. 2758-2761.
- [41] F. Fan, J. Yang, V. Vassilev and A. U. Zaman, "Bandwidth Investigation on Half-Height Pin in Ridge Gap Waveguide," in *IEEE Transactions on Microwave Theory and Techniques*, vol. 66, no. 1, pp. 100-108, Jan. 2018.
- [42] Dongquan Sun, Xiang Chen, Jing-Ya Deng, Li-Xin Guo, Wanzhao Cui, Kang Yin, Zhenhua Chen, Changfei Yao, Feng Huang, "Gap Waveguide With Interdigital-Pin Bed of Nails for High-Frequency Applications," in *IEEE Transactions on Microwave Theory and Techniques*, vol. 67, no. 7, pp. 2640-2648, July 2019.
- [43] A. Hessel, M. H. Chen, R. C. M. Li, and A. A. Oliner, "Propagation in periodically loaded waveguides with higher symmetries," *Proc. IEEE*, vol. 61, no. 2, pp. 183–195, Feb. 1973.
- [44] O. Quevedo-Teruel, M. Ebrahimpouri, and M. N. M. Kehn, "Ultrawideband metasurface lenses based on off-shifted opposite layers," *IEEE Antennas Wireless Propag. Lett.*, vol. 15, pp. 484–487, Dec. 2016.
- [45] M. Ebrahimpouri, E. Rajo-Iglesias, Z. Sipus and O. Quevedo-Teruel, "Cost-Effective Gap Waveguide Technology Based on Glide-Symmetric Holey EBG Structures," in *IEEE Transactions on Microwave Theory and Techniques*, vol. 66, no. 2, pp. 927-934, Feb. 2018.
- [46] E. Rajo-Iglesias, M. Ebrahimpouri and O. Quevedo-Teruel, "Wideband Phase Shifter in Groove Gap Waveguide Technology Implemented With Glide-

- Symmetric Holey EBG," in *IEEE Microwave and Wireless Components Letters*, vol. 28, no. 6, pp. 476-478, June 2018.
- [47] M. Ebrahimpouri, A. Algaba Brazalez, L. Manholm and O. Quevedo-Teruel, "Using Glide-Symmetric Holes to Reduce Leakage Between Waveguide Flanges," in *IEEE Microwave and Wireless Components Letters*, vol. 28, no. 6, pp. 473-475, June 2018.
- [48] A. Monje-Real, N. J. G. Fonseca, O. Zetterstrom, E. Pucci and O. Quevedo-Teruel, "Holey Glide-Symmetric Filters for 5G at Millimeter-Wave Frequencies," in *IEEE Microwave and Wireless Components Letters*, vol. 30, no. 1, pp. 31-34, Jan. 2020.
- [49] C. E. Chrisostomidis, M. Guglielmi, P. R. Young, and S. Lucyszyn, "Application of chained functions to low-cost microwave band-pass filters using standard PCB etching techniques", *European Microwave Conference Proceedings*, Paris, France, vol. 3, pp. 40-43, Oct. 2000.
- [50] S.-W. Wong, R. S. Chen, K. Wang, Z.-N. Chen, and Q.-X. Chu, "U-shape slots structure on substrate integrated waveguide for 40-GHz bandpass filter using LTCC technology," *IEEE Trans. Components, Packag. Manuf. Technol.*, vol. 5, no. 1, pp. 128–134, Jan. 2015.
- [51] A. L. Borja, A. Belenguer, H. Esteban and V. E. Boria, "design and performance of a high-Q narrow bandwidth bandpass filter in empty substrate integrated coaxial line at Ku-band," in *IEEE Microwave and Wireless Components Letters*, vol. 27, no. 11, pp. 977-979, Nov. 2017.
- [52] M. S. Sorkherizi, A. Khaleghi, and P.-S. Kildal, "Direct-coupled cavity filter in ridge gap waveguide," *IEEE Trans. Components, Packag. Manuf. Technol.*, vol. 4, no. 3, pp. 490–495, Mar. 2014.
- [53] M. S. Sorkherizi and A. A. Kishk, "Completely tuned coupled cavity filters in defected bed of nails cavity," *IEEE Trans. Components, Packag. Manuf. Technol.*, vol. 6, no. 12, pp. 1865-1872, Dec. 2016.
- [54] A. U. Zaman, P.-S. Kildal, and A. A. Kishk, "Narrow-band microwave filter using high-Q groove gap waveguide resonators with manufacturing flexibility and no sidewalls," *IEEE Trans. Components, Packag. Manuf. Technol.*, vol. 2, no. 11, pp. 1882–1889, Nov. 2012.

- [55] E. A. Alos, A. U. Zaman, and P.-S. Kildal, "Ka-band gap waveguide coupled-resonator filter for radio link diplexer application," *IEEE Trans. Components, Packag. Manuf. Technol.*, vol. 3, no. 5, pp. 870–879, Jan. 2013.
- [56] B. Ahmadi and A. Banai, "Direct coupled resonator filters realised by gap waveguide technology," *IEEE Trans. Microw. Theory Tech.*, vol. 63, no. 10, pp. 3445–3452, Aug. 2015.
- [57] B. Al-Juboori, Y. Huang, D. Klugmann, M. Hussein and J. Zhou, "Millimeter wave cross-coupled bandpass filter based on groove gap waveguide technology," *UK-Europe-China Workshop on Millimetre Waves and Terahertz Technologies (UCMMT)*, Liverpool, 2017, pp. 1-4.
- [58] A. del Olmo-Olmeda, M. Baquero-Escudero, V. E. Boria-Esbert, A. Valero-Nogueira and A. J. Berenguer-Verdú, "A novel band-pass filter topology for millimeter-wave applications based on the groove gap waveguide," *2013 IEEE MTT-S International Microwave Symposium Digest (MTT)*, Seattle, WA, 2013, pp. 1-4.
- [59] A. Berenguer, M. Baquero-Escudero, D. Sanchez-Escuderos, B. Bernardo-Clemente and V. E. Boria-Esbert, "Low insertion loss 61 GHz narrow-band filter implemented with Groove Gap Waveguides," *European Microwave Conference*, Rome, 2014, pp. 191-194.
- [60] J. Hirokawa, H. Arai, and N. Goto, "Cavity backed wide slot antenna," *Proc. Inst. Elect. Eng.*, vol. 136, no. 1, pt. H, pp. 29–33, Feb. 1989.
- [61] H. Morishita, K. Hirasawa and K. Fujimoto, "Analysis of a cavity-backed annular slot antenna with one point shorted," in *IEEE Transactions on Antennas and Propagation*, vol. 39, no. 10, pp. 1472-1478, Oct. 1991.
- [62] H. Chu, C. Jin, W. Sun, J. Chen and Y. Guo, "Substrate-Integrated Millimeter-Wave Short Backfire Antenna Excited by a Novel Quad-Slot Cavity-Back Feed," in *IEEE Transactions on Components, Packaging and Manufacturing Technology*, vol. 5, no. 11, pp. 1694-1699, Nov. 2015.
- [63] Q. Wu, J. Yin, C. Yu, H. Wang and W. Hong, "Low-Profile Millimeter-Wave SIW Cavity-Backed Dual-Band Circularly Polarised Antenna," in *IEEE Transactions on Antennas and Propagation*, vol. 65, no. 12, pp. 7310-7315, Dec. 2017.

- [64] S. Mukherjee, A. Biswas and K. V. Srivastava, "Broadband Substrate Integrated Waveguide Cavity-Backed Bow-Tie Slot Antenna," in *IEEE Antennas and Wireless Propagation Letters*, vol. 13, pp. 1152-1155, 2014.
- [65] J. Yan, F. Xu, K. Cao and J. Qian, "Planar slot antenna based on triangle substrate integrated waveguide cavity," *IEEE International Conference on Ubiquitous Wireless Broadband (ICUWB)*, Nanjing, 2016, pp. 1-3.
- [66] D. Sánchez-Escuderos, M. Ferrando-Rocher, J. I. Herranz-Herruzo and A. Valero-Nogueira, "Single-Layer Dual-Band Slot-Array Antenna in Gap Waveguide Technology," *13th European Conference on Antennas and Propagation (EuCAP)*, Krakow, Poland, 2019.
- [67] S. Ranjan Mishra, K. L. Sheeja, and N. P. Pathak, "Split ring resonator inspired microstrip filtenna for Ku-band application," *J. Eur. des Syst. Autom.*, vol. 50, nos. 4–6, pp. 391–403, Dec. 2017.
- [68] A. A. C. Alves, L. G. da Silva, E. C. V. Boas, D. H. Spadoti and A. Cerqueira S., "Mechanically Tunable Horn Filtenna for mmWaves," *13th European Conference on Antennas and Propagation (EuCAP)*, Krakow, Poland, 2019.
- [69] Z. Gao, W. Hong, R. Lu and C. Wang, "A Planar Filtenna Array Implemented by Embedding the Filtering Function into the SIW Power Divider," *International Symposium on Antennas and Propagation (ISAP)*, Xi'an, China, 2019, pp. 1-3.
- [70] K. R. Mahmoud and A. M. Montaser, "Design of Compact mmWave Tunable Filtenna Using Capacitor Loaded Trapezoid Slots in Ground Plane for 5G Router Applications," in *IEEE Access*, vol. 8, pp. 27715-27723, 2020.
- [71] S. Yu, W. Hong, C. Yu, H. Tang, J. Chen and Z. Kuai, "Integrated millimeter wave filtenna for Q-LINKPAN application," *6th European Conference on Antennas and Propagation (EUCAP)*, Prague, 2012, pp. 1333-1336.
- [72] H. Chu and Y. Guo, "A Filtering Dual-Polarised Antenna Subarray Targeting for Base Stations in Millimeter-Wave 5G Wireless Communications," in *IEEE Transactions on Components, Packaging and Manufacturing Technology*, vol. 7, no. 6, pp. 964-973, June 2017.
- [73] H. Tang, C. Tong, J. Chen, C. Shao, W. Qin and W. Yang, "Differentially SIW TE₂₀-Mode Fed Substrate Integrated Filtering Dielectric Resonator Antenna for

- 5G Millimeter Wave Application," *IEEE International Conference on Computational Electromagnetics (ICCEM)*, Shanghai, China, 2019, pp. 1-3.
- [74] H. Jin, G. Q. Luo, W. Wang, W. Che and K. Chin, "Integration Design of Millimeter-Wave Filtering Patch Antenna Array With SIW Four-Way Anti-Phase Filtering Power Divider," in *IEEE Access*, vol. 7, pp. 49804-49812, 2019.
- [75] X. Liu, H. Wang, S. Quan, X. Jiang, W. Xu and D. Xu, "Design of a W band filter antenna array with low sidelobe level using gap waveguide," *11th International Symposium on Antennas, Propagation and EM Theory (ISAPE)*, Guilin, 2016, pp. 132-134.
- [76] H. S. Farahani and W. Bösch, "A Novel Compact High-Gain Filtenna Using Gap Waveguide Technology," *IEEE International Symposium on Antennas and Propagation and USNC-URSI Radio Science Meeting*, Atlanta, GA, USA, 2019, pp. 2043-2044.
- [77] H. Oraizi, M. Hamedani, D. Zarifi and A. Amini, "Design of filter-horn antenna based on groove gap waveguide technology for V-band application," *12th European Conference on Antennas and Propagation (EuCAP 2018)*, London, 2018, pp. 1-4.
- [78] R. E. Amaya, A. Momciu, and I. Haroun, "High-performance, compact quasi-elliptic band pass filters for V-band high data rate radios," *IEEE Trans. Components, Packag. Manuf. Technol.*, vol. 3, no. 3, pp. 411–416, Mar. 2013.
- [79] Q. Guo, X. Y. Zhang, L. Gao, Y. C. Li and J. Chen, "Microwave and Millimeter-Wave LTCC Filters Using Discriminating Coupling for Mode Suppression," *IEEE Transactions on Components, Packaging and Manufacturing Technology*, vol. 6, no. 2, pp. 272-281, Feb. 2016.
- [80] S. W. Wong, K. Wang, Z.-N. Chen, and Q.-X. Chu, "Electric coupling structure of substrate integrated waveguide (SIW) for the application of 140-GHz bandpass filter on LTCC," *IEEE Trans. Components, Packag. Manuf. Technol.*, vol. 4, no. 2, pp. 316–322, Feb. 2014.
- [81] K. Wang, S.-W. Wong, G.-H. Sun, Z. N. Chen, L. Zhu and Q.-X. Chu, "Synthesis method for substrate-integrated waveguide bandpass filter with even-order Chebyshev response," *IEEE Trans. Components, Packag. Manuf. Technol.*, vol. 6, no. 1, pp. 126-135, Jan. 2016.

- [82] Y. Li, L.-A. Yang, L. Du, K. Zhang, and Y. Hao, "Design of millimeter-wave resonant cavity and filter using 3-D substrate-integrated circular waveguide," *IEEE Microw. Wirel. Components Lett.*, vol. 27, no. 8, pp. 706–708, Aug. 2017.
- [83] X. Shang, H. Yang, D. Glynn, and M. J. Lancaster, "Submillimeter-wave waveguide filters fabricated by SU-8 process and laser micromachining," *IET Microwaves, Antennas Propag. Spec.*, vol. 11, no. 14, pp. 2027–2034, Dec. 2017.
- [84] O. Sushko, M. Pigeon, R. S. Donnan, T. Kreouzis, C. G. Parini and R. Dubrovka, "Comparative study of sub-THz FSS filters fabricated by inkjet printing, microprecision material printing, and photolithography," *IEEE Trans. on Terahertz Science and Technology*, vol. 7, no. 2, pp. 184-190, Mar. 2017.
- [85] Y.-S. He, A. Barannik, N. Cherpak, L. Sun, V. Skresanov, Y. Bian, J. Wang, M. Natarov, and V. Zolotaryov, "Novel design of band-pass waveguide filter with HTS E-plane insert," *IEEE Trans. Appl. Supercond.*, vol. 27, no. 4, pp. 4–7, Jun. 2017.
- [86] C. Arnold, J. Parlebas, and T. Zwickber, "Reconfigurable waveguide filter with variable bandwidth and center frequency," *IEEE Trans. Microw. Theory Tech.*, vol. 62, no. 8, pp. 1663–1670, Aug. 2014.
- [87] D. Sun and J. Xu, "A novel iris waveguide bandpass filter using air gapped waveguide technology," *IEEE Microwave and Wireless Components Letters*, vol. 26, no. 7, pp. 475-477, Jul. 2016.
- [88] W. J. Otter and S. Lucyszyn, "3-D printing of microwave components for 21st century applications," *IEEE MTT-S International Microwave Workshop Series on Advanced Materials and Processes for RF and THz Applications (IMWS-AMP)*, Chengdu, 2016.
- [89] Z. Bing, Y.-X. Guo, H. Zirath, and Y. P. Zhang, "Investigation on 3-D-printing technologies for millimeter-wave and terahertz applications," *Proc. IEEE*, vol. 105, no. 4, pp. 723–736, Apr. 2017.
- [90] M. D'Auria, W. J. Otter, J. Hazell, B. T. W. Gillatt, C. Long-Collins, N. M. Ridler, and S. Lucyszyn, "3-D printed metal-pipe rectangular waveguides," *IEEE Trans. Components, Packag. Manuf. Technol.*, vol. 5, no. 9, pp. 1339-1349, Sep. 2015.

- [91] W. J. Otter, N. M. Ridler, H. Yasukochi, K. Soeda, K. Konishi, J. Yumoto, M. Kuwata-Gonokami and S. Lucyszyn, "3D printed 1.1 THz waveguides," *IET Electronics Letters*, vol. 53, no. 7, pp. 471-473, Mar. 2017.
- [92] B. Zhang and H. Zirath, "Metallic 3-D printed rectangular waveguides for millimeter-wave applications," *IEEE Trans. Components, Packag. Manuf. Technol.*, vol. 6, no. 5, pp. 796-804, May 2016.
- [93] W. J. Otter and S. Lucyszyn, "Hybrid 3-D-printing technology for tunable THz applications," *Proc. IEEE*, vol. 105, no. 4, pp. 756–767, Apr. 2017.
- [94] A. Tamayo-Domínguez, J. Fernández-González and M. Sierra-Pérez, "Groove gap waveguide in 3-D printed technology for low loss, weight, and cost distribution networks," in *IEEE Transactions on Microwave Theory and Techniques*, vol. 65, no. 11, pp. 4138-4147, Nov. 2017.
- [95] Ereš, Zoran; Vukomanović, Mladen; Šipuš, Zvonimir, "Gap waveguide leaky wave antenna realised in 3D printing technology," *22nd International Conference on Applied Electromagnetics and Communications (ICECom)*, Zagreb, 2016.

Chapter 3. Filters and Filtering Antennas

Network Theory

3.1. Introduction

Filters are vital components in almost every RF/microwave communications system. The theory of filter design was first introduced and developed during the 1930s to the 1950s. In 1960, filter functions were mathematically generated [1]. In this chapter, a brief introduction to filter definition and types in terms of attenuation characteristics, amplitude responses, bandwidth and design technology is provided. Then, filter design theory and formulas along with an example showing the design procedure are presented. Also, the design formulae of a rectangular cavity resonator and a filtering antenna are provided.

3.2. Filter Network

A Filter is a two-port frequency-selective device to attenuate signals of the undesired frequency range (stop-band) while allowing desired ones (pass-band) to pass from a port to another. Filters can be classified according to the following parameters:

A- Frequency selection (attenuation characteristics):

- Low-pass Filter: Low insertion loss below a specified cut-off frequency.
- High-pass Filter: Low insertion loss above a specified cut-off frequency.
- Band-pass Filter: Low insertion loss across a specified frequency band.
- Band-stop Filter: High insertion loss across a specified frequency band.

B- Amplitude response (the location of the poles and zeros of the transmission function):

- Equal-ripple passband amplitude response: Chebyshev.
- Maximally-flat passband amplitude response: Butterworth.
- Elliptic, Quasi-Elliptic, Bessel, Linear Phase, etc.

C- Technology: Lumped, planar, waveguide, etc.

D- Frequency bandwidth: Narrowband and broadband.

As mentioned above, filters can be classified according to the technology that utilised to build. A lumped element-based filter circuit is formed of capacitors, inductors and resistors. The simplest method to attenuate a signal quickly is by increasing the number of lumped elements in a periodic topology or a circuit leading to a higher-order (N). The ladder topology is the most commonly used for periodic topology in filter design [2]. Fig. 3.1. depicts the schematic of a general two-port filter network that is driven by a voltage source (e_s) with the internal impedance (Z_s) and terminated by the load impedance (Z_L).

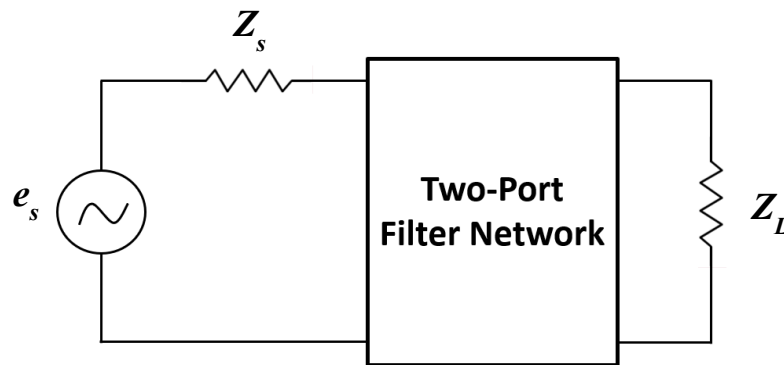


Fig. 3.1. A two-port filter network.

3.2.1. Filter Design by the Insertion Loss Method

In this section, a filter design procedure based on the insertion loss method is introduced [3]. In the insertion loss method, a filter response is defined by its insertion loss IL , or power loss ratio, P_{LR} :

$$P_{LR} = \frac{\text{Power available from source}}{\text{Power delivered to load}}$$

$$IL = 10 \log P_{LR}$$

Many general filter specifications can be obtained, but *maximally flat*, *equal ripple*, *elliptic function* and *linear phase* responses are the most common.

In the following sections, after defining the filter specifications, a design of low-pass filter prototypes that are normalised in terms of impedance and frequency is demonstrated. The normalisation simplifies the design of filters for arbitrary frequency, impedance and filter type (low-pass, high-pass, bandpass, or bandstop). The low-pass filter prototypes are then scaled to the desired frequency and impedance. The final step is replacing the lumped-elements with distributed circuit elements for implementation at microwave frequencies. This design process is illustrated in Fig. 3.2.

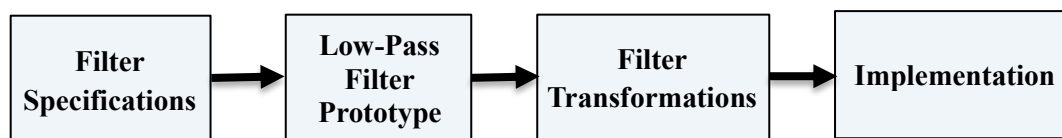


Fig. 3.2. The process of filter design by the insertion loss method

A- Filter specifications

Before starting the design of any RF or microwave filter, the factors that drive the hardware design should be mentioned. These factors are the filter specifications. Some of these specifications are filter type, frequency response type, desired frequency of operation, passband & stopband frequency range and maximum allowed attenuation. More details of this part can be found in this chapter and Chapter 4.

B- Low-Pass Filter Prototype

The low-pass filter prototypes are lumped elements networks that have been synthesised to obtain a transfer function of the desired filter. The elements of the low-pass filter prototype are capacitors and inductors of the ladder networks, which are known as *g*-values, as shown in Fig. 3.3. In a low-pass filter prototype, the order of the filter is equal to the number of reactive elements. To manifest flexibility, ease of use and tabulation, the component values of the low-pass filter prototype have been

normalised having a source impedance of $R_o = 1$ and a cut-off frequency of $\Omega_c = 1$ rad/sec [3]. To calculate the values of the lumped elements of a low-pass filter prototype, it is important to know the filter response function (Butterworth, Chebyshev, Equal-Ripple, etc.) and the filter order (the number of filter resonators).

To design a filter based on its coupling matrix, the filter specifications should be specified first. Then, a low-pass filter prototype of a specific response, e.g. Chebyshev, is considered. For Chebyshev low-pass filter prototype with a passband ripple L_{Ar} dB and the cut-off frequency $\Omega_c=1$, the g values for the two-port prototype networks, shown in Fig. 3.3. , can be calculated using the following formulae [2], [3]:

$$g_o = 1,$$

$$g_1 = \frac{2}{\gamma} \sin\left(\frac{\pi}{2N}\right), \quad (3.1a)$$

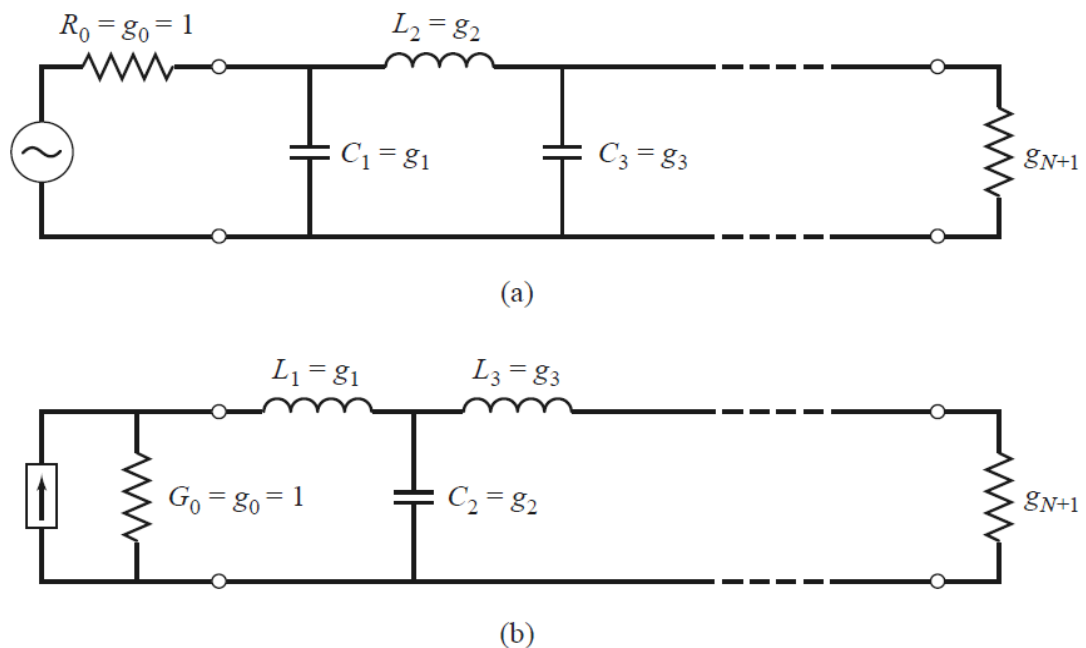


Fig. 3.3. Ladder circuits of Lumped elements for low-pass filter prototypes and their element definitions. (a) Prototype beginning with a shunt element. (b) Prototype beginning with a series element.

$$g_i = \frac{1}{g_{i-1}} \frac{4 \sin\left[\frac{(2i-1)\pi}{2N}\right] \cdot \sin\left[\frac{(2i-3)\pi}{2N}\right]}{\gamma^2 + \sin^2\left[\frac{(i-1)\pi}{N}\right]} \quad \text{for } i = 2, 3, \dots, N \quad (3.1b)$$

$$g_{n+1} = \begin{cases} 1 & \text{for } N \text{ odd} \\ \coth^2\left(\frac{\beta}{4}\right) & \text{for } N \text{ even} \end{cases} \quad (3.1c)$$

where

$$\beta = \ln \left[\coth \left(\frac{L_{Ar}}{17.37} \right) \right]$$

$$\gamma = \sinh \left(\frac{\beta}{2N} \right)$$

C- Frequency and Elements Transformations (or Scaling)

In the previous section, the low-pass filter prototype was established and the values of its lumped elements were computed based on a normalised design having a source impedance of $g_o = 1$ ohm and a cut-off frequency of $\Omega_c = 1$ rad/sec. Here, this design can be scaled in terms of impedance and frequency, and converted to give high-pass, bandpass or bandstop characteristics.

Frequency Scaling

Since all the filters designed in this thesis are bandpass filters, so the transformation procedure of a bandpass response is mentioned here. Let us assume that ω_1 and ω_2 refer to the lower and upper angular frequencies of the passband, respectively. Then a bandpass response can be obtained using the following frequency substitution:

$$\Omega = \frac{\Omega_c}{FBW} \left(\frac{\omega}{\omega_o} - \frac{\omega_o}{\omega} \right) \quad (3.2a)$$

$$FBW = \frac{\omega_2 - \omega_1}{\omega_o} \quad (3.2b)$$

$$\omega_o = \sqrt{\omega_1 \omega_2} \quad (3.2c)$$

where Ω is the low-pass prototype frequency, Ω_c is the low-pass prototype normalised cut-off frequency ($\Omega_c = 1$), ω is the practical filter angular frequency, ω_0 denotes the centre angular frequency and FBW is defined as the fractional bandwidth. A summary of prototype filter frequency transformations for different types of filters is illustrated in Table 3.1.

Impedance Scaling

In the low-pass filter prototype design, the source and load resistances are unity (except for equal-ripple filters with an even number of resonators, which have non-unity load resistance). If we denote all the scaled quantities with a prime, the new filter component values can be obtained by multiplying all the components of the low-pass prototype filter in Fig. 3.3. by the practical design impedance R_{pr} [3]

$$R'_o = R_o R_{pr}$$

$$C'_1 = \frac{C_1}{R_{pr}}$$

$$L'_2 = L_2 R_{pr}$$


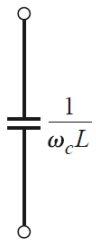
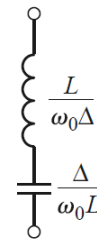
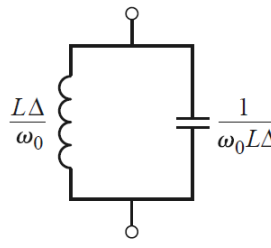

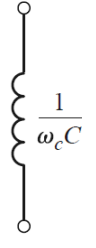
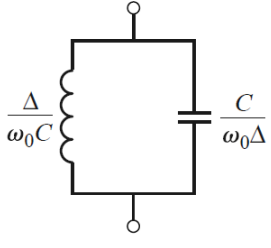
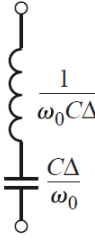
$$C'_3 = \frac{C_3}{R_{pr}}$$

$$g'_{N+1} = g_{n+1} R_{pr}$$

(3.3)

where R_o , C_1 , L_2 and C_3 are the component values for the original prototype.

Table 3.1. Summary of Prototype Filter Frequency Transformations (Δ =FBW) [3].

Low-pass	High-pass	Bandpass	Bandstop
			
			

D- Filter Implementation

The prototype filter designed above generally works well at low frequencies. At higher RF and microwave frequencies, two problems arise. First is the limitation of the lumped-element (inductors and capacitors), where they are available for a limited range of values suitable for low frequencies. They can be replaced by their approximation of distributed elements, open-circuited or short-circuited transmission line stubs. The second is that at microwave frequencies the spaces between filter elements cannot be neglected. These issues can be tackled by different approaches. One of these approaches is using Richards' transformation, which can be used to convert lumped elements to transmission line sections. Then, Kuroda's identities can be used to physically separate filter elements by using transmission line sections. Another approach is using impedance (K) and admittance (J) Inverters. Such inverters are especially useful for bandpass or bandstop filters with narrow ($<10\%$) bandwidths.

3.2.2. Bandpass Filter Design Example

In this section, a bandpass filter design example using the insertion loss method is presented. The filter specifications are shown in Table 3.2. First, the filter order $N = 5$

is estimated by using the graphs and equations in [3]. Second, a 5th-order low-pass filter prototype with its g -values is chosen. The g -values of the 5th-order Chebyshev low-pass filter prototype with a passband equal ripple of 0.1 dB for a normalised low-pass cut-off frequency $\Omega_c = 1$ are obtained by using (3.1) to be: $g_0 = g_6 = 1.0$, $g_1 = g_5 = 1.1468$, $g_2 = g_4 = 1.3712$ and $g_3 = 1.9750$. Then, the frequency and impedance scaling of the lumped elements of the prototype is done using (3.2) and (3.3), respectively. The scaled lumped elements of the BPF are:

$$R'_o = R_{pr} R_o = 50 \text{ ohms}$$

$$C'_1 = C'_5 = \frac{C_1}{\omega_o FBW R_{pr}} = 5.2148 \text{ pF}$$

$$L'_1 = L'_5 = \frac{FBW R_{pr}}{\omega_o C_1} = 3.8219 \text{ pH}$$

$$C'_2 = C'_4 = \frac{FBW}{\omega_o L_2 R_{pr}} = 1.2785 \text{ fF}$$

$$L'_2 = L'_4 = \frac{L_2 R_{pr}}{\omega_o FBW} = 15.588 \text{ nH}$$

$$C'_3 = \frac{C_3}{\omega_o FBW R_{pr}} = 8.9809 \text{ pF}$$

$$L'_1 = \frac{FBW R_{pr}}{\omega_o C_3} = 2.2192 \text{ pH}$$

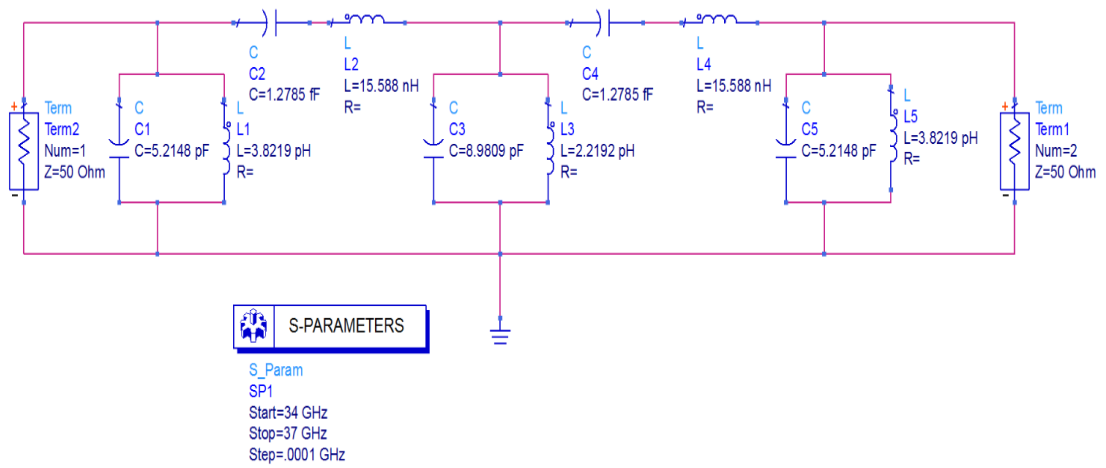
The proposed bandpass filter is firstly simulated using an ideal lumped-element circuit and using a transmission line schematic. The simulations were conducted using two computer-aided design (CAD) packages, Advanced Design System (ADS) 2011.10 and Sonnet 14.54. Fig. 3.4. shows the schematic lumped-element circuit of the designed 5th-order Chebyshev BPF with its S-parameters.

Table 3.2. Bandpass Filter Specifications.

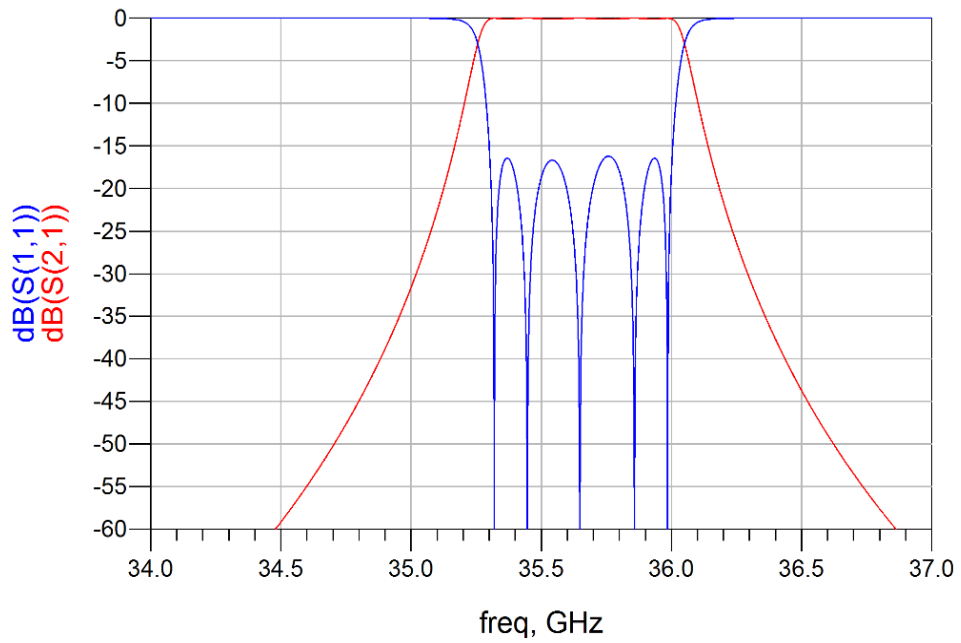
Parameter	Value
Frequency response	Chebyshev (equal ripple 0.1 dB)
Centre frequency (GHz)	35.6
Fractional bandwidth (<i>FBW</i>) (%)	2
Insertion loss (dB)	< 1
Return loss (dB)	≥ 16
Lower/upper rejection (dB)	50
Terminated impedance (ohms)	50

At high frequency, lumped-element circuits exhibit inaccuracy because the wavelength becomes comparable to the physical dimensions of the circuit. Therefore, for better performance, distributed elements have been used to represent the circuit components at high frequencies. The bandpass filter based on lumped elements circuit, shown in Fig. 3.4. , has been converted into its equivalent distributed elements model as shown in Fig. 3.5. The distributed elements have been implemented based on the filter specifications and by using Line Calculator tool (LineCalc) in the ADS package, so as to calculate the dimensions of transmission line resonators.

Based on series microstrip line end-coupled resonators, the designed BPF has been simulated. The S-parameters of simulated results are shown in Fig. 3.6. It can be noticed that there is an improvement of about 6 dB in the simulated reflection coefficient S_{11} between -14 dB in Fig. 3.6. (before optimisation) and -20 dB in Fig. 3.6. (after optimisation).



(a)



(b)

Fig. 3.4. A 5th-order Chebyshev BPF with a passband equal ripple of 0.1 dB. (a) The scaled lumped elements of the BPF schematic. (b) The filter S-parameters.

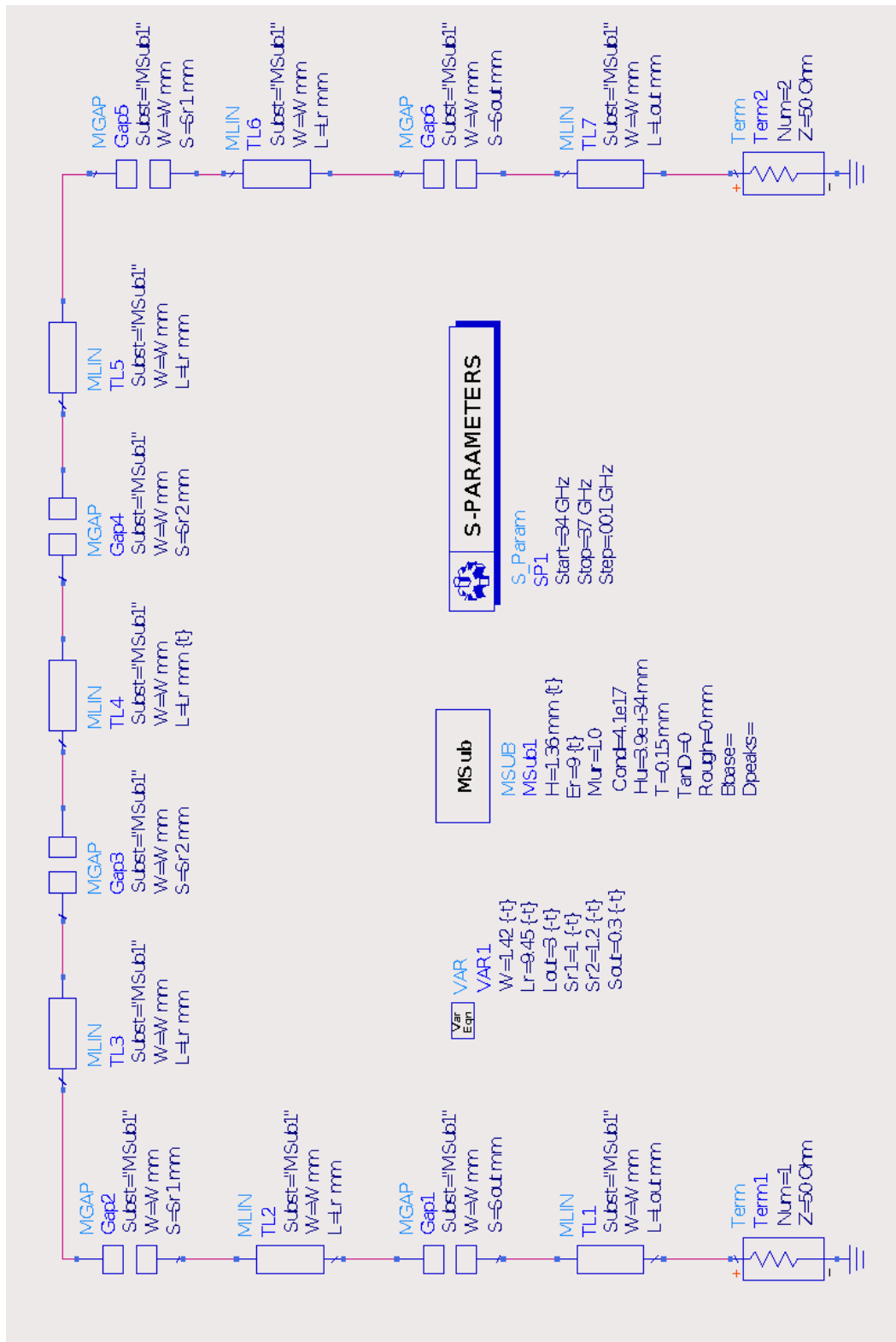


Fig. 3.5. ADS schematic diagram of a 5-pole Chebyshev BPF.

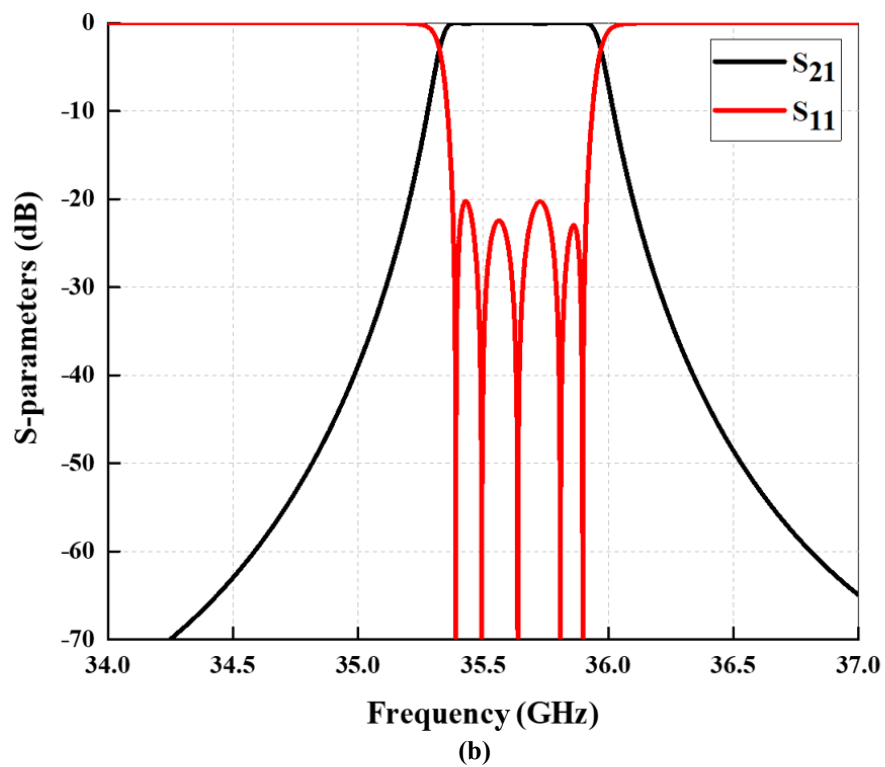
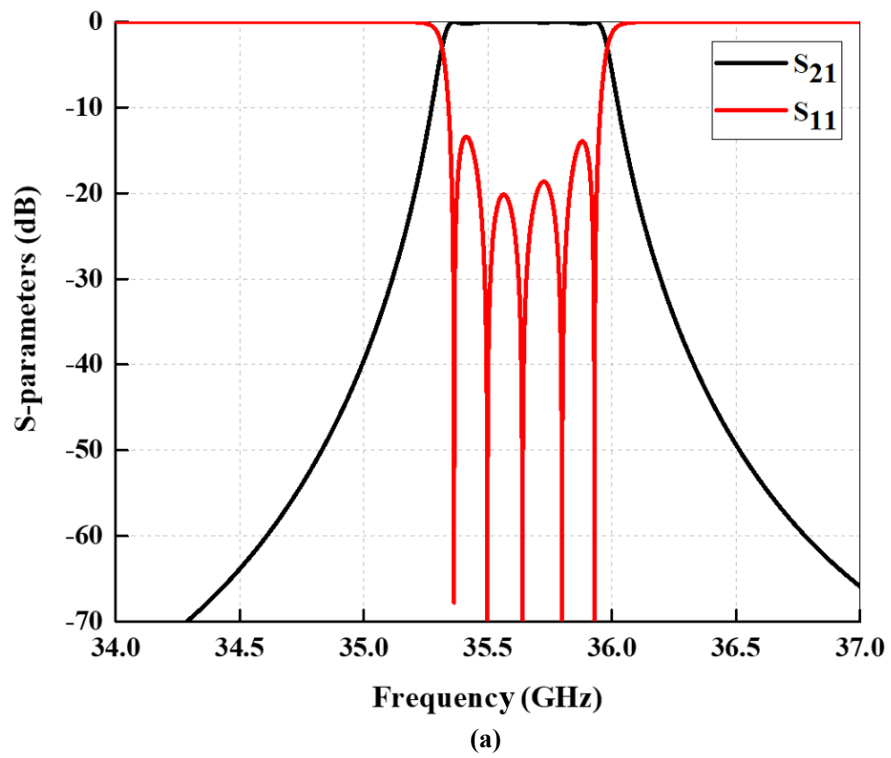


Fig. 3.6. Simulated S-parameters of a 5-pole Chebyshev BPF. (a) Before optimisation. (b) After optimisation.

3.2.3. Coupling Matrix Synthesis

Coupling matrix is a scheme used normally in microwave filters for the coupled structure analysis. Reconfiguring the circuit configuration and synthesis of the circuit are simplified by such matrix operations [4]. The coupling matrix theory is mainly suitable for narrow-band filtering circuits, as the theory is based on the narrow bandwidth assumption. The indices of a coupling matrix of a filter are the design parameters of that filter. These parameters are the coupling coefficients between the filter resonators and the external quality factors with the source and load of the filter. Based on the procedure/steps of filter design by the insertion loss method, the coupling coefficients and the external quality factors can be easily calculated.

To design a filter based on a coupling matrix, the filter specifications should be specified first. Then, a low-pass filter prototype of a specific response, e.g. Chebyshev, is considered. For Chebyshev low-pass filter prototype with a passband ripple L_{Ar} dB and the cut-off frequency $\Omega_c=1$, the g -values for the two-port networks shown in Fig. 3.3. can be calculated using the formulae in [2], [3]. After obtaining the g -values, the coupling coefficients $K_{i,i+1}$ and the external quality factors Q_{ex} can be obtained as follows:

$$K_{i,i+1} = \frac{FBW}{\sqrt{g_i g_{i+1}}}, \quad i = 1, \dots, N - 1 \quad (3.4a)$$

$$Q_{ex1} = \frac{g_0 g_1}{FBW} \quad (3.4b)$$

$$Q_{exN} = \frac{g_N g_{N+1}}{FBW} \quad (3.4c)$$

Then, the coupling coefficients can be arranged in a coupling matrix according to the desired configuration of the filter as follows:

$$k = \begin{bmatrix} k_{11} & k_{12} & \cdots & k_{1N} \\ k_{21} & k_{22} & \cdots & k_{2N} \\ \vdots & \vdots & \ddots & \vdots \\ k_{N1} & k_{N2} & \cdots & k_{NN} \end{bmatrix} \quad (3.5)$$

Accordingly, the S-parameters can be found as follows:

$$S_{21} = 2 \frac{1}{\sqrt{q_{ex1} \cdot q_{exn}}} [A]_{n1}^{-1} \quad (3.6a)$$

$$S_{11} = \pm \left(1 - \frac{2}{q_{ex1}} [A]_{11}^{-1} \right) \quad (3.6b)$$

with

$$[A] = [q] + p[U] - j[k] \quad (3.6c)$$

where $[U]$ is the $n \times n$ (n is a filter order) unit or identity matrix, $[q]$ is an $n \times n$ matrix with all entries zero, except for $q_{11} = 1/q_{ex1}$ and $q_{nn} = 1/q_{exn}$, and $[k]$ is the so-called general coupling matrix, which is an $n \times n$ reciprocal matrix (that is, $k_{ij} = k_{ji}$) and is allowed to have nonzero diagonal entries k_{ii} for an asynchronously tuned filter. In the next chapter, a mmWave BPF based on gap waveguide technology using coupling matrix theory will be designed.

3.2.4. Resonators Coupling

Generally, the coupling between resonators can be realised in different manners. According to the physical structure of the couplings, they can be classified into three types: electric coupling, magnetic coupling and mix coupling. On the other hand, based on the sequence digit of resonators, there are two main types of couplings: direct-coupling and cross-coupling.

A- Self-Coupled Resonators

In general, all the entries in a coupling matrix K are nonzero. The entries on the main diagonal are named self-couplings. The self-coupling coefficient K_{ii} is related to the self-resonant frequency of the resonator i in a filter. For the case of asynchronous tuning, K_{ii} can be defined by

$$K_{ii} = 2 \left(\frac{f_{0i}^2 - f_0^2}{f_{0i}^2 + f_0^2} \right) \quad (3.7)$$

Where f_{0i} is the resonant frequency of the resonator i and f_0 is the desired centre frequency.

B- Direct-Coupled Resonators

Direct-coupling or in-line coupling can be produced by making a coupling between any two sequentially numbered (adjacent) resonators. In Fig. 3.7. , the solid lines represent the direct-coupling between the resonators. Many filters have been designed based on this type of coupling [5]-[7]. The response of filters designed based on this configuration, as discussed in the previous sections, has a skirt flatter than that designed based on cross-coupled resonators, due to the absence of transmission zeros, as will be discussed later.

C- Cross-Coupled Resonators and Transmission Zeros

Many wireless communications require RF bandpass filters with high selectivity. To improve the selectivity of a filter, the rejection below and/or above the passband needs to be improved by adding transmission zeros below and/or above the filter passband. To do so, usually, two methods are adopted. The first approach is by using shunt resonators at the beginning and end of the designed filter [8]. This approach is not preferable because the size may, however, be large. The second approach is by introducing a cross-coupling between a pair of non-sequentially numbered (non-contiguous) resonators [9]. Generally, filters that use the cross-coupling result in a compact structure, and hence, they become more attractive especially for those systems where size is important. Using the cross-coupling technique to generate transmission zero reduces the number of resonating elements needed and this, in turn, reduces the insertion loss, component size and manufacturing cost, albeit at the expense of topology.

To achieve high selectivity in filters, the most common methods are either increase the number of resonators which leads to higher loss and larger size, or using the cross-coupling technique to generate transmission zero. In this work, cross-coupling will be employed. This type of coupling needs to be applied between non-contiguous resonators as depicted in Fig. 3.7. Many configurations or topologies can be adopted to introduce a cross-coupling between its resonators. In Fig. 3.8. , 4th-order and 6th-order BPF are chosen to show the resonators configuration of filters with a cross-coupling.

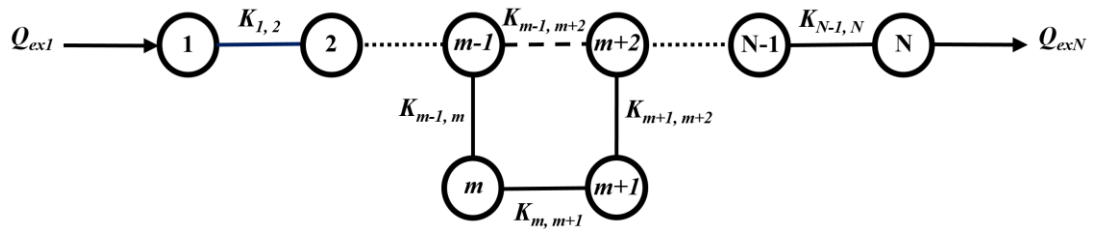


Fig. 3.7. General coupling structure of the bandpass filters with a single pair of attenuation poles at finite frequencies. Each circle represents a resonator, the solid lines represent a direct-coupling between the resonators, the dashed line refers to a cross-coupling and the dotted lines mean that there is a number of resonators in between. $m = N/2$.

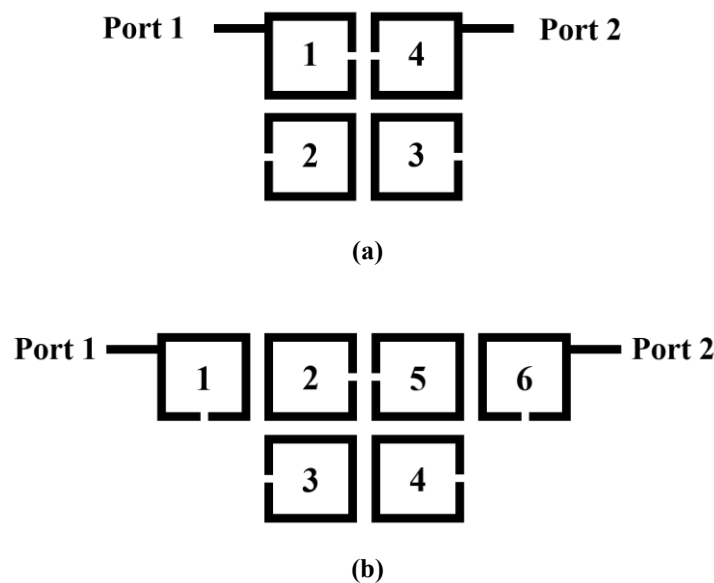


Fig. 3.8. Configurations of (a) 4th-order and (b) 6th-order bandpass filter exhibiting a single pair of transmission zeros at finite frequencies.

The external quality factors and coupling coefficients of the cross-coupled bandpass filters, similar to that in Fig. 3.7. can be obtained in terms of circuit elements of a low-pass prototype filter shown in Fig. 3.9. which consists of lumped capacitors and ideal admittance inverters. Based on the low-pass filter elements the filter's design parameters can be calculated as follows:

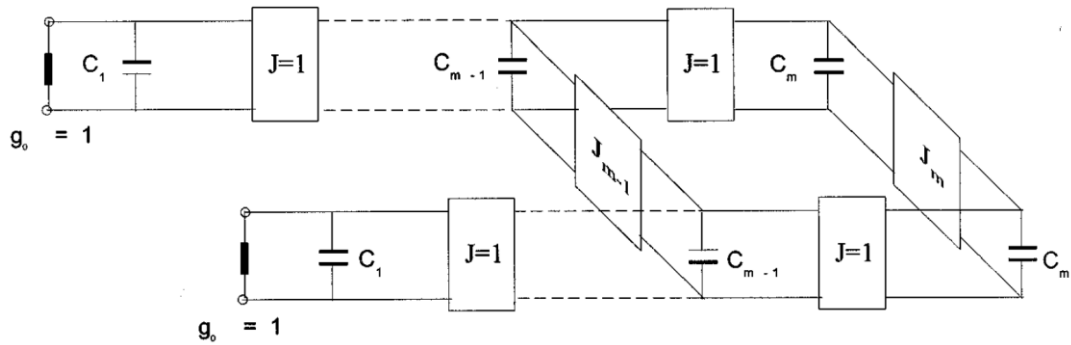


Fig. 3.9. A low-pass filter prototype (starting with a shunt capacitor) for a cross-coupled bandpass filter.

$$Q_{ex1} = Q_{exN} = \frac{C_1}{FBW} \quad (3.8a)$$

$$K_{i,i+1} = K_{N-i,N-i+1} = \frac{FBW}{\sqrt{C_i C_{i+1}}}, \quad i = 1, \dots, N/2 \quad (3.8b)$$

$$K_{m,m+1} = \frac{FBW \cdot J_m}{C_m}, \quad m = N/2 \quad (3.8c)$$

$$K_{m-1,m+2} = \frac{FBW \cdot J_{m-1}}{C_{m-1}}, \quad m = N/2 \quad (3.8d)$$

where C_s are the capacitances of the lumped capacitors, J_s are the characteristic admittances of the inverters, and again N is the order of the filter. The values of the C_s and J_s can be extracted from the design formulae in [9], see Appendix A.

It is worth mentioning that the sign of coupling may only be a matter for cross-coupled resonator filters. The positive or negative sign of coupling is relative, which means

that if we may refer to one particular coupling as a positive coupling then the negative coupling would imply that its phase response is opposite to that of the positive coupling [2]. Therefore, the signs for the coupling coefficients $K_{m,m+1}$ and $K_{m-1,m+2}$ in (3.8c) and (3.8d) are relative; it does not matter which one is positive or negative as long as their signs are opposite.

3.3. Waveguide Cavity Resonator

As stated in Chapter 2, a groove gap waveguide structure is equivalent to a conventional rectangular waveguide and consequently supports the propagation of TE/TM modes. Therefore, the analysis of a waveguide cavity resonator can be applied for a groove gap waveguide cavity resonator. The geometry of a rectangular cavity is shown in Fig. 3.10. The transverse electric fields (E_x , E_y) of the TE_{mn} or TM_{mn} rectangular waveguide mode can be written as [3]

$$\bar{E}_t(x, y, z) = \bar{e}(x, y)(A^+ e^{-j\beta_{mn}z} + A^- e^{j\beta_{mn}z}) \quad (3.9)$$

where $\bar{e}(x, y)$ is the transverse variation of the mode, and A^+ , A^- are arbitrary amplitudes of the forward and backward travelling waves. The propagation constant β of the m , n^{th} TE or TM mode is

$$\beta_{mn} = \sqrt{k^2 - \left(\frac{m\pi}{a}\right)^2 - \left(\frac{n\pi}{b}\right)^2} \quad (3.10)$$

where $k = \omega\sqrt{\mu\epsilon}$, and μ and ϵ are the permeability and permittivity of the material filling the cavity, respectively.

Applying the condition that $\bar{E}_t = 0$ at $z = 0$ to eq. (3.9) implies that $A^+ = -A^-$ (as we should expect for reflection from a perfectly conducting wall). Then the condition that $\bar{E}_t = 0$ at $z = d$ leads to the equation

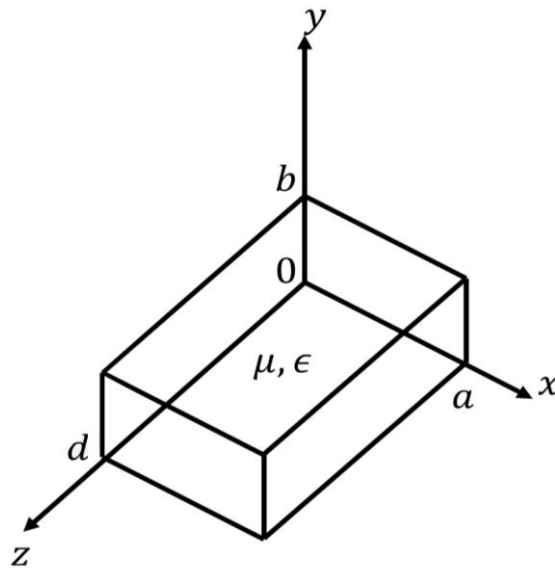


Fig. 3.10. A rectangular cavity resonator.

$$\bar{E}_t(x, y, d) = -\bar{e}(x, y)A^+ 2j \sin \beta_{mn}d = 0 \quad (3.11)$$

The only nontrivial ($A^+ \neq 0$) solution occurs for $\beta_{mn}d = \ell\pi$, $\ell = 1, 2, 3, \dots$, which implies that the cavity must be an integer multiple of a half-guide wavelength (λ_g) long at the resonant frequency. No nontrivial solutions are possible for other lengths, or for frequencies other than the resonant frequencies. A resonance wave number for the rectangular cavity can be defined as

$$k_{mn\ell} = \sqrt{\left(\frac{m\pi}{a}\right)^2 + \left(\frac{n\pi}{b}\right)^2 + \left(\frac{\ell\pi}{d}\right)^2} \quad (3.12)$$

Then we can refer to the $TE_{mn\ell}$ or $TM_{mn\ell}$ resonant mode of the cavity, where the indices m, n, ℓ indicate the number of variations in the standing wave pattern in the x, y, z directions, respectively. The resonant frequency of the $TE_{mn\ell}$ or $TM_{mn\ell}$ mode is given by

$$f_{mnl} = \frac{ck_{mnl}}{2\pi\sqrt{\mu_r\epsilon_r}} = \frac{c}{2\pi\sqrt{\mu_r\epsilon_r}} \sqrt{\left(\frac{m\pi}{a}\right)^2 + \left(\frac{n\pi}{b}\right)^2 + \left(\frac{\ell\pi}{d}\right)^2} \quad (3.13)$$

if $b < a < d$, the dominant resonant mode (lowest resonant frequency) will be the TE₁₀₁ mode, corresponding to the TE₁₀ dominant waveguide mode in a shorted guide of length $\lambda_g/2$.

$$\lambda_g = \frac{\lambda_0}{\sqrt{1 - (\lambda_0/\lambda_c)^2}} \quad (3.14)$$

where $\lambda_0 = c/f$ is the free-space wavelength, f is frequency in (Hz) and λ_c is the cut-off wavelength

$$\lambda_c = \frac{2}{\sqrt{(m/a)^2 + (n/b)^2}} \quad (3.15)$$

3.4. Antenna Theory

3.4.1. Overview of Antennas

An antenna is a key passive device used for transmitting and/or receiving radio frequency signals used in wireless communication links. In a transmitter, the antenna radiates the electromagnetic wave into the free-space. Whereas in a receiver, it receives the electromagnetic wave from the space and sends it into the receiver system. The performance of antennas can be described in terms of reflection coefficient, bandwidth, gain, radiation patterns, directivity and efficiency. A typical radiation pattern of an antenna is illustrated in Fig. 3.11. The lobes of the radiation pattern are classified into: main, side, minor and back lobes [10].

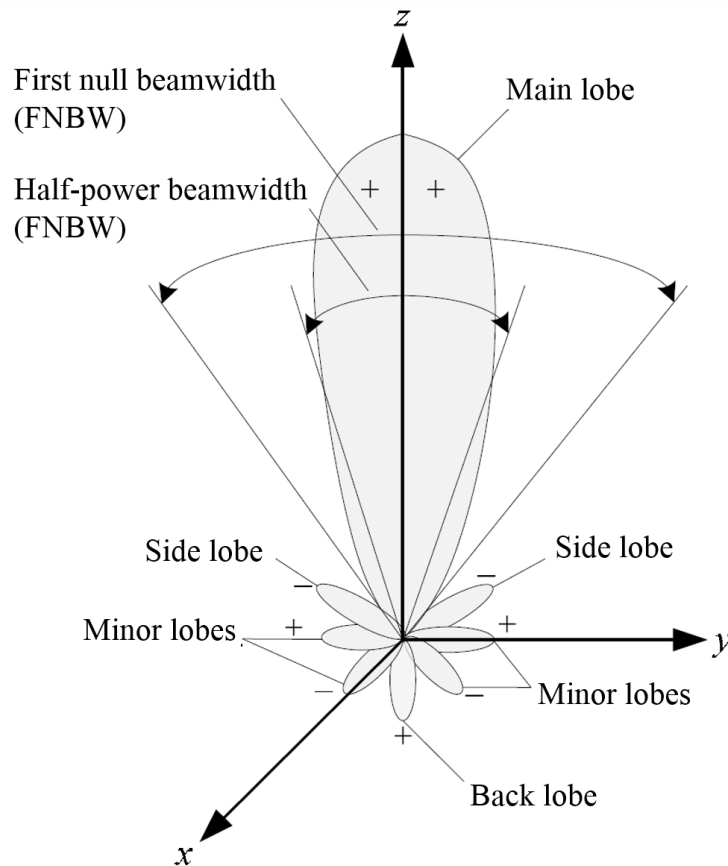


Fig. 3.11. Three-dimensional radiation pattern of an antenna [10].

3.4.2. Filtering Antenna

The antenna and the bandpass filter are key components in any RF front end. They are conventionally designed separately and connected using a matching network. The filter is usually positioned after the antenna to reject spurious signals received by the antenna. To minimise size and expense of circuits, it is highly recommended to combine the bandpass filter and the antenna into a single device that simultaneously performs both filtering and radiating functions. Such a device eliminates the need for pre-filtering stage in the receiver and improves noise performance. Comparing to a conventional antenna, the frequency response of the filtering antenna is anticipated to be highly selective (steep roll-off) at the edges of the passband due to the filter functionality.

Recently, the concept of filtering antenna has been proposed by integrating a bandpass filter and an antenna into a single component with filtering and radiating functions simultaneously to reduce the size and loss [11] - [21]. Different techniques have been used to design such a component, for example, planar technology [11], [12], SIW [13] - [16], conventional waveguide [17], [18] and gap waveguide [19]- [21].

Fig. 3.10. Fig. 3.12. shows a typical N^{th} -order filtering antenna (BPF + antenna) equivalent circuit. This model consists of a set of resonators representing a BPF operating at a specific frequency followed by a final resonator that acts as an antenna that resonates at the same resonant frequency as the BPF resonators. Filtering antenna design is based on the filter synthesis approach, which uses an antenna radiator as the last resonator of the filter. With the help of filter specifications, all the parameters of the filtering antenna equivalent lumped circuit model, shown in Fig. 3.12. , can be calculated [2]

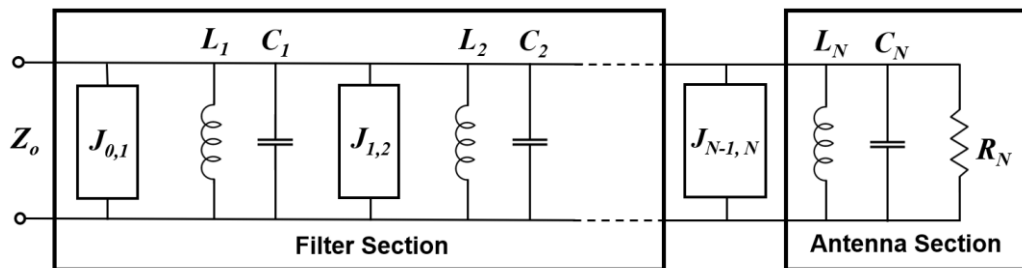


Fig. 3.12. Equivalent circuit of a typical N^{th} -order filtering antenna (bandpass filter + antenna) [22].

$$R_N = \frac{Z_0}{g_2} \quad (3.16a)$$

$$C_1 = C_2 = C_N = \frac{g_3}{2\pi f_0 Z_0 \Delta} \quad (3.16b)$$

$$L_1 = L_2 = L_N = \frac{1}{4\pi^2 f_o^2 C_3} \quad (3.16c)$$

$$J_{0,1} = \sqrt{\frac{\Delta}{g_0 g_1} \frac{2\pi f_o C_1}{Z_o}} \quad (3.16d)$$

$$J_{i,i+1} = 2\pi f_o \Delta \sqrt{\frac{C_i C_{i+1}}{g_i g_{i+1}}}, \quad i=1, 2, \dots, N-1 \quad (3.16e)$$

$$Q_{e1} = \frac{1}{Z_o J_{0,1}^2} \sqrt{\frac{C_1}{L_1}} = \frac{g_0 g_1}{\Delta} \quad i=1, 2, \dots, N-1 \quad (3.16f)$$

$$K_{i,i+1} = \frac{J_{i,i+1}}{2\pi f_o \sqrt{C_i C_{i+1}}} = \frac{\Delta}{\sqrt{g_i g_{i+1}}}, \quad i=1, 2, \dots, N-1 \quad (3.16g)$$

where Δ is the fractional bandwidth of the designed BPF, R_N , C_s , L_s and J_s are the lumped elements of the filtering antenna circuit model and Z_o is the characteristic impedance of the circuit.

3.5. Summary

In this chapter, an overview of RF filter design by the insertion loss method has been described. A 5th-order Chebyshev BPF has been designed and its parameters have been computed based on the procedure of the insertion loss technique. With the aid of ADS software, the schematic lumped-element circuit of the designed filter has been simulated. The S-parameters of the simulated filter have been plotted. Because ideal lumped-element circuits are often unattainable at high frequency, distributed elements have been used to represent the circuit components of the same filter. The filter has been designed based on series coupled line resonators structure. Also, coupling matrix synthesis, cross-coupling and transmission zeros have been presented. Finally, the design formulae of a rectangular cavity resonator and a filtering antenna have been

stated. All components in the next chapters will be designed based on the procedure and formulas mentioned in this chapter.

References

- [1] J. D. Rhodes, *Theory of Electrical Filters*. Pitman Press Ltd, Bath, Great Britain. 1976.
- [2] J.-S. Hong, *Microstrip Filters for RF/Microwave Applications*, 2nd edition. Hoboken, N.J.: Wiley, 2011.
- [3] D. M. Pozar, *Microwave Engineering*, 4th edition. John Wiley, 2000.
- [4] R. J. Cameron, C. M. Kudsia, and R. R. Mansour, *Microwave filters for communication systems: fundamentals, design, and applications*. Hoboken, N.J.: Wiley ; Chichester : John Wiley [distributor], 2007.
- [5] E. A. Alos, A. U. Zaman, and P.-S. Kildal, "Ka-band gap waveguide coupled-resonator filter for radio link diplexer application," *IEEE Trans. Components, Packag. Manuf. Technol.*, vol. 3, no. 5, pp. 870–879, Jan. 2013.
- [6] M. S. Sorkherizi, A. Khaleghi, and P.-S. Kildal, "Direct-coupled cavity filter in ridge gap waveguide," *IEEE Trans. Components, Packag. Manuf. Technol.*, vol. 4, no. 3, pp. 490–495, Mar. 2014.
- [7] M. S. Sorkherizi and A. A. Kishk, "Completely tuned coupled cavity filters in defected bed of nails cavity," *IEEE Trans. Components, Packag. Manuf. Technol.*, vol. 6, no. 12, pp. 1865-1872, Dec. 2016.
- [8] S. J. Hedges and R. G. Humphreys, "An extracted pole microstrip elliptic function filter using high temperature superconductors," in *Proc. EuMC*, 1994, pp. 517–521.
- [9] J.-S. Hong and M. J. Lancaster, "Design of highly selective microstrip bandpass filters with a single pair of attenuation poles at finite frequencies," in *IEEE Transactions on Microwave Theory and Techniques*, vol. 48, no. 7, pp. 1098-1107, July 2000.
- [10] C. A. Balanis, *Antenna Theory Analysis and Design*. 3rd ed. New Jersey, USA: John Wiley & Sons; 2005.

-
- [11] Z. Gao, W. Hong, R. Lu and C. Wang, "A Planar Filtenna Array Implemented by Embedding the Filtering Function into the SIW Power Divider," *2019 International Symposium on Antennas and Propagation (ISAP)*, Xi'an, China, 2019.
- [12] K. R. Mahmoud and A. M. Montaser, "Design of Compact mm-Wave Tunable Filtenna Using Capacitor Loaded Trapezoid Slots in Ground Plane for 5G Router Applications," in *IEEE Access*, vol. 8, pp. 27715-27723, 2020.
- [13] S. Yu, W. Hong, C. Yu, H. Tang, J. Chen and Z. Kuai, "Integrated millimeter wave Filtenna for Q-LINKPAN application," *2012 6th European Conference on Antennas and Propagation (EUCAP)*, Prague, 2012, pp. 1333-1336.
- [14] H. Chu and Y. Guo, "A Filtering Dual-Polarised Antenna Subarray Targeting for Base Stations in Millimeter-Wave 5G Wireless Communications," in *IEEE Transactions on Components, Packaging and Manufacturing Technology*, vol. 7, no. 6, pp. 964-973, June 2017.
- [15] H. Jin, G. Q. Luo, W. Wang, W. Che and K. Chin, "Integration Design of Millimeter-Wave Filtering Patch Antenna Array With SIW Four-Way Anti-Phase Filtering Power Divider," in *IEEE Access*, vol. 7, pp. 49804-49812, 2019.
- [16] H. Tang, C. Tong, J. Chen, C. Shao, W. Qin and W. Yang, "Differentially SIW TE₂₀-Mode Fed Substrate Integrated Filtering Dielectric Resonator Antenna for 5G Millimeter Wave Application," *2019 IEEE International Conference on Computational Electromagnetics (ICCEM)*, Shanghai, China, 2019.
- [17] F. Chen, J. Chen, Q. Chu and M. J. Lancaster, "X-Band Waveguide Filtering Antenna Array With Nonuniform Feed Structure," in *IEEE Transactions on Microwave Theory and Techniques*, vol. 65, no. 12, pp. 4843-4850, Dec. 2017.
- [18] A. A. C. Alves, L. G. da Silva, E. C. V. Boas, D. H. Spadoti and A. Cerqueira S., "Mechanically Tunable Horn Filtenna for mm-waves," *2019 13th European Conference on Antennas and Propagation (EuCAP)*, Krakow, Poland, 2019.
- [19] X. Liu, H. Wang, S. Quan, X. Jiang, W. Xu and D. Xu, "Design of a W band filter antenna array with low sidelobe level using gap waveguide," *2016 11th International Symposium on Antennas, Propagation and EM Theory (ISAPE)*, Guilin, 2016, pp. 132-134.
- [20] H. Oraizi, M. Hamedani, D. Zarifi and A. Amini, "Design of filter-horn antenna based on groove gap waveguide technology for V-band application," *12th*

European Conference on Antennas and Propagation (EuCAP 2018), London, 2018.

- [21] H. S. Farahani and W. Bösch, "A Novel Compact High-Gain Filtenna Using Gap Waveguide Technology," *2019 IEEE International Symposium on Antennas and Propagation and USNC-URSI Radio Science Meeting*, Atlanta, GA, USA, 2019, pp. 2043-2044.
- [22] J. B. Jadhav, P. J. Deore, "Filtering antenna with radiation and filtering functions for wireless applications," *Journal of Electrical Systems and Information Technology*, vol. 4, no. 1, pp. 125-134, 2017.

Chapter 4. Millimetre-Wave Bandpass Filter Design Based on Gap Waveguide

This chapter presents a new design of a groove gap waveguide (also known as a waffle-iron) bandpass filter at the Ka-band (26.5 - 40 GHz). In this work, a high-selectivity response is achieved with a low number of resonators by introducing cross-coupling between one pair of non-adjacent resonators, to produce two transmission zeros around the passband. The filter is fabricated using two technologies: computer numerical control (CNC) machining technology and high-resolution metalised polymer jetting (PolyJet) 3D printing technology.

4.1. Introduction

Low loss, low mass and easiness of manufacture for bandpass filters operating at millimetre-wave (mmWave) frequencies are of high importance for aerospace (unmanned drone, manned aircraft, satellite and interplanetary mission) applications. A large number of mmWave bandpass filters (BPFs) using various design and fabrication technologies have been reported over the past few decades. For high-frequency microwave/mmWave applications, designers prefer metal-pipe rectangular waveguide solutions, due to their low loss and high power-handling capabilities. Typical examples of waveguide BPF implementations have been demonstrated at the X-band (8.2-12.4 GHz) [1] and Ku-band (12.4-18 GHz) [2].

One of the drawbacks of conventional waveguide components is the poor electrical contact between joined waveguide parts, especially at mmWave frequencies. To mitigate this, a very accurate machining process is required. In contrast, planar solutions are compatible with the monolithic microwave integrated circuit (MMIC) applications, although the associated ohmic losses are relatively high, especially at mmWave frequencies [3], [4]. Substrate integrated waveguide (SIW) technology has also been used to implement BPFs at mmWave frequencies [5]. Although SIWs

present good integration capabilities, when compared to conventional waveguides, they can still suffer from high dielectric losses.

Air-filled SIW [6] and empty SIW (ESIW) [7], [8] have been proposed for manufacturing “empty” waveguides without having a dielectric substrate, but at the same time, they are completely integrated into planar circuits. This method is compromised between the merits of conventional waveguide technologies, such as low losses, and the features of planar circuits, such as low cost and easy compact integration. However, the Q-factor is still much lower than the conventional rectangular waveguides. The reason behind that is, in conventional waveguides, the volume is much larger, which results in more energy being stored than that in ESIWs. To overcome this constraint, a novel integrated structure was proposed in [9] to embed very high Q-factor filters based on the ESIW with a higher profile. Nevertheless, due to the use of microstrip feed lines and transitions (from microstrip to ESIW), losses will increase.

Gap waveguide was proposed as an alternative to conventional metal-pipe rectangular waveguides, at extremely high frequencies (EHF) and beyond [10], as it avoids the use of sidewalls. Because of the small dimensions of the structures at mmWave frequencies, fabrication of conventional waveguide components using longitude-cut fabrication techniques is challenging, due to radiation leakage from the physical connection mismatches of the waveguide pieces. Moreover, poor metal contact also leads to other undesirable effects, such as passive intermodulation (PIM) [11]. Gap waveguides consist of two parallel plates, being open from the sides. One of the plates is flat, which ideally acts as a perfect electrical conducting plane, while the other has a periodic structure of metal pins that are created to act as an artificial magnetic conductor [10], [12].

By choosing specific pin dimensions, a cut-off frequency for parallel-plate modes can be established; prohibiting wave propagation. To provide a path for electromagnetic propagation, a groove gap waveguide (GGW) or ridge gap waveguide is formed among the pins, where the waves transfer through the groove or ridge, respectively [10]-[13]. Similar to conventional rectangular waveguides, gap waveguides are usually

manufactured using machining technology (e.g., by milling or drilling metal structures).

Low-cost gap waveguides have been proposed in [14]-[17]. In the former two, half-height pins are employed in gap waveguide technology, making the fabrication process of the pin surface easier. However, an accurate manufacturing process is still needed. In the latter two, a novel cost-effective method to manufacture integrated waveguide structures at high frequencies has been presented. In this method, instead of pins, a truncated glide-symmetric holey EBG structure is adopted.

Gap waveguides are regarded as a compromise solution for mmWave BPFs. Unlike planar and SIW technologies, gap waveguide filters are characterised by their high Q-factor and, thus, low loss at mmWave frequencies. Also, the perfect contact between the top and bottom plates (required with conventional waveguides) are no longer needed, where a lattice of periodic pins can be created on the borders of one of the parallel plates in order to function as a high impedance surface.

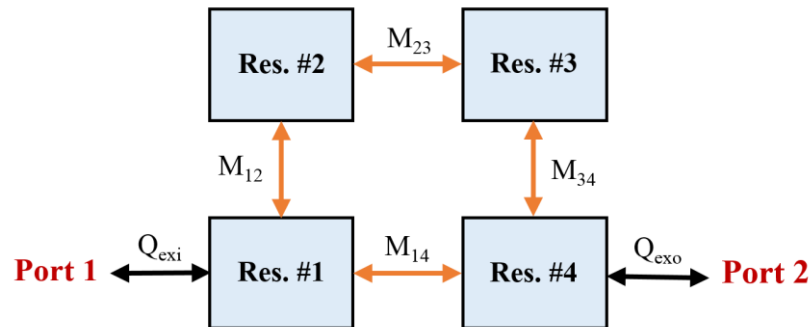
4.2. Gap Waveguide-Based Bandpass Filter Design

4.2.1. Filter Specifications and Synthesis

A mmWave BPF is designed and simulated based on GW technology, having the high selectivity design specifications given in Table 4.1. In this work, a high-selectivity response is achieved with a low number of resonators by introducing a positive cross-coupling between one pair of non-adjacent resonators, to produce two transmission zeros around the passband. The filter centre frequency is chosen to be at the mmWave band. The topology of this compact quadruplet BPF is shown in Fig. 4.1. The coupling coefficient (M) between resonators and the external quality factor (Q_{ex}) can be determined from the circuit elements of the low-pass prototype filter [25]-[27]. With reference to Fig. 4.1, M_{ij} is the coupling coefficient between two resonators, where i and j identify different resonator numbers, while Q_{exi} and Q_{exo} represent the input and output external quality factors or the coupling between the first/last resonators and the source/load, respectively.

Table 4.1. Target bandpass filter design specifications.

Parameter	Value
Filter Type	Quasi-elliptic
Centre Frequency (GHz)	35.65
Fractional Bandwidth (<i>FBW</i>) (%)	1.4
Insertion Loss (dB)	< 0.5
Return Loss (dB)	> 15

**Fig. 4.1. The topology of the designed quadruplet bandpass filter.**

4.2.2. Coupling Matrix and Design Procedure

On the (bottom) plate containing the periodic array of pins, the tips of these pins are separated from the (top) flat plate with a gap (g). Based on the dispersion diagram in [28], the dimensions of the periodic pins shown in Fig. 4.2 are chosen to cover Ka-band frequencies. In a gap waveguide, the height of the pins h is approximately $\lambda/4$ and the air gap separation distance $g < \lambda/4$, where λ is the wavelength at the centre frequency. To create a groove gap waveguide, some of the pins are removed to form four air-filled cavity resonators, as illustrated in Fig. 4.2. To obtain resonance at 35.65 GHz, initially, the geometric shape of the cavities was chosen to be square. The length of each cavity can be obtained from eq. (3.11). The associated cavity mode is confined between the flat areas of both parallel plates and rows of side pins. Increasing the

number of side pins rows will decrease the undesired leakage. However, it increases the structural complexity and size. To reduce the size and complexity of the structure with a reasonable leakage, two rows of side pins are sufficient in this work. Fig. 4.3 exhibits the electric field for a single gap-waveguide resonator with two and three rows of side pins. It can be observed that the leakage at the third row of sided pins in Fig. 4.3b is lower than -40 dB which can be neglected for most applications. The resonant frequency of each resonator can be determined from its dimensions. In this design, the 35.65 GHz cavity resonator was achieved with dimensions of $5.9 \times 5.9 \text{ mm}^2$. To achieve direct-resonator coupling, coupling pillars are longitudinally centred in parallel with two periodic pins between the adjacent resonators, as will be illustrated later.

Generally, to design any BPF, three fundamental variables should be known: resonant frequency (f_o) of each resonator, coupling coefficients (M) between coupled resonators and external quality factor (Q_e) which is the coupling between first/last resonators and source/load, respectively. It is assumed that all resonators are tuned at the same centre frequency, which is 35.65 GHz. The other two parameters, M and Q_e can be determined in terms of circuit elements of a low-pass prototype filter as explained in Chapter 3. Based on the filter design specifications in Table 4.1 and the filter topology in Fig. 4.1, by applying the equations (3.8a-d), the following coupling matrix can be created:

$$m = \begin{bmatrix} 0 & -1.2 & 0 & 0.24 \\ -1.2 & 0 & -1.1 & 0 \\ 0 & -1.1 & 0 & -1.2 \\ 0.24 & 0 & -1.2 & 0 \end{bmatrix}$$

$$m_{ij} = \frac{M_{ij}}{FBW}$$

where m is the normalised coupling coefficient with i and j as matrix indices, and FBW is the fractional bandwidth of the filter. The external quality factor has been calculated to be 48.878.

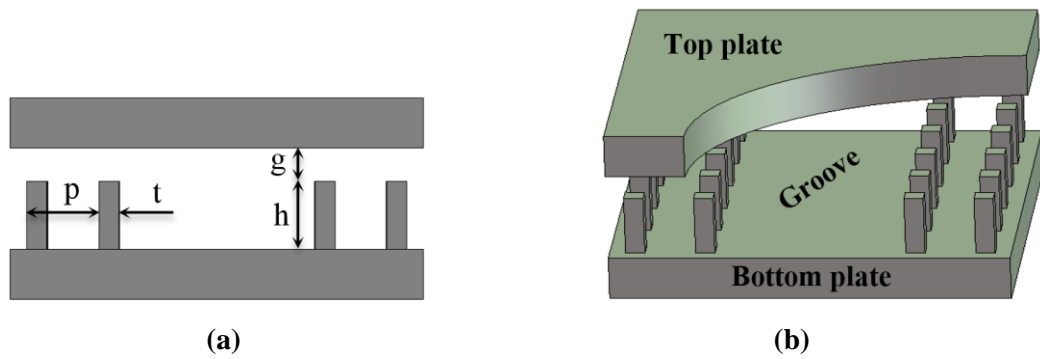


Fig. 4.2. Gap waveguide periodic structure: (a) Cross-section; (b) 3D perspective view. (Dimensions listed in Table 4.2).

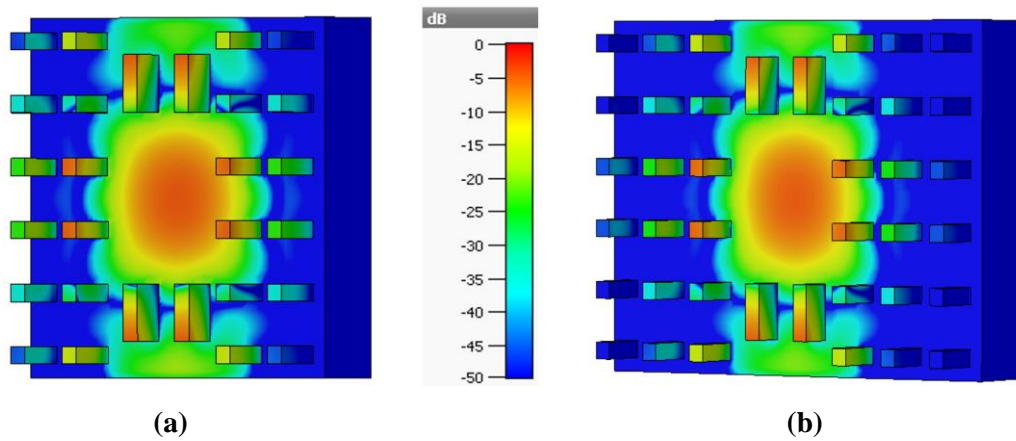


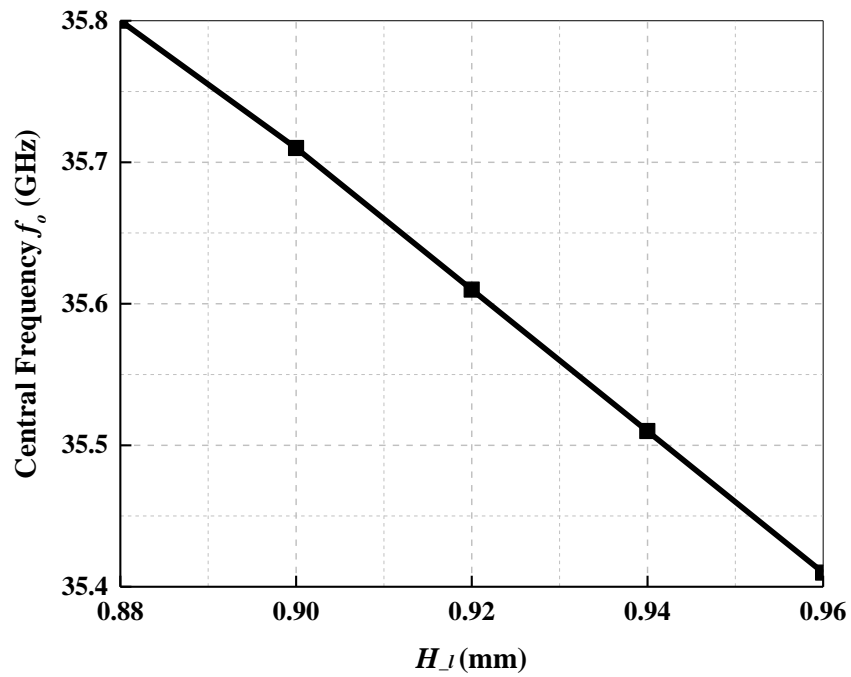
Fig. 4.3. Electric field distribution of one resonator in a groove gap waveguide with a weak internal coupling with side pins of (a) two rows and (b) three rows.

To study the effect of each dimension, the following are the design curves that show the relationship between these dimensions and the filter parameters. Couplings between the input source and resonator #1 and also between resonator #4 and the output load are realised by placing two pairs of pillars (H), with the first and fourth resonators connected to WR-28 (26.5-40 GHz) rectangular waveguide ports, respectively. The length of H (H_l) controls the resonant frequency, while the height (H_h) controls the external quality factor, as shown in Fig. 4.4(a) and Fig. 4.4(b), respectively. Although the resonant frequency is slightly affected by the change of the input/output pillars height, this can be compensated by optimising the input/output pillars length. The normalised coupling coefficient between resonator #1 and resonator

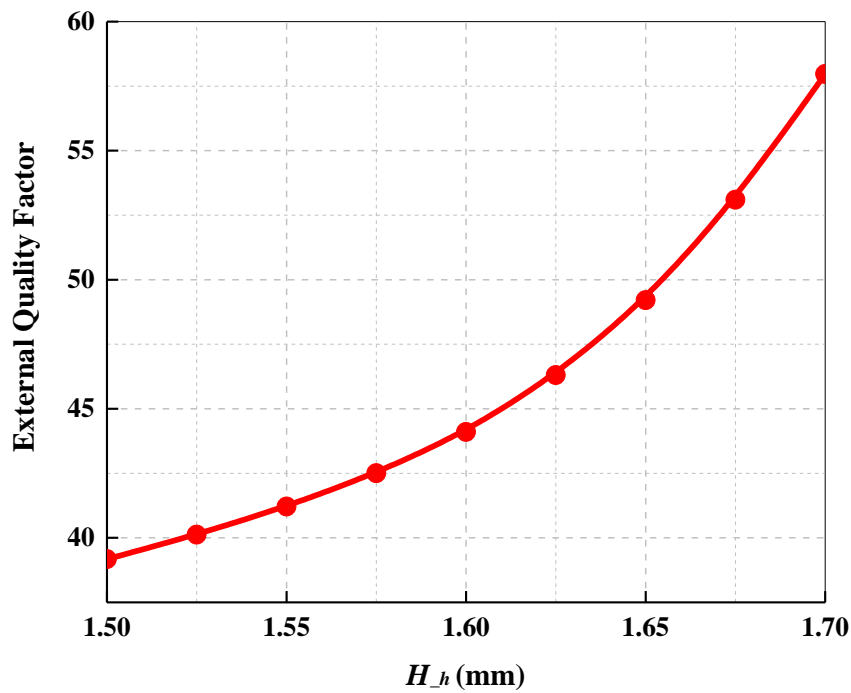
#2, m_{12} ($m_{12} = M_{12} / FBW$), is plotted as a function of the pillar length (P_{12_l}) and pillar height (P_{12_h}) in Fig. 4.5(a) and Fig. 4.5(b), respectively. Due to the symmetry of the filter structure, P_{12} and P_{34} are identical. The dimensions of P_{23} were evaluated in the same way (results are not shown).

Table 4.2. Initial and optimised BPF spatial dimensions (Unit: mm).

Parameter	Description	Initial Value	Optimised Value
g	Gap separation	1.00	1.00
t	Pin thickness	0.50	0.70
h	Pin height	2.00	2.10
p	pin period	2.00	2.20
P_{12_h}	Pillar height between res. #1 and res. #2	1.77	1.70
P_{12_l}	Pillar length between res. #1 and res. #2	1.27	1.25
P_{23_h}	Pillar height between res. #2 and res. #3	2.20	2.33
P_{23_l}	Pillar length between res. #2 and res. #3	1.23	1.22
$iris_w$	Iris width	1.86	1.90
H_h	Input/output pillar height	1.64	1.67
H_l	Input/output pillar length	0.91	0.92



(a)



(b)

Fig. 4.4. (a) Centre frequency of a doubly-loaded resonator as a function of H_l mm ($H_h = 1.5$ mm). (b) External quality factor as a function of H_h mm ($H_l = 1.2$ mm).

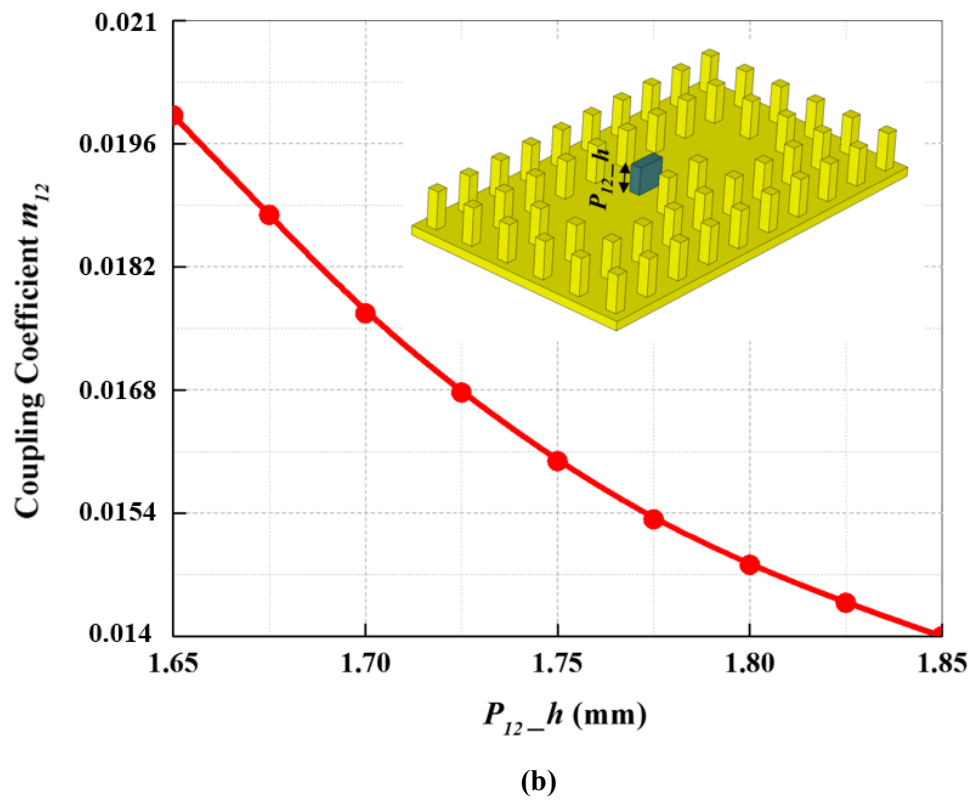
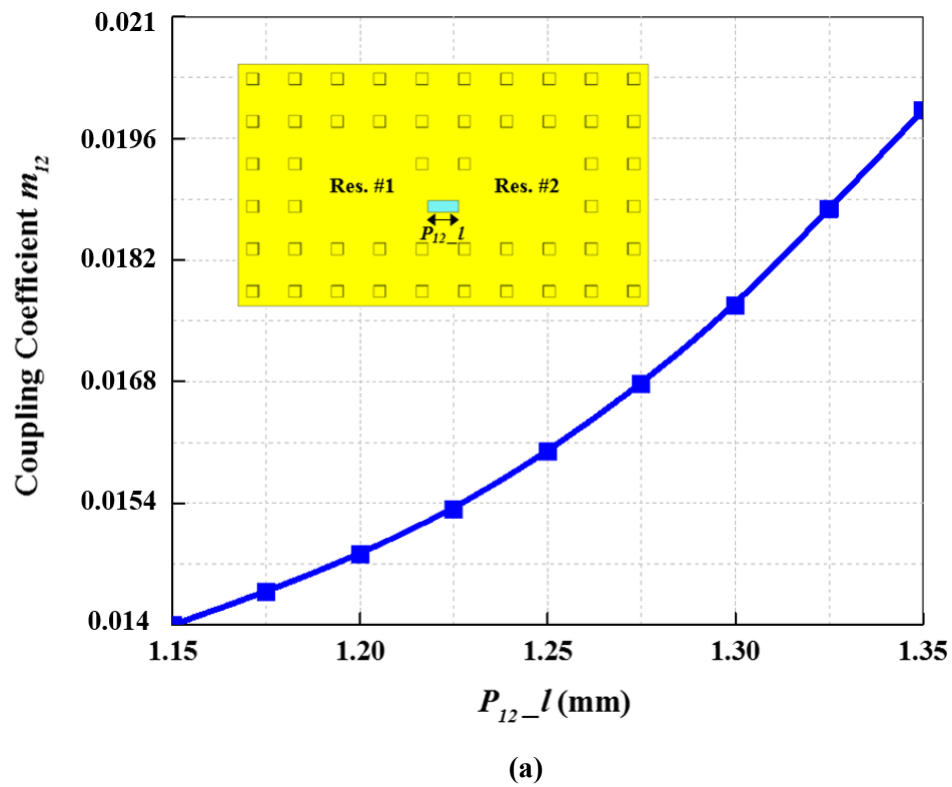


Fig. 4.5. Coupling coefficient m_{12} as a function of (a) P_{12-l} and (b) P_{12-h} .

The coupling coefficients m_{12} , m_{23} and m_{34} are electrical due to the use of capacitive pillars between the adjacent resonators. To have a symmetric response with one TZ on each side of the passband, the coupling coefficient between the non-adjacent resonators, m_{14} in our design, should be positive [29]. To realise a positive cross-coupling, a pair of inductive irises are placed between resonator #1 and resonator #4. The thickness of each iris is the same as the thickness of the pin. The normalised coupling coefficient m_{14} is plotted as a function of the iris width ($iris_w$), as shown in Fig. 4.6. The effect of $iris_w$ against the transmission coefficient is plotted in Fig. 4.7. One can notice that when the $iris_w$ increases, the positions of the transmission zeros move away from the passband, leading to reducing the filter selectivity. However, the stopband rejection below and above the passband improves when $iris_w$ increases, as can be seen in Fig. 4.7. A final optimisation process is then applied to finely tune the dimensions of the filter structure, to fully meet the target frequency response specifications. The initial and optimised structural dimensions are given in Table 4.2.

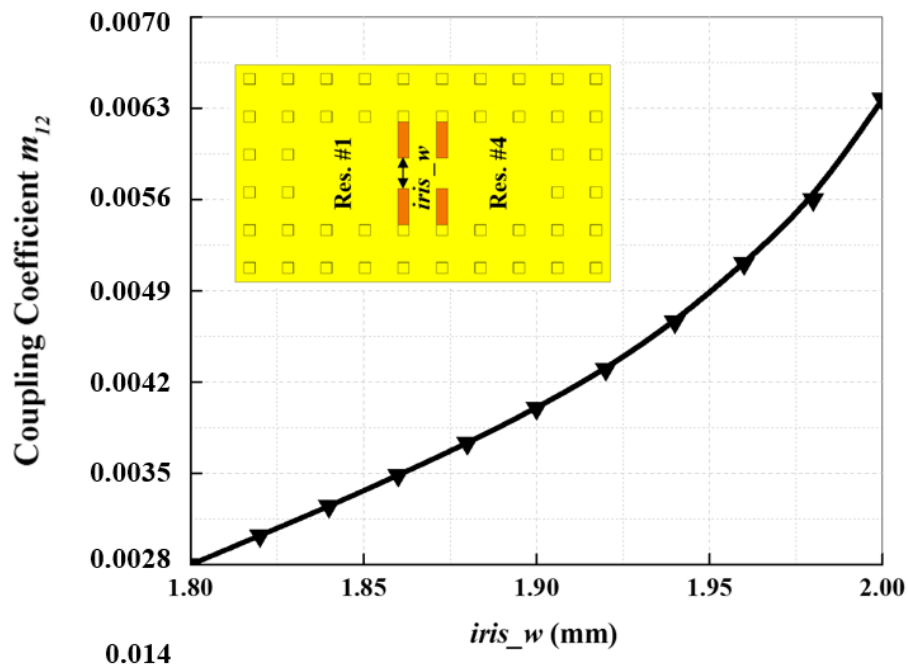


Fig. 4.6. Coupling coefficient m_{14} as a function of $iris_w$ (with $iris_h = h + g$).

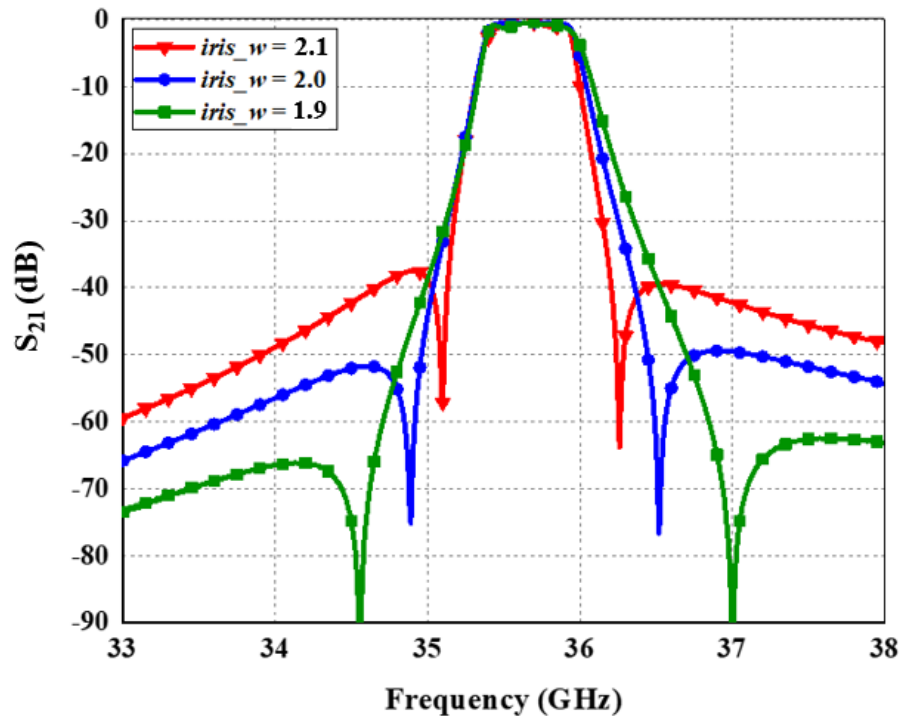


Fig. 4.7. The effect of $iris_w$ against the transmission zeros locations, i.e. the filter selectivity, and the stopband rejection (Unit: mm).

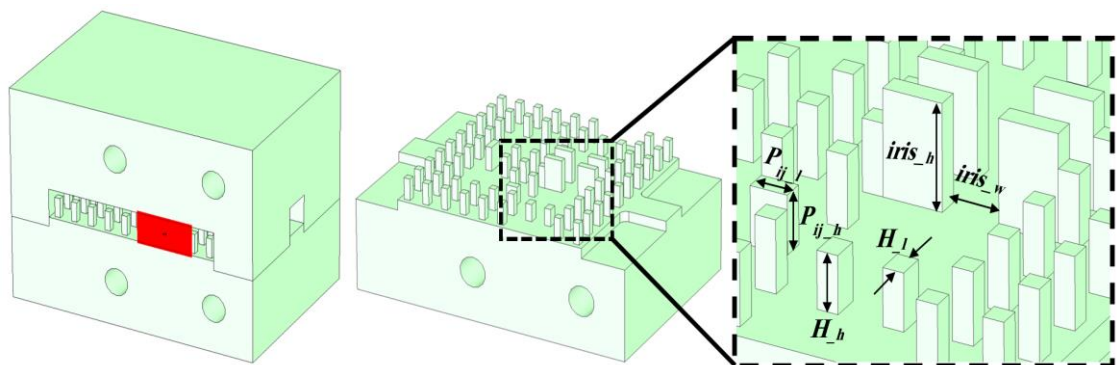


Fig. 4.8. The proposed filter structure (dimensional values are listed in Table 4.2).

4.3. Simulations and Measurements

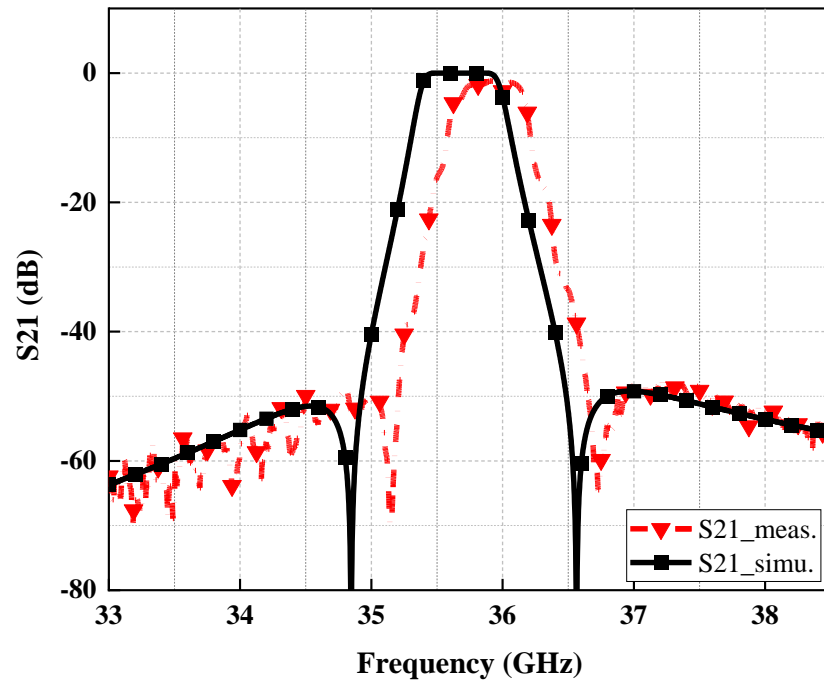
4.3.1. Filter Specifications and Synthesis

Full-wave electromagnetic simulations were undertaken using CST MICROWAVE STUDIO®. The whole structure of the optimised BPF is shown in Fig. 4.8. The simulated S-parameters of the final optimised filter are shown in Fig. 4.9. It can be seen that the simulated performance satisfies the design specifications. The minimum insertion loss IL within the passband is 0.4 dB (with a passband average of 0.45 dB) and the passband return loss RL is better than 22 dB. Two transmission zeros are introduced at 34.89 GHz and 36.52 GHz, as a result of the cross-coupling between Resonators #1 and #4. Near-symmetrical stopband attenuation is predicted to be ~50 dB.

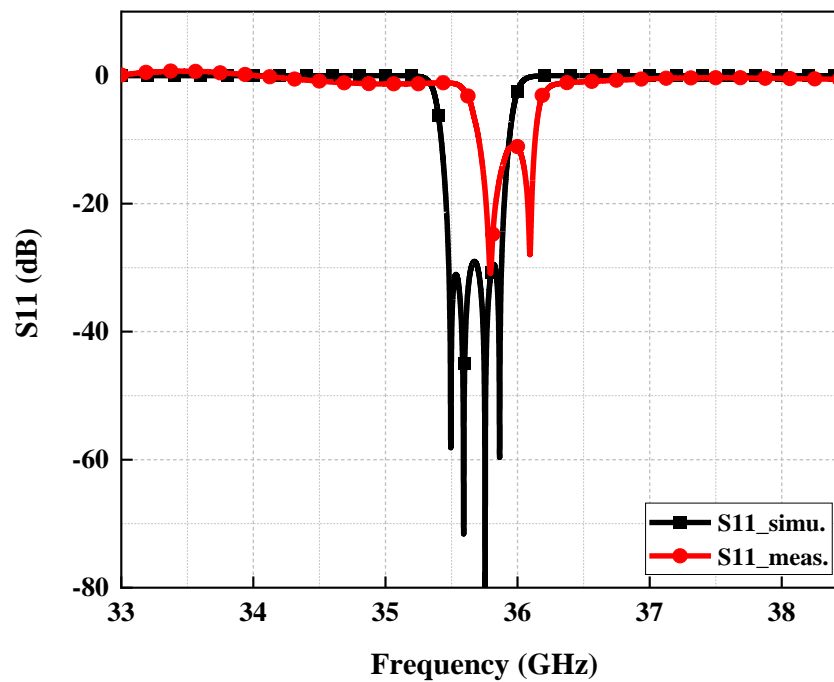
4.3.2. Fabrication Process and Measurements

The designed 4th-order BPF is fabricated using two different manufacturing technologies, CNC machining technology and high-resolution metalised PolyJet 3D printing technology. First, a prototype of the optimised filter is fabricated from brass using a CNC milling machine. The fabricated groove gap waveguide filter is illustrated in Fig. 4.10. The overall size of the fabricated filter is $31.5 \times 21.5 \times 23.1 \text{ mm}^3$, including the fixing stands. The prototype consists of two parallel plates, the bottom plate is etched to create the periodic texture and to form four cavity resonators, while the top plate is left flat.

In contrast to conventional waveguide structures, no sidewalls are needed with gap waveguides. That means an electric contact between the two parallel plates is not required. For hollow waveguides, an electric contact is needed. The joints between the top and bottom parts of the waveguide usually suffer from a physical mismatch due to surface roughness problem which leads to the increase of loss, especially at high frequencies.



(a)



(b)

Fig. 4.9. The simulated and measured results of the metal machined BPF prototype.
(a) Transmission coefficient S_{21} . (b) Reflection coefficient S_{11} .

The prototype BPF was measured using an Anritsu 37369A vector network analyzer (VNA) with standard WR-28 (26-40 GHz) waveguide flange interfaces. A Thru-Reflect-Line (TRL) calibration technique was first performed to calibrate the VNA, the cables and the waveguide. The measured results of the metal machined BPF prototype are shown in Fig. 4.9, where reasonable agreement with the simulated ones is achieved. It can be seen that there is a slight frequency shift (170 MHz) in the measured results towards the high frequencies. Such a small frequency shift is mainly due to some corners or edges which are not accurately fabricated. The measured insertion loss is 1.2 dB. The measured return loss is 11 dB. This difference between the simulated and measured results is expected due to the fabrication tolerance. Better performance can be obtained if another CNC machine with higher accuracy is used..

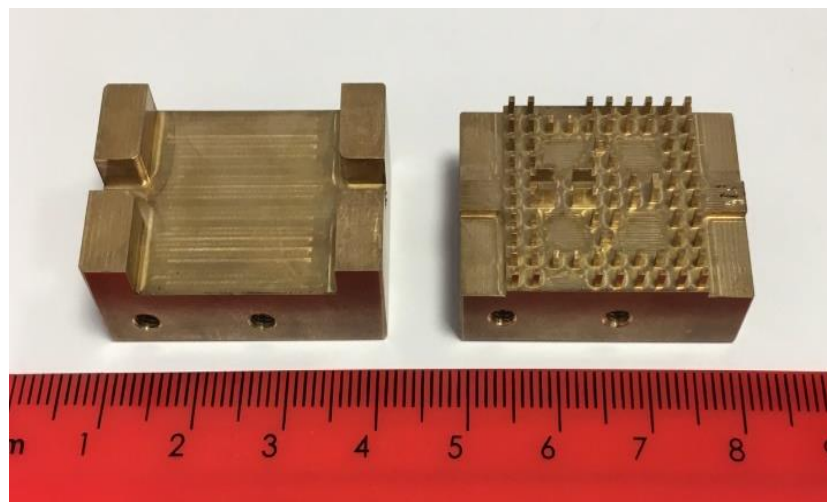


Fig. 4.10. Photo of the fabricated top (left) and bottom (right) plates of the brass metal machined BPF prototype.

Second, the optimised BPF is fabricated using a 3D Systems' ProJet 2500 printer, which provides near state-of-the-art resolution ($800 \times 900 \times 790$ DPI, $32 \mu\text{m}$ layers). As illustrated in Fig. 4.8, the filter structure is split into two parts; this simplifies the fabrication process of the pins, as well as avoid problems with metal plating. The parts were formed by jetting of photopolymers from multiple nozzles, to form each layer that is immediately selectively UV cured, to form structure and support areas as defined by

the CAD file. This technology represents the highest resolution in the commercial 3D printing of plastics that can be achieved for large structures. Once printed, the parts were baked at 60°C, to allow the supporting wax to melt away. To further remove any wax residue, the parts were cleaned further in a 70°C ultrasonic bath of EZ-Rinse for 15 minutes and a room temperature ultrasonic bath of IPA for 15 minutes. These cleaned parts were then commercially electroless-plated with 20 µm thick copper, exceeding five skin depths of thickness at the lowest frequency of operation. The final PolyJet 3D printed and copper-plated BPF prototype is shown in Fig. 4.11.

The measured results of the metalised PolyJet 3D printed BPF are shown in Fig. 4.12. In the passband, the measured insertion and return losses are 0.5 dB and 21 dB; only 0.1 dB and 1 dB different from predictions, respectively. The measured transmission zeros are slightly further out than predicted. This slight difference between the simulations and measurements is mainly due to manufacturing tolerance. The width of irises between resonator #1 and resonator #4 is a few microns wider than that in the design. Nevertheless, it should be noted that there were no iterations to the fabrication and no tuning was needed to achieve these measured results.

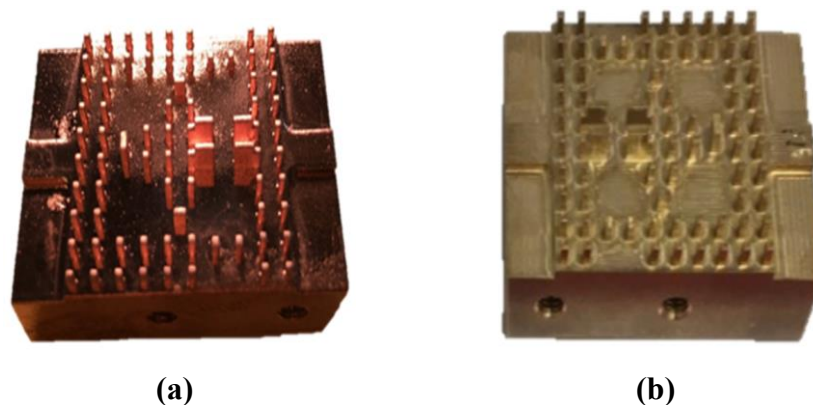


Fig. 4.11. Prototypes of the Ka-band BPF: (a) Metalised PolyJet 3D printed BPF (weighing just 17 g). (b) CNC metal machined BPF (weighing 112 g).

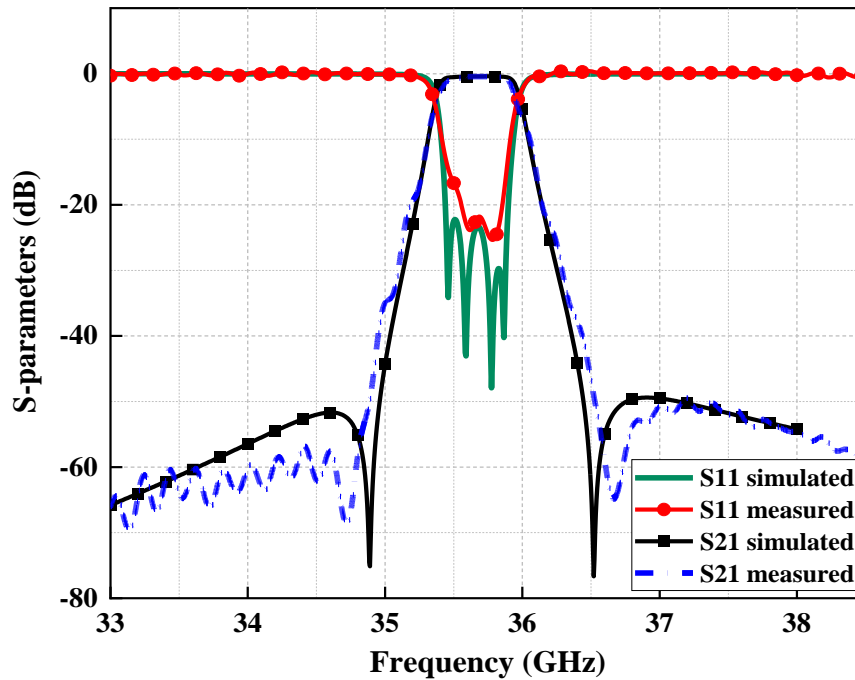
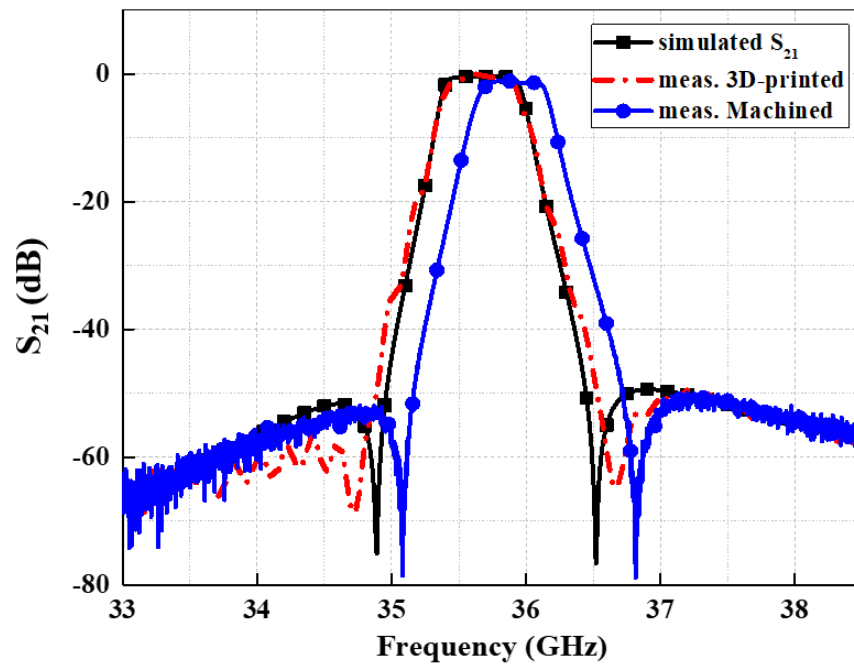


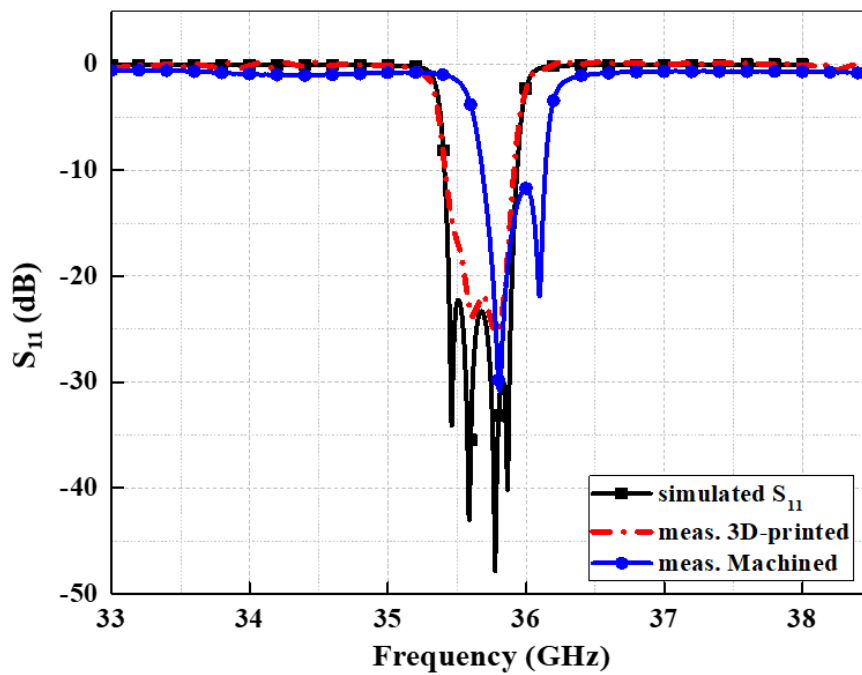
Fig. 4.12. Simulated and measured results of the metalised PolyJet 3D printed BPF.

The 3D printed and CNC machined counterparts are compared in terms of performance. The measured transmission and reflection coefficients, S_{21} and S_{11} , of both prototypes are shown in Fig. 4.13, along with the simulated results. It can be seen that there are obvious differences between the measured results of the 3D printed and machined filters. The measured insertion and return losses for the machined filter were 1.2 dB and 11 dB, respectively; significantly worse than the PolyJet 3D printed counterpart. The insertion loss is more with the CNC BPF, because of the lower bulk conductivity of brass when compared to copper.

Moreover, when compared to the machined filter, a negligible frequency shift is observed with the PolyJet 3D printed counterpart. These improvements are mainly due to the high fabrication accuracy offered by PolyJet 3D printing. Though the precision of CNC machines is usually higher than that of PolyJet 3D printers, it is difficult to keep the accuracy equal over a whole structure (changes over the manufacturing time period) especially with such a complex bed of nails. In addition to the excellent measured performance, another important advantage of the 17 g PolyJet 3D printed component is the dramatic reduction in mass, when compared to the 112 g brass CNC machined counterpart; an 85% weight reduction, while having the same geometric dimensions.



(a)



(b)

Fig. 4.13. Comparison among simulated results, measured performances of the PolyJet 3D printed filter and measured performances of the CNC machined filter: (a) S_{21} (b) S_{11} .

Table 4.3. A comparison with other mmWave CNC machining-based GGW BPFs

Meas. Freq. (GHz)	Manufac. Tech.	Filter Order	FBW (%)	IL (dB)	RL (dB)	Band Reject (dB)	Dimensions (mm)	Ref.
37.37	CNC Machining	7	1.5	1	17	60	61.6×12.0×2.8	[20]
35	CNC Machining	3	1	1	9	35	17.8×16.0×12.7	[21]
61	CNC Machining	5	2.5	1.5	13	60	NA	0
35.65	CNC Machining	4	1.4	1.2	11.7	50	21.0×21.0×3.1	This work
35.65	PolyJet 3D Printing	4	1.4	0.5	21	50	21.0×21.0×3.1	This work

Finally,

Table 4.3 compares the designed and fabricated filters with recently reported mmWave GGW-based BPFs, fabricated using machining technology (mass was not included, due to a lack of available data). It can be seen that our PolyJet 3D printed BPF has the lowest insertion loss and the second narrowest bandwidth. Furthermore, good selectivity was achieved with high stopband attenuation. Clearly, the low mass and excellent measured performance of our prototype filter make it a potential solution for aerospace applications.

4.4. Summary

A narrow and high selective BPF operates at a centre frequency of 35.65 GHz and a fractional bandwidth of 1.4% has been designed. A high selectivity has been realised by introducing a cross-coupling between two non-adjacent resonators. The filter is fabricated using two technologies: CNC machining technology and high-resolution metalised PolyJet 3D printing technology. The measured results are in excellent agreement with predictions, without having any design iterations or post-fabrication tuning. The metalised 3D printed filter presents many advantages, when compared to

other manufacturing technologies, in terms of mass (lighter weight), performance (lower loss), development time and cost. The designed and fabricated filter is expected to be as a potential device for aerospace applications.

References

- [1] C. Carceller, P. Soto, V. E. Boria, and M. Guglielmi, "Design of hybrid folded rectangular waveguide filters with transmission zeros below the passband," *IEEE Trans. Microw. Theory Tech.*, vol. 64, no. 2, pp. 475–485, Feb. 2016.
- [2] Y.-S. He, A. Barannik, N. Cherpak, L. Sun, V. Skresanov, Y. Bian, J. Wang, M. Natarov, and V. Zolotaryov, "Novel design of band-pass waveguide filter with HTS E-plane insert," *IEEE Trans. Appl. Supercond.*, vol. 27, no. 4, pp. 4–7, Jun. 2017.
- [3] I. D. Robertson and S. Lucyszyn (Editors), "RFIC and MMIC Design and Technology", Published by the IEE, Nov. 2001.
- [4] S. Lucyszyn (Editor), "Advanced RF MEMS", Cambridge University Press, Cambridge, Aug. 2010.
- [5] S.-W. Wong, R. S. Chen, K. Wang, Z.-N. Chen, and Q.-X. Chu, "U-shape slots structure on substrate integrated waveguide for 40-GHz bandpass filter using LTCC technology," *IEEE Trans. Components, Packag. Manuf. Technol.*, vol. 5, no. 1, pp. 128–134, Jan. 2015.
- [6] F. Parment, A. Ghiotto, T. Vuong, J. Duchamp and K. Wu, "Air-filled substrate integrated waveguide for low-loss and high power-handling millimeter-wave substrate integrated circuits," in *IEEE Transactions on Microwave Theory and Techniques*, vol. 63, no. 4, pp. 1228-1238, April 2015.
- [7] A. Belenguer, H. Esteban and V. E. Boria, "Novel empty substrate integrated waveguide for high-performance microwave integrated circuits," in *IEEE Transactions on Microwave Theory and Techniques*, vol. 62, no. 4, pp. 832-839, April 2014.
- [8] A. L. Borja, A. Belenguer, H. Esteban and V. E. Boria, "design and performance of a high-Q narrow bandwidth bandpass filter in empty substrate integrated coaxial line at Ku-band," in *IEEE Microwave and Wireless Components Letters*,

- vol. 27, no. 11, pp. 977-979, Nov. 2017.
- [9] J. A. Martinez, J. J. de Dios, A. Belenguer, H. Esteban and V. E. Boria, "Integration of a very high quality factor filter in empty substrate-integrated waveguide at Q-band," in *IEEE Microwave and Wireless Components Letters*, vol. 28, no. 6, pp. 503-505, June 2018.
- [10] P.-S. Kildal, E. Alfonso, A. Valero-Nogueira, and E. Rajo-Iglesias, "Local metamaterial-based waveguides in gaps between parallel metal plates," *IEEE Antennas Wirel. Propag. Lett.*, vol. 8, pp. 84–87, Feb. 2009.
- [11] C. Vicente and H.L. Hartnagel, "Passive intermodulation analysis between rough rectangular waveguide flanges", *IEEE Trans. Microwave Theory Tech.*, vol. 53, no.8, pp. 2515 - 2525, Aug. 2005.
- [12] M. G. Silveirinha, C. A. Fernandes, and J. R. Costa, "Electromagnetic characterisation of textured surfaces formed by metallic pins," *IEEE Trans. Antennas Propag.*, vol. 56, no. 2, pp. 405–415, Feb. 2008.
- [13] A. U. Zaman, P.-S. Kildal, and A. A. Kishk, "Narrow-band microwave filter using high-Q groove gap waveguide resonators with manufacturing flexibility and no sidewalls," *IEEE Trans. Components, Packag. Manuf. Technol.*, vol. 2, no. 11, pp. 1882–1889, Nov. 2012.
- [14] F. Fan, J. Yang and P. Kildal, "Half-height pins - a new pin form in gap waveguide for easy manufacturing," *2016 10th European Conference on Antennas and Propagation (EuCAP)*, Davos, 2016, pp. 1-4.
- [15] F. Fan, J. Yang, V. Vassilev and A. U. Zaman, "Bandwidth investigation on half-height pin in ridge gap waveguide," in *IEEE Transactions on Microwave Theory and Techniques*, vol. 66, no. 1, pp. 100-108, Jan. 2018.
- [16] M. Ebrahimpouri, E. Rajo-Iglesias, Z. Sipus and O. Quevedo-Teruel, "Cost-effective gap waveguide technology based on glide-symmetric holey EBG structures," in *IEEE Transactions on Microwave Theory and Techniques*, vol. 66, no. 2, pp. 927-934, Feb. 2018.
- [17] E. Rajo-Iglesias, M. Ebrahimpouri and O. Quevedo-Teruel, "Wideband phase shifter in groove gap waveguide technology implemented with glide-symmetric holey EBG," in *IEEE Microwave and Wireless Components Letters*, vol. 28, no. 6, pp. 476-478, June 2018.
- [18] M. S. Sorkherizi, A. Khaleghi, and P.-S. Kildal, "Direct-coupled cavity filter

- in ridge gap waveguide," *IEEE Trans. Components, Packag. Manuf. Technol.*, vol. 4, no. 3, pp. 490–495, Mar. 2014.
- [19] M. S. Sorkherizi and A. A. Kishk, "Completely tuned coupled cavity filters in defected bed of nails cavity," *IEEE Trans. Components, Packag. Manuf. Technol.*, vol. 6, no. 12, pp. 1865–1872, Dec. 2016.
- [20] E. A. Alos, A. U. Zaman, and P.-S. Kildal, "Ka-band gap waveguide coupled-resonator filter for radio link diplexer application," *IEEE Trans. Components, Packag. Manuf. Technol.*, vol. 3, no. 5, pp. 870–879, Jan. 2013.
- [21] B. Ahmadi and A. Banai, "Direct coupled resonator filters realised by gap waveguide technology," *IEEE Trans. Microw. Theory Tech.*, vol. 63, no. 10, pp. 3445–3452, Aug. 2015.
- [22] B. Al-Juboori, Y. Huang, D. Klugmann, M. Hussein and J. Zhou, "Millimeter wave cross-coupled bandpass filter based on groove gap waveguide technology," *UK-Europe-China Workshop on Millimetre Waves and Terahertz Technologies (UCMMT)*, Liverpool, 2017, pp. 1-4.
- [23] A. del Olmo-Olmeda, M. Baquero-Escudero, V. E. Boria-Esbert, A. Valero-Nogueira and A. J. Berenguer-Verdú, "A novel band-pass filter topology for millimeter-wave applications based on the groove gap waveguide," *2013 IEEE MTT-S International Microwave Symposium Digest (MTT)*, Seattle, WA, 2013, pp. 1-4.
- [24] A. Berenguer, M. Baquero-Escudero, D. Sanchez-Escuderos, B. Bernardo-Clemente and V. E. Boria-Esbert, "Low insertion loss 61 GHz narrow-band filter implemented with Groove Gap Waveguides," *European Microwave Conference*, Rome, 2014, pp. 191-194.
- [25] J.-S. Hong and M. J. Lancaster, "Design of highly selective microstrip bandpass filters with a single pair of attenuation poles at finite frequencies," *IEEE Trans. Microw. Theory Tech.*, vol. 48, no. 7, pp. 1098–1107, Jul. 2000.
- [26] J.-S. HONG, *Microstrip Filters for RF/Microwave Applications*, 2nd edition. Hoboken, N.J: Wiley, 2011.
- [27] D. M. Pozar, *Microwave Engineering*, 4th edition. John Wiley, 2000.
- [28] H. Raza, J. Yang, P. Kildal and E. Alfonso, "Resemblance between gap waveguides and hollow waveguides," in *IET Microwaves, Antennas & Propagation*, vol. 7, no. 15, pp. 1221-1227, 10 December 2013.

- [29] M. Sharifi Sorkherizi and A. A. Kishk, "Self-Packaged, Low-Loss, Planar Bandpass Filters for Millimeter-Wave Application Based on Printed Gap Waveguide Technology," in *IEEE Transactions on Components, Packaging and Manufacturing Technology*, vol. 7, no. 9, pp. 1419-1431, Sept. 2017.

Chapter 5. A Novel Gap Waveguide Structure: Analysis and Investigation

5.1. Introduction

In gap waveguides, different pin geometries have been proposed. The existing pin forms as a full-length pin are square pins [1], as shown in Fig. 5.1(a), circular pins [11], inverted pyramid-shaped pins [12] and double cone pins [13]. The former two are the basic forms while the latter two were proposed for wideband performance enhancement. However, all the above forms are based on a full-length pin form, i.e. the pins will be long and thin, which poses a difficulty for low-cost manufacturing.

Recently, different pins forms have been introduced. The half-height-pin form, shown in Fig. 5.1(b), is proposed for reducing the fabrication cost [14]. In this form, the full-height conventional pins on one of the two parallel plates are divided into two half-height pins placed on either plate. However, that increases the number of pins to double which may lead to increased manufacturing time. An interdigital-pins bed of nails has been proposed in [15], as shown in Fig. 2.5(c) in Chapter 2. The metal pins are allocated to the two plates alternatively, where each pin is surrounded by four pins of the other plate. The advantage of the interdigital-pin lattice is that a minimum pin gap could be achieved, reducing the diameter of the milling cutter to its radius. This makes it possible to manufacture EBG structures operating at higher frequencies using the same machining centre. However, in such a configuration, the alignment between the two textures will be the main challenge.

For a conventional gap waveguide with dimensions of a standard rectangular waveguide port ($a=2b$), since the pins height is a quarter-wavelength of the centre frequency of the passband, its corresponding frequency is very close to the lower cut-off frequency of the fundamental TE_{10} mode in a rectangular waveguide. Although, as a gap waveguide structure, the effect of wave shielding is the best at this frequency,

rectangular waveguides usually are not used at the cut-off frequencies. So, by using conventional full-height pins, the wave shielding effect will not be fully utilised. However, by adding a wall, the frequency where the wave shielding is most effective will be shifted higher. Hence, the wave shielding will be much more effective at the new operating frequency.

A new pin form is proposed that can overcome the bandwidth limitation. Unlike a unit cell in the conventional gap waveguide which consists of full-height pins as a unit-cell, the unit-cell of the proposed pin-form consists of a pin mounted on a wall. This form of pins has the following advantages compared to the conventional forms:

- (i) The wave shielding will be much more effective at the operating band using the proposed pins/wall combination compared to the traditional full-height pins.
- (ii) The bandwidth of the passband can be enhanced by moving the upper edge of the passband towards higher frequencies due to the use of shorter pins instead of full-height pins, with the same cross-section dimensions (width and height).
- (iii) A good matching between a groove gap waveguide structure and a standard waveguide port can be achieved without the need for a transition.
- (iv) The solid wall in the proposed pin-form can be exploited to make a horizontal slot to be used for wave radiation (as will be shown in Chapter 6) which is not possible with the full-height pins. This is the first time that the sidewalls of gap waveguides can be used for slot radiation.

5.2. The Proposed Unit-Cell Geometry

Since the emergence of gap waveguide technology [1], different pin geometries/forms have been proposed. Fig. 5.1 shows the unit cell geometry of three forms of gap waveguide structures: the traditional (full-height) pin [1], the half-height pin [14] and the proposed pin/wall form. The traditional form of pins is a full-height pin mounted

on one of the parallel plates while the other plate is kept flat. Different shapes of pins are reported in the review, but the square geometry, shown in Fig. 5.1(a), is the most common one. The half-height-pin form, shown in Fig. 5.1(b), is proposed to reduce the fabrication cost of gap waveguide structures. In this form, the full-height conventional pins on one of the parallel plates are divided into two half-height pins located on either plate.

The proposed pin-form consists of a pin mounted on a solid wall as shown in Fig. 5.1(c). The height of the pins and the wall is the same in this case, but the ratio between them can be varied. Both the walls and the pins are created on one of the parallel plates to act as an AMC while the other plate is kept flat (no walls and no pins) to act as a PEC. In all these three pin forms, the height of the pins should be correspondent to the quarter wavelength of the operating frequency.

5.3. S-parameters Investigation

In this section, the scattering parameters (S-parameters) of two-port back-to-back groove gap waveguide structures based on both the traditional and proposed pin-form are investigated. Fig. 5.2 shows the schematic of the bottom plate of three two-port back-to-back groove gap waveguide channels with different types of periodic textures with two rows of pins on each side of the groove: the traditional pins (full-height pin), the proposed pin-form (wall and pin combination) and full-wall (similar to conventional rectangular waveguide but there is a small gap between the top of sidewalls and the upper plate). Each guiding channel consists of two metal plates, where the bottom plate contains the textured surface on the sides with a groove in between while the top plate is kept flat (the top plates of all the structures in Fig. 5.2 are removed to show the groove or cavity and the texture). Two rows of the periodic texture are considered in these three structures. Both the conventional and the proposed structures have exactly the same dimensions of the unit cell of the periodic texture, except the dimension related to the height of pin and wall. In the conventional structure, the pin height h_p of the unit-cell is 2.4 mm ($0.24\lambda_{30\text{ GHz}}$) and no wall is included. While in the proposed structure, pin height h_p = wall height h_w = 1.2 mm

($0.12\lambda_{30\text{ GHz}}$), where $\lambda_{30\text{ GHz}}$ is the wavelength at 30 GHz. Other dimensions of both structures are as follows: air gap height $h_a = 0.1\text{ mm}$ ($0.01\lambda_{30\text{ GHz}}$), pin width or thickness $w = 1\text{ mm}$ ($0.1\lambda_{30\text{ GHz}}$), the periodicity of the pins $p = 3\text{ mm}$ ($0.3\lambda_{30\text{ GHz}}$). The boundary conditions on the sides of the structures are open.

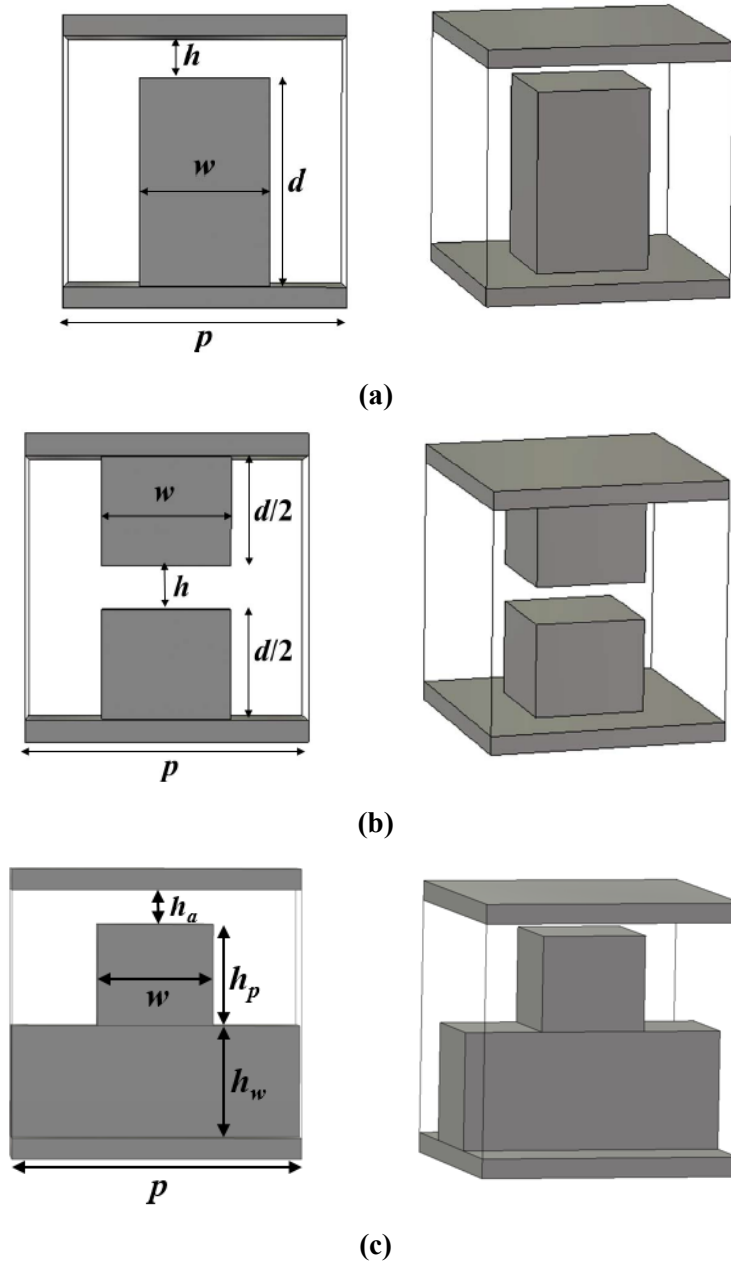


Fig. 5.1. The unit cell geometry of three pin forms for gap waveguide technology. (a) Traditional full-height pin. (b) Half-height pin. (c) Proposed wall and pin form.

As is well known, the electrical contact between the two plates in gap waveguides is not needed for the operation in the stopband of the structure [1]. These structures have the same dimensions, the only difference is the geometry of the pin-form. The total channel length in the direction of wave propagation of the structures is 71 mm. It is worth mentioning that different lengths of guiding channels (48 mm and 101 mm) are also investigated but it is noticed that there is no noticeable difference to be included in this study. High-frequency simulation software, CST, is used for simulation where brass is used as the metal material for all the structures. The width of the groove (similar to the broad dimension in a conventional rectangular waveguide) of all the structures are chosen the same as that of the WR-28 standard rectangular waveguide, which is suitable for Ka-band applications. The height of the groove (the distance between the two parallel plates) in the structures in Fig. 5.2 is chosen to be the quarter wavelength of the frequency 30 GHz which is 2.5 mm. The height of the waveguide port used in this study is the same height of the groove (2.5 mm) to avoid the mismatch problem. In a later study in this chapter, the groove height will be equalised to the height of a standard waveguide port (flange).

The reflection coefficients of both the conventional and the proposed groove gap waveguide structures shown in Fig. 5.2 are investigated for different pins periods (p). Many values of p are tested in this study starting from 1.1 mm to 5 mm with a step of 0.1 mm. Including the results of all the values of p leads to too many curves in one plot and it will not be easy to follow, so just a few values of p were needed to show the difference in performance between the conventional and the proposed groove gap waveguide structures as shown in Fig. 5.3. The reflection coefficients of the conventional and the proposed structures are shown in Fig. 5.3(a) and (b), respectively. In both results, it can be seen that the lower limit of the passband is about 21 GHz which is corresponding to the wavelength $\lambda=14.224$ mm where the width of the groove ($a = \lambda/2 = 7.112$) determines the lower cut-off frequency just similar to the conventional rectangular waveguides. The width of the groove a is the same in both structures. The upper limit of the passband is determined by the height of pins on the sides of the groove as long as the period p is less than $\lambda/4$ of the operating frequency. Otherwise, pins period is the dominant factor in determining the upper limit frequency.

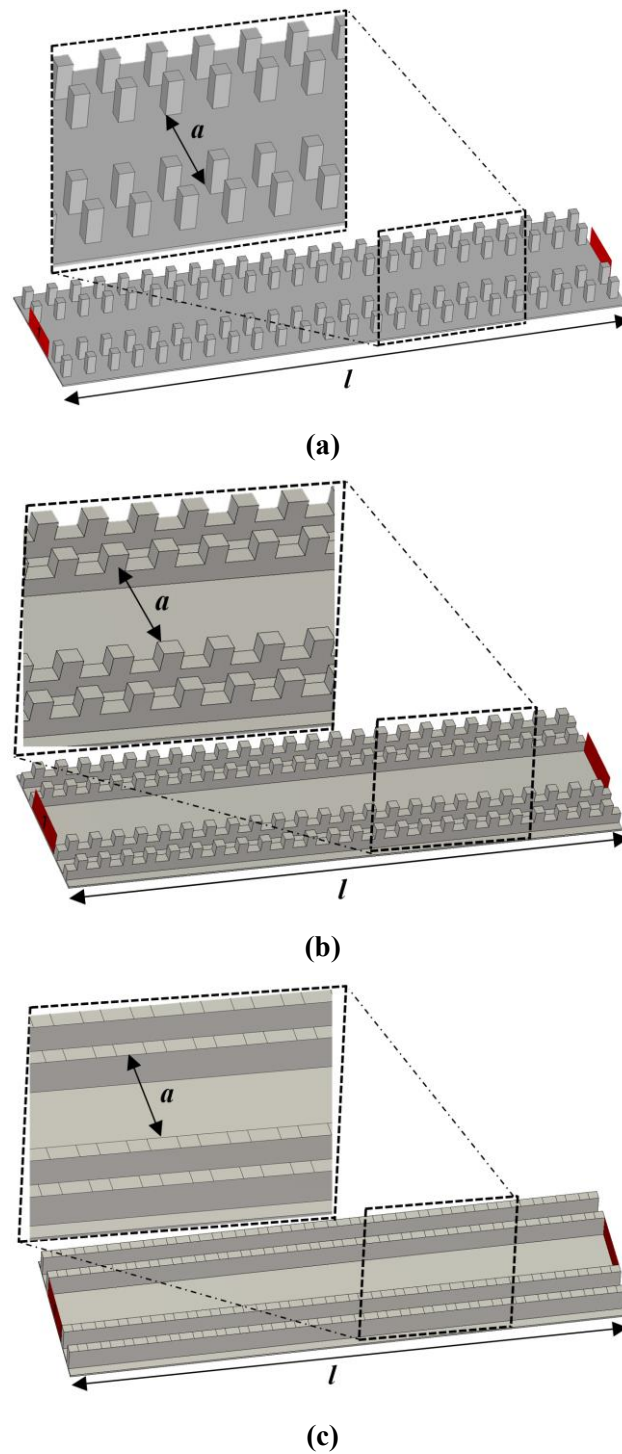
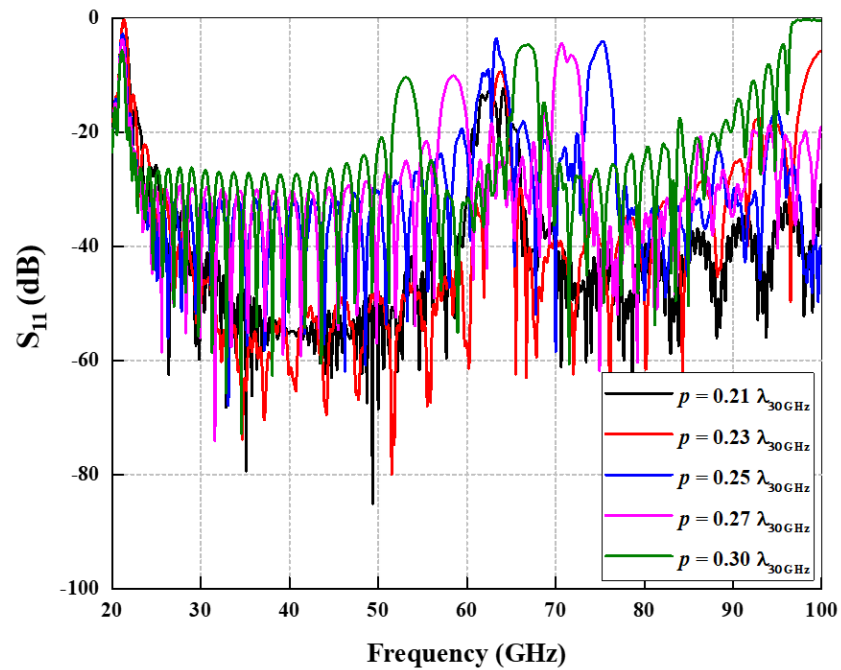


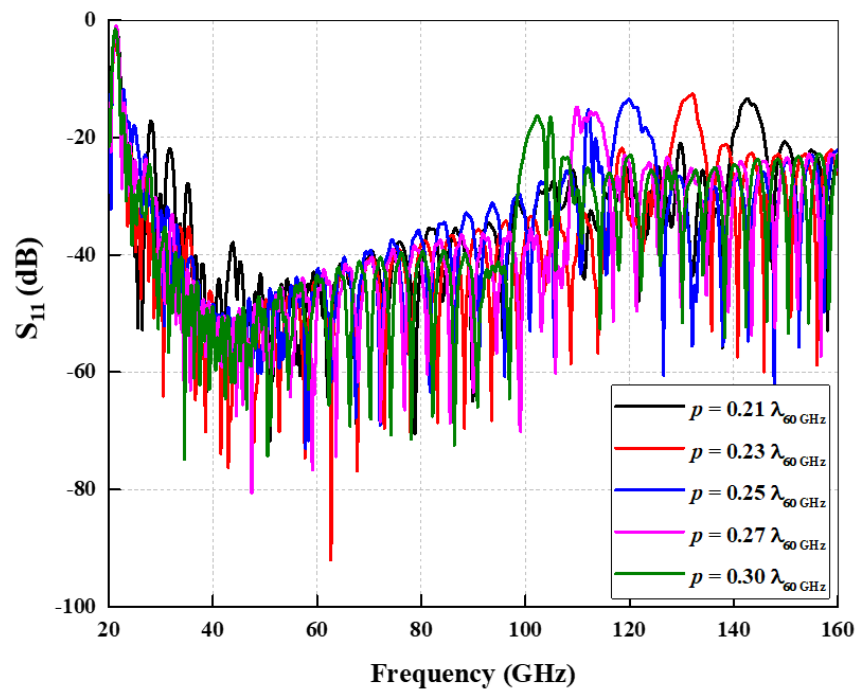
Fig. 5.2. Three two-port back-to-back groove gap waveguide channels with different types of periodic texture with two rows of pins on each side of the groove: (a) the traditional pins (full-pin), (b) the proposed pin-form (wall and pin combination) and (c) full-wall texture. All structures have the same channel length $l = 71$ mm, the same groove width $a = 7.112$ mm and the same groove height $b = 2.5$ mm. The top plates of all the structures are removed to show the groove and the texture.

In Fig. 5.3(a), in the full-height pins case where the pin height $h_p = 2.4$ mm ($h_p = b - h_a$), the frequency of the upper limit is about 62 GHz (the theoretical value is 62.5 GHz) which corresponds to the second harmonic of the frequency of 31.25 GHz with a quarter wavelength of 2.4 mm. However, in Fig. 5.3(b), it can be noted that the upper limit is moved to the frequency 122 GHz (twice that in the case of the traditional form). This is because the pins height in the proposed form is shortened to the half of the traditional one. Theoretically, the periodic structure creates a high impedance surface on both sides of the groove starting from the cut-off frequency (determined by the broad dimension of the groove, as stated above) keeping the EM wave confined inside the groove and following the direction of propagation until a frequency at which the pins height equals the half-wavelength of that frequency. Then the surface impedance at the top of pins is reduced to its lowest value leading to a leakage of the EM waves through the gaps between and above the pins, according to the concept of gap waveguide technology [11].

Fig. 5.4 depicts the relative bandwidth ($f_{\text{end}}/f_{\text{start}}$) as a function of the period p for the structures shown in Fig. 5.2(a) and (b) with the same cross-section of the two grooves, where f_{start} and f_{end} are the start and the end frequencies of the passband, respectively. Starting from the largest value of the period p towards its lower values, the relative bandwidth increases for both structures at a similar level. At this stage, the effect of the period in determining the upper limit of the passband is the dominant compared to the effect of pins height. This increase in the bandwidth continues until the period approaches the quarter wavelength of the operating frequency. After this point, the bandwidth of the traditional structure stays in a constant level when the period p equals 2.5 mm ($\lambda_{30 \text{ GHz}}/4$). However, the bandwidth of the proposed pin-form keeps increasing until the period approaches 1.2 mm ($\lambda_{60 \text{ GHz}}/4$). As a conclusion, with the same cross-section of the groove gap waveguide structure, the passband bandwidth can be almost doubled by changing the geometry of the side pins.



(a)



(b)

Fig. 5.3. S_{11} of two-port back-to-back groove gap waveguide channels for different pin periods of (a) the traditional structure and (b) the proposed structure.

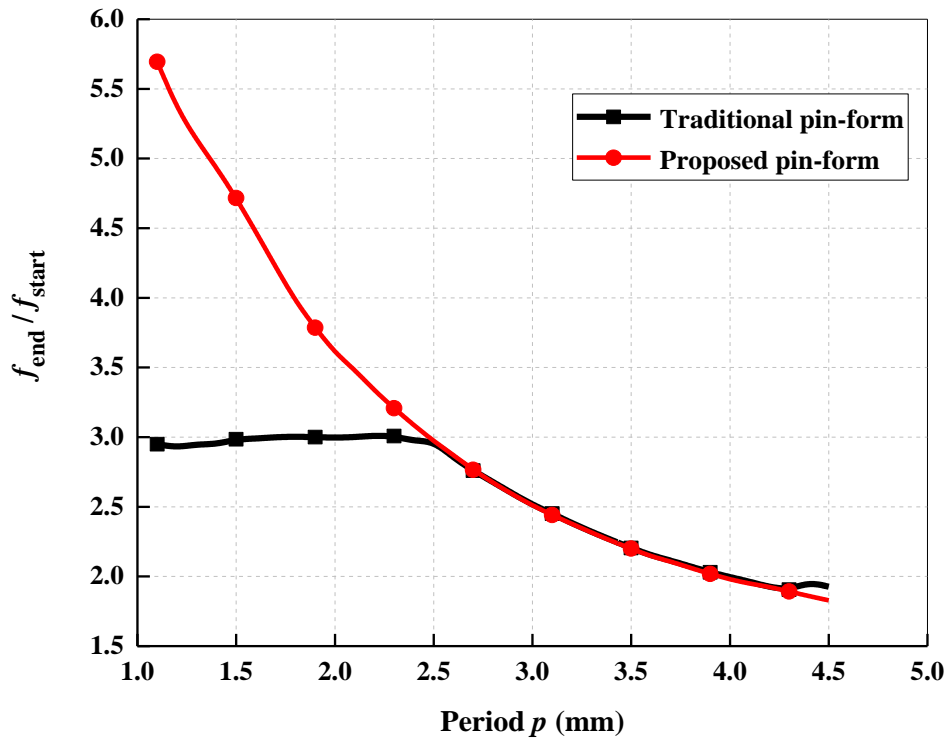


Fig. 5.4. Relative bandwidth (f_{end}/f_{start}) as a function of the period p for two-port back-to-back groove gap waveguide channels based on both the traditional pin-form and the proposed pin-form.

The Full-wall texture shown in Fig. 5.2(c) is indeed a conventional rectangular waveguide with sidewalls but with an intentionally made gap between the top of sidewalls and the upper plate. It can be seen in Fig. 5.5 that the case of full-wall has more leakage due to the absence of the periodic structure with a quarter wavelength height and hence no high impedance surface can be realised unless many walls with very narrow gaps ($\ll \lambda_{30 GHz}$) between them are created [16].

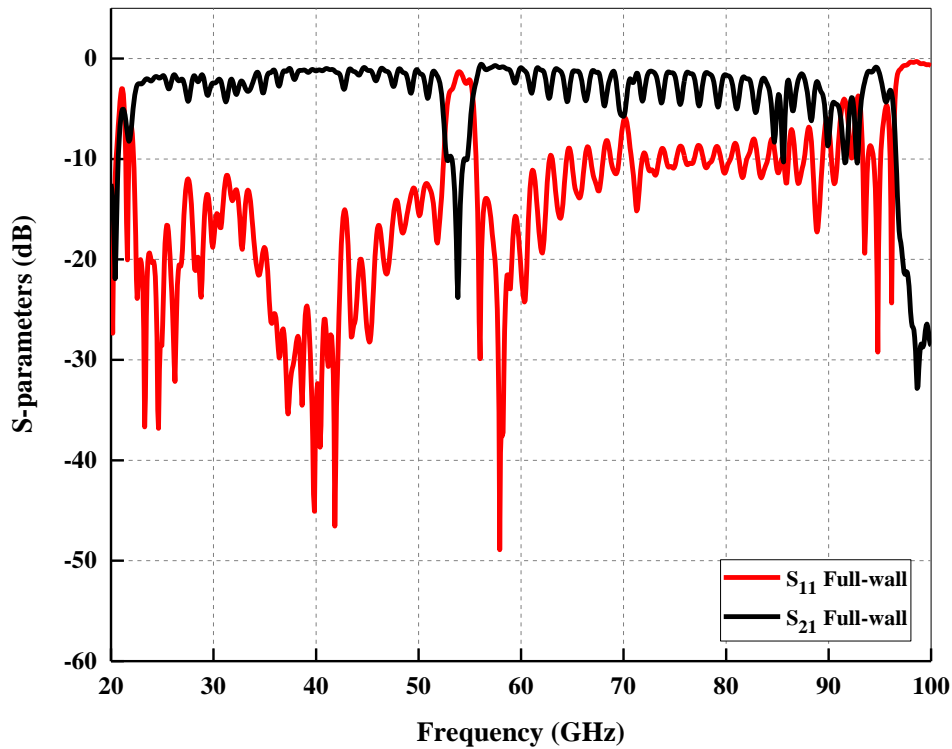


Fig. 5.5. The S-parameters of a back-to-back groove gap waveguide channel with a full-wall texture on each side of the groove as shown in Fig. 5.2(c).

Fig. 5.6 shows a comparison of the S-parameters of two 2-port back-to-back groove gap waveguide channels based on the proposed pin-form with 1-row and 2-row pins on each side of the groove. The unit-cell dimensions are as follows: $h_p = h_w = 1.2$ mm ($0.12\lambda_{30\text{ GHz}}$), $h_a = 0.1$ mm ($0.01\lambda_{30\text{ GHz}}$), $w = 1$ mm ($0.1\lambda_{30\text{ GHz}}$) and $p = 1.2$ mm ($0.12\lambda_{30\text{ GHz}}$), where $\lambda_{30\text{ GHz}}$ is the wavelength at 30 GHz. The boundary conditions on the sides of the structures are open. From the simulations, there is no appreciable difference between the 1-row and 2-row pin forms that can be noticed. Therefore, for the rest of this chapter and the next chapter, all structures will be considered based on one row of the pin-form. With this advantage, we can exploit the solid wall of the proposed structure to make a horizontal slot for wave radiation which is not possible with the conventional gap waveguide structures. This feature will be exploited to design cavity-backed slot antennas in Chapter 6.

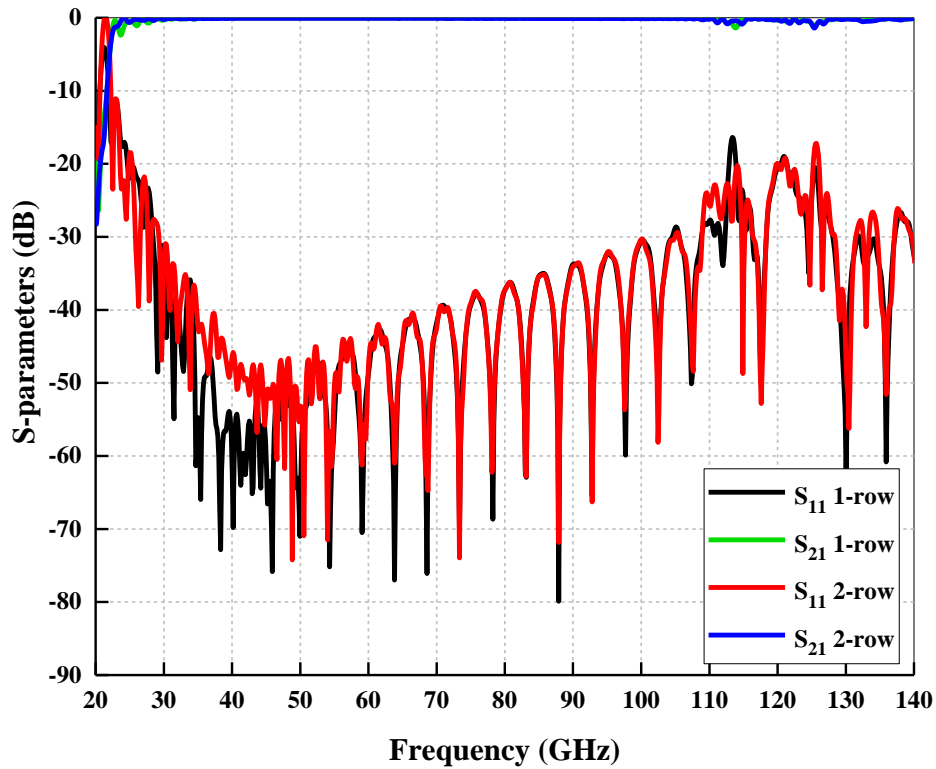


Fig. 5.6. Comparison of the S-parameters of two 2-port back-to-back groove gap waveguide channels based on the proposed pin-form with one row and two rows of pins on each side of the groove.

Fig. 5.7 shows the schematic of the bottom plate (the top plate is removed for clarity) of a two-port back-to-back groove gap waveguide channel with one row of a half-height periodic pins on each side of the groove, which is proposed in [14]. Each half-height pin is located on one of the two parallel plates. The dimensions of the unit cell of the periodic texture used in Fig. 5.7 are the same as those of the traditional pins in Fig. 5.2(a) but the full-height pin is divided into two half-height pins with a height of $h_p = 1.2 \text{ mm}$ ($0.12\lambda_{30 \text{ GHz}}$). The S-parameters of two-port back-to-back groove gap waveguide channels with sidewalls consist of traditional, half-height and proposed pin forms with one row of pins on each side of the groove are depicted in Fig. 5.8. The periodicity of pins in all the three structures equals the quarter wavelength of the operating frequency. It can be noticed from Fig. 5.8 that, for the same cross-section of the groove gap waveguide structure, the reflection coefficient of the half-height pins structure is quite similar to that in the traditional full-height. While wide bandwidth can be achieved with the proposed pin form.

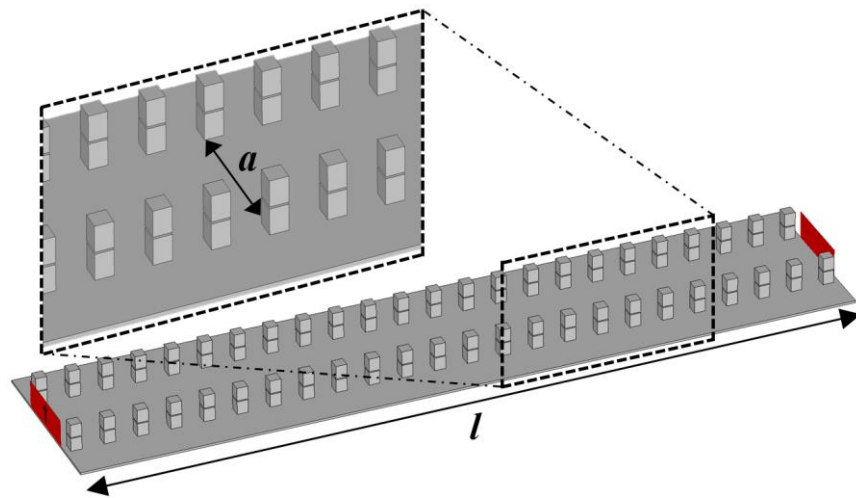


Fig. 5.7. Two-port back-to-back groove gap waveguide channel with half-height pin periodic texture with one row of pins on each side of the groove with a channel length $l = 71$ mm, a groove width $a = 7.112$ mm and a groove height $b = 2.556$ mm. The top plate is removed to show the groove and the texture.

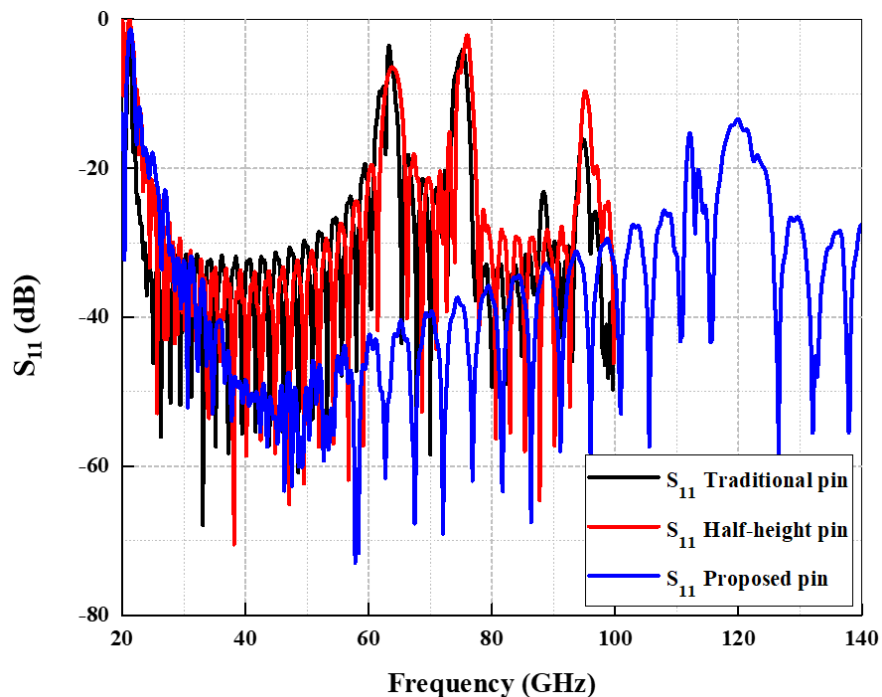


Fig. 5.8. S_{11} of two-port back-to-back groove gap waveguide channels of the traditional, half-height and proposed pin forms with one row of pins on each side of the groove. The periodicity of pins in all the three structures equals the quarter wavelength of the operating frequency.

In conventional rectangular waveguides, the lowest cut-off frequency can be determined by the broad dimension of the waveguide channel. Similarly, in groove gap waveguide structures, the lowest cut-off frequency can be determined by the broad dimension of the groove cross-section. Usually, the unit-cell dimensions are chosen to cover a stopband with an operating frequency away from the cut-off frequency. Using these unit-cells in a periodic structure as two sidewall confines the EM waves inside the groove. They prevent the waves from leaking out through the gap as long as the pins height approaches the quarter wavelength of the operating frequency.

The distance between the two parallel plates in gap waveguides represents the summation of the pin height plus the air gap height between the top of the pins and the top plate. Since the pins height determines the centre frequency of the passband in gap waveguides at which the highest impedance surface can be achieved, it needs to be short enough to be away from the cut-off frequency. Let us now consider the use of the standard waveguide flanges (waveguide-to-coaxial adapters) in the measurement of a conventional groove gap waveguide structure. The width and height of the window of such standard waveguide adapters are fixed. To match the waveguide flange window with the groove window, the cross-sections of both of them need to be identical. In terms of width, it is easy to realise a gap waveguide with a groove that has the same width as the standard waveguide adapter. In this case, both of them will have the same cut-off frequency. However, in terms of height, by using the traditional pin-form (full-height pins), the two heights cannot be the same. Where, for a conventional gap waveguide with dimensions of a standard rectangular waveguide port ($a=2b$), when the pins height is quarter-wavelength, its corresponding frequency is the lower cut-off frequency (f_c , the lower cut-off frequency of the fundamental TE_{10} mode) of the waveguide. The wave shielding effect is the best at this frequency. However, waveguides usually will not be operated at the cut-off frequencies. This difference in the height between the two parts causes a mismatch problem unless an additional matching circuit is used. To avoid this problem, we need to either increase the pins height or enlarge the air gap. In either case, the operation of the gap waveguide will be affected.

Increasing the pins height while maintaining a small air gap as depicted in Fig. 5.9(a) can be one of the solutions for such an issue, but this leads to a potential problem. Because the pins height is almost the same as the distance between the parallel plates, the centre frequency of the operating passband will approach the cut-off frequency of the gap waveguide channel as shown in Fig. 5.10, which is not preferable in most applications. Another solution to keep the height of the joint parts the same is maintaining short pins while increasing the air gap height (see Fig. 5.9(b)) but this reduces the operating bandwidth of the structure as shown in Fig. 5.10. The passband bandwidth is inversely proportional to the air gap height [1].

To mitigate the above challenges, the proposed gap waveguide pin-form using pins mounted on a wall (act as a ground) can shorten the pins as well as maintain a small air gap. To prove this, a back-to-back groove gap waveguide channel with a width and a height exactly the same as the standard WR-28 waveguide adapter is designed.

Fig. 5.11 shows the reflection coefficients of both the conventional and the proposed groove gap waveguide structures shown in Fig. 5.2(a) and (b) for the ratio wall height (h_w):pin height (h_p) of 1/8:7/8. The groove in both structures has a cross-section with dimensions (a and b) exactly the same as the WR-28 standard rectangular waveguide. These dimensions provide a waveguide operating band of 26.5-40 GHz. It can be noticed that over the entire waveguide operating band, the reflection coefficient of the proposed gap waveguide structure (pins/wall combination) has better performance than that in the traditional structure (full-height pins). Also, the upper limit of the passband is shifted to a higher frequency leading to an increased bandwidth. The wall:pin ratio can be varied to obtain different performances based on the specifications of the potential design.

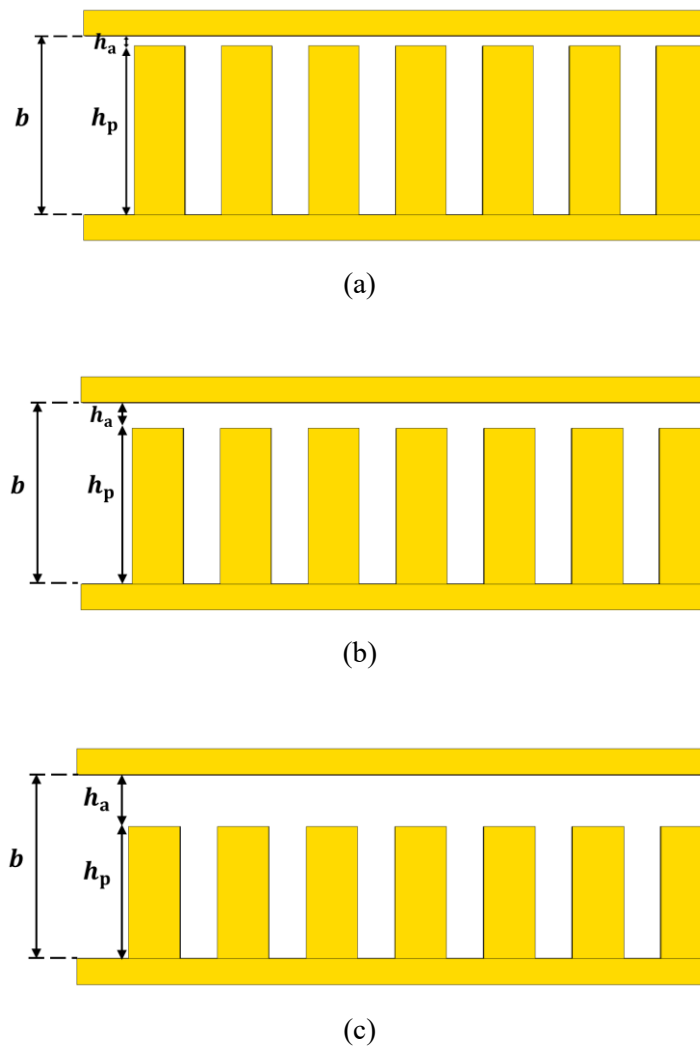


Fig. 5.9. A side view of back-to-back groove gap waveguide channels with a width and a height exactly the same as the standard WR-28 waveguide adapter. The sidewalls consist of traditional full-height pins with different h_p s and h_a s: (a) $h_p=3.456$ mm and $h_a=0.1$ mm, (b) $h_p=2.956$ mm and $h_a=0.5$ mm and (c) $h_p=2.456$ mm and $h_a=1$ mm.

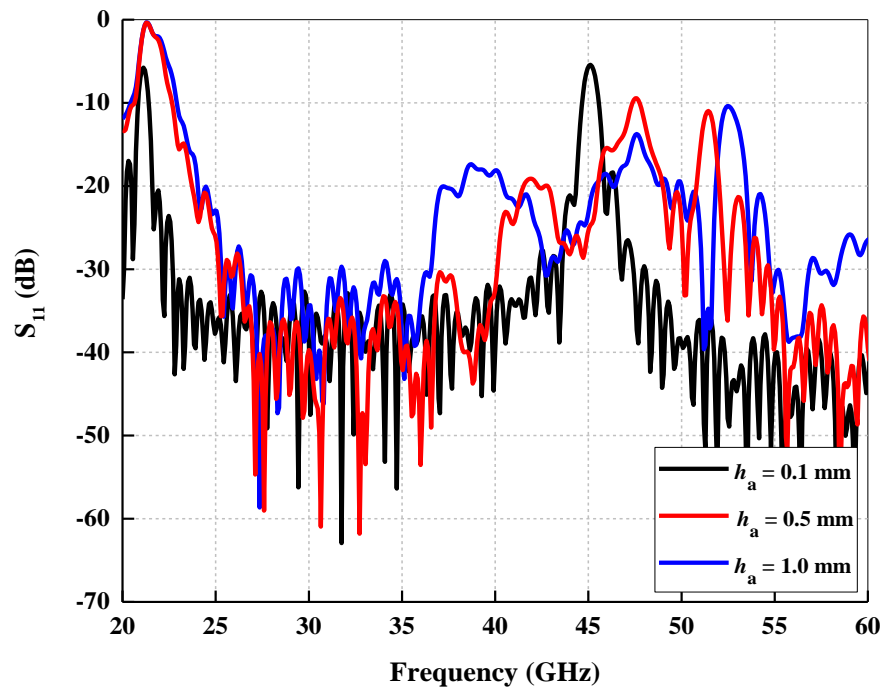


Fig. 5.10. The reflection coefficients of the three cases of back-to-back groove gap waveguide channels shown in Fig. 5.9.

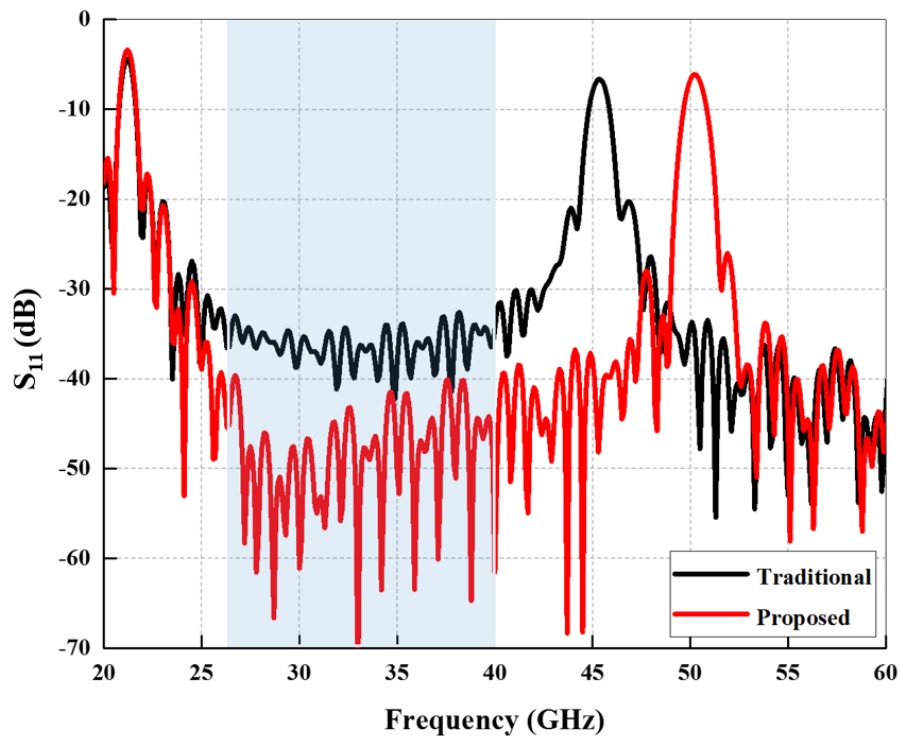
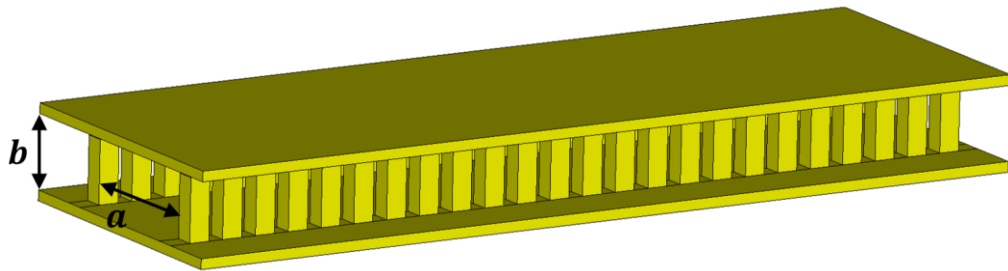
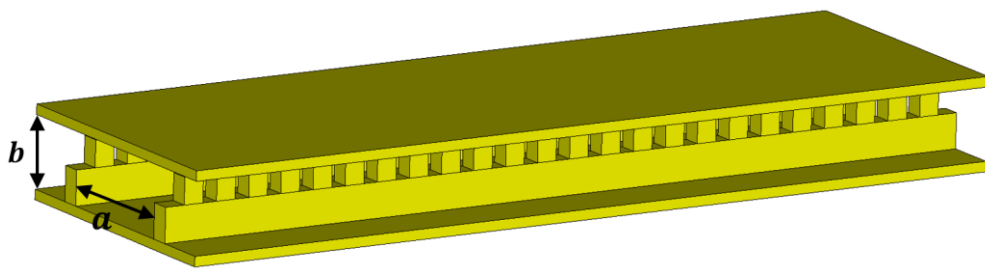


Fig. 5.11. A comparison between the reflection coefficients of back-to-back groove gap waveguide channel based on two types of sidewalls: the traditional full-height pins and the proposed pin/wall combination with a ratio $h_w:h_p = 1/8:7/8$.

Two back-to-back groove gap waveguide structures with a width and a height exactly the same as the standard WR-28 waveguide adapter are designed. The sidewalls consisting of traditional full-height pins and the proposed pin-form are considered as shown in Fig. 5.12(a) and (b), respectively. The reflection coefficients of these two structures are investigated for different pins periods (p) and shown in Fig. 5.13(a) and (b), respectively. When p is less than h_p , the upper edge of the passband is mainly determined by the pins height. While once p becomes equal or larger than h_p , the period between the pins will be the dominant parameter in determining the passband bandwidth as the upper edge of the passband will be dramatically affected.

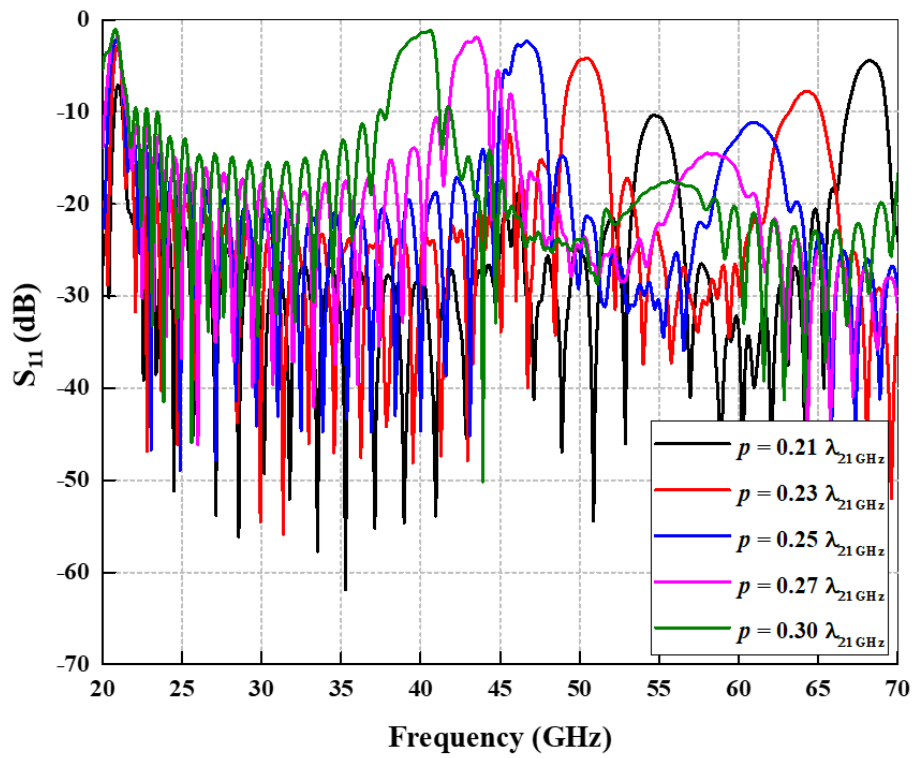


(a)

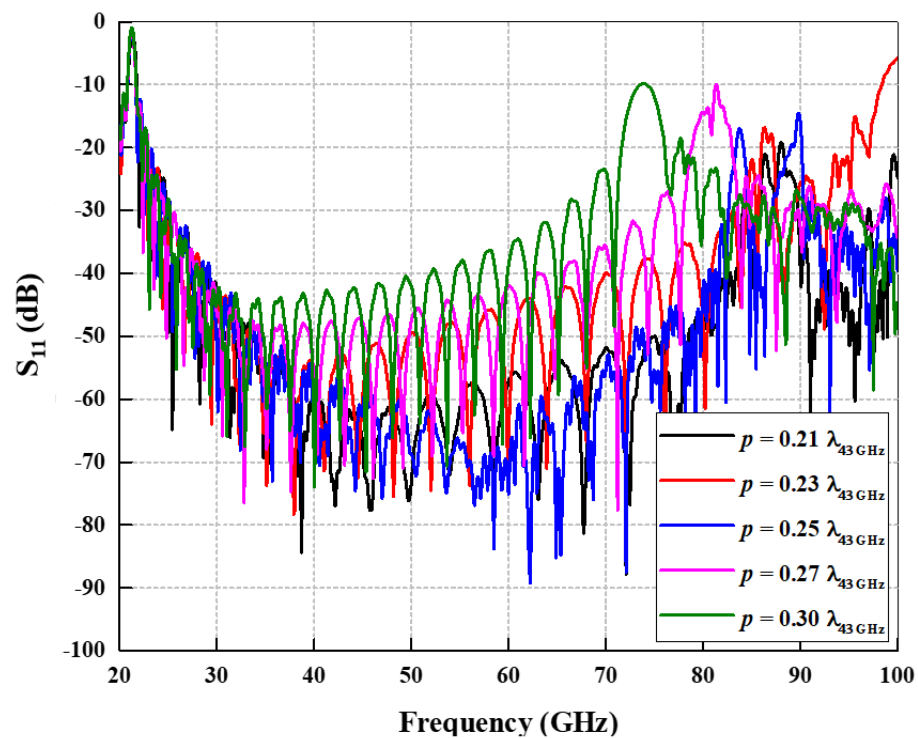


(b)

Fig. 5.12. Back-to-back groove gap waveguide channels with a width and a height exactly the same as the standard WR-28 waveguide adapter ($a=2b$). The one-row sidewalls are represented by (a) traditional full-height pins and (b) proposed pin-form.



(a)



(b)

Fig. 5.13. The reflection coefficients of back-to-back groove gap waveguide channels shown in Fig. 5.12 for different pins periods with sidewalls consisting of (a) the traditional full-height pins and (b) the proposed pin/wall form.

Last, in the proposed pin-form, different ratios between the wall height (h_w) and pin height (h_p) are considered. The ratio $h_w:h_p$ is changed through five ratios with a step of 0.25 as follows: 0:1 (no wall and full-pin), 0.25:0.75, 0.5:0.5, 0.75:0.25 and 1:0 (full-wall and no pin). Fig. 5.14 shows the reflection coefficients of all these ratios. When $h_w:h_p$ is 0:1, i.e. full-height pins, the upper edge of the passband will be limited to a lower value compared to the other ratios. With the increase of h_w which means decrease of h_p , the upper limit of the passband moves towards higher frequencies due to the shortening of the pins. In other words, it can be said that increasing the wall height compared to pin height leads to widening the passband bandwidth. When $h_w=h_p$, the upper edge of the passband moves towards a frequency almost twice as the frequency of the full-height pins because the pins height is reduced to the half, and hence the passband bandwidth is doubled. When $h_w>h_p$ (very small pins), although the upper limit of the passband may be even farther, the performance at lower frequencies near the lower cut-off frequency deteriorates. Finally, the worst obtained results is with the full-wall case (no pins) due to the absence of the periodic structure, i.e the absence of the high impedance surface.

As a conclusion, with the proposed pin-form, the realised bandwidth will be much wider than 2:1, the single-mode bandwidth of a traditional waveguide. On the one hand, the broad bandwidth can be fully utilised by combining the proposed pin-form with other design techniques, such as ridge gap waveguides. On the other hand, to achieve the best in-band performance, the ratio $h_w:h_p$ needs to be chosen carefully to obtain the most effective combination of walls and pins heights to keep waves in the middle of the operating waveguide passband.

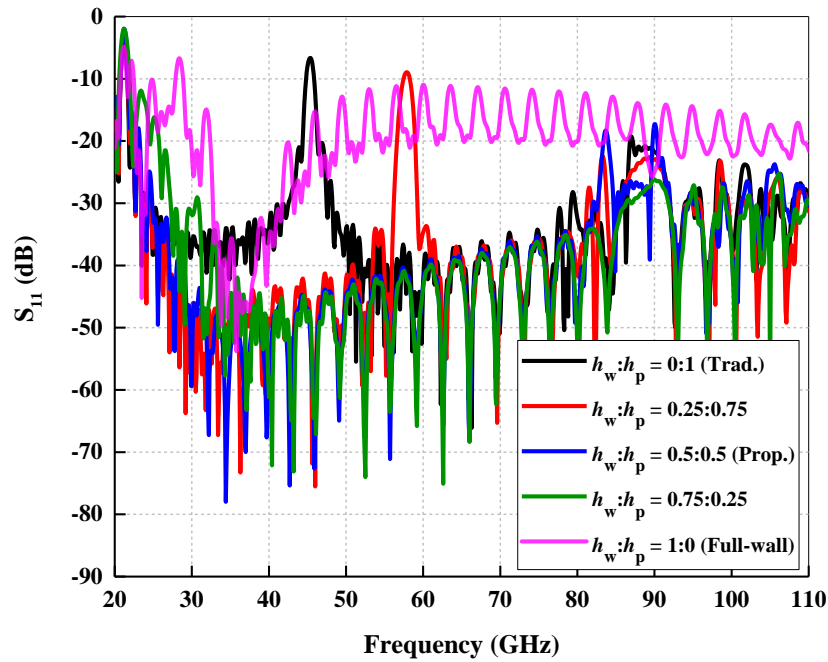


Fig. 5.14. The reflection coefficients of back-to-back groove gap waveguide channel with sidewalls consisting of the proposed pin-form with different $h_w:h_p$ ratios.

5.4. Summary

A novel pin-form of gap waveguide structure has been proposed. In the conventional gap waveguide structures, full-height pins were used as a unit cell. Also, half-height pins were suggested to ease the fabrication process. In this work, pins mounted on a wall has been proposed to form the sidewalls that surround a groove to realise a gap waveguide structure. The S-parameters of back-to-back gap waveguide channels based on the traditional pins, half-height pins and the new pin-form have been analysed. With the proposed gap waveguide pin-form, four main advantages can be obtained: the wave shielding effect will be much better at the operating band compared to the traditional pin-form, the bandwidth can be enhanced, better matching between the designed component and standard waveguide adapters can be achieved without the need for a transition and the sidewalls can be used for wave radiation via a slot created at the solid wall as it will be realised in Chapter 6.

References

- [1] P.-S. Kildal, E. Alfonso, A. Valero-Nogueira, and E. Rajo-Iglesias, "Local metamaterial-based waveguides in gaps between parallel metal plates," *IEEE Antennas Wireless Propag. Lett.*, vol. 8, no. 4, pp. 84–87, Apr. 2009.
- [2] M. S. Sorkherizi, A. Khaleghi, and P.-S. Kildal, "Direct-coupled cavity filter in ridge gap waveguide," *IEEE Trans. Compon., Packag., Manuf. Technol.*, vol. 4, no. 3, pp. 490–495, Mar. 2014.
- [3] E. A. Alós, A. U. Zaman, and P.-S. Kildal, "Ka-band gap waveguide coupled-resonator filter for radio link diplexer application," *IEEE Trans. Compon., Packag., Manuf. Technol.*, vol. 3, no. 5, pp. 870–879, May 2013.
- [4] A. U. Zaman, P.-S. Kildal, and A. A. Kishk, "Narrow-band microwave filter using high-Q groove gap waveguide resonators with manufacturing flexibility and no sidewalls," *IEEE Trans. Compon., Packag., Manuf. Technol.*, vol. 2, no. 11, pp. 1882–1889, Nov. 2012.
- [5] H. Raza and J. Yang, "Compact UWB power divider packaged by using gap-waveguide technology," in *Proc. 6th Eur. Conf. Antennas Propag. (EuCAP)*, Prague, Czech Republic, Mar. 2012, pp. 2938–2942.
- [6] J. Yang and H. Raza, "Empirical formulas for designing gap waveguide hybrid ring coupler," *Microw. Opt. Technol. Lett.*, no. 8, pp. 1917–1920, 2013.
- [7] Bahaa Al-Juboori, Jiafeng Zhou, Yi Huang, Muaad Hussein, Ahmed Alieldin, William J. Otter, Dirk Klugmann, Stepan Lucyszyn, "Lightweight and Low-Loss 3-D Printed Millimeter-Wave Bandpass Filter Based on Gap-Waveguide," in *IEEE Access*, vol. 7, pp. 2624–2632, 2019.
- [8] P.-S. Kildal, A. U. Zaman, E. Rajo-Iglesias, E. Alfonso, and A. Valero Nogueira, "Design and experimental verification of ridge gap waveguide in bed of nails for parallel-plate mode suppression," *IET Microw., Antennas Propag.*, vol. 5, no. 3, pp. 262–270, Feb. 2011.
- [9] E. Pucci, A. U. Zaman, E. Rajo-Iglesias, and P.-S. Kildal, "New low loss inverted microstrip line using gap waveguide technology for slot antenna applications," in *Proc. 5th Eur. Conf. Antennas Propag. (EuCAP)*, Rome, Italy, Apr. 2011, pp. 979–982.

-
- [10] E. Rajo-Iglesias and P.-S. Kildal, "Groove gap waveguide: A rectangular waveguide between contactless metal plates enabled by parallel-plate cut-off," in *Proc. 4th Eur. Conf. Antennas Propag. (EuCAP)*, Barcelona, Spain, Apr. 2010.
- [11] E. Rajo-Iglesias and P.-S. Kildal, "Numerical studies of bandwidth of parallel-plate cut-off realised by a bed of nails, corrugations and mushroom-type electromagnetic bandgap for use in gap waveguides," *IET Microw., Antennas Propag.*, vol. 5, no. 3, pp. 282–289, Feb. 2011.
- [12] A. U. Zaman, V. Vassilev, P.-S. Kildal, and A. Kishk, "Increasing parallel plate stop-band in gap waveguides using inverted pyramid-shaped nails for slot array application above 60 GHz," in *Proc. 5th Eur. Conf. Antennas Propag. (EuCAP)*, Rome, Italy, Apr. 2011, pp. 2254–2257.
- [13] S. I. Shams and A. A. Kishk, "Double cone ultra wide band unit cell in ridge gap waveguides," in *Proc. IEEE Antennas Propag. Soc. Int. Symp. (APSURSI)*, Jul. 2014, pp. 1768–1769.
- [14] F. Fan, J. Yang, V. Vassilev and A. U. Zaman, "Bandwidth Investigation on Half-Height Pin in Ridge Gap Waveguide," in *IEEE Transactions on Microwave Theory and Techniques*, vol. 66, no. 1, pp. 100-108, Jan. 2018.
- [15] Dongquan Sun, Xiang Chen, Jing-Ya Deng, Li-Xin Guo, Wanzhao Cui, Kang Yin, Zhenhua Chen, Changfei Yao, Feng Huang, "Gap Waveguide With Interdigital-Pin Bed of Nails for High-Frequency Applications," in *IEEE Transactions on Microwave Theory and Techniques*, vol. 67, no. 7, pp. 2640-2648, July 2019.
- [16] D. Sievenpiper, Lijun Zhang, R. F. J. Broas, N. G. Alexopolous and E. Yablonovitch, "High-impedance electromagnetic surfaces with a forbidden frequency band," in *IEEE Transactions on Microwave Theory and Techniques*, vol. 47, no. 11, pp. 2059-2074, Nov. 1999.
- [17] CST Microwave Studio. CST, Inc. [Online]. Available: <http://www.cst.com>.

Chapter 6. A Cavity-Backed Slot Antenna and Filtering Antenna Based on Gap Waveguide Using Novel Sidewalls

Based on the new gap waveguide structure proposed in Chapter 5, a cavity-backed slot antenna (CBSA) and a cavity-backed slot filtering antenna (CBSFA) are designed and simulated by cutting a window at the end of a guiding structure. Two different bands are used to design these components; for the CBSA, the X-band is chosen while the Ka-band is adopted for the CBSFA. The resonant frequency of the CBSA is 10GHz and that of the CBSFA is 30.5 GHz. The fractional bandwidth (FBW) is 5% and 6.3% for the CBSA and CBSFA, respectively. Both antennas are fabricated using computer numerical control (CNC) milling technology. The simulated and measured results of the proposed antennas are in good agreement.

6.1. Cavity-Backed Slot Antenna (CBSA)

6.1.1. Concept of CBSA

An extensive review of cavity-backed slot antennas operating at mmWave frequency bands is conducted in Chapter 2. CBSA consists of a resonant metal cavity, having a slot for electromagnetic wave radiation. A slot antenna is often compared to a conventional half-wave dipole consisting of two flat metal strips, where the metal strips have dimensions that perfectly fits into a slot cut out of a large metal sheet. Therefore, based on Babinet's principle, a complementary dipole is another name for a slot antenna, as shown in Fig. 6.1.

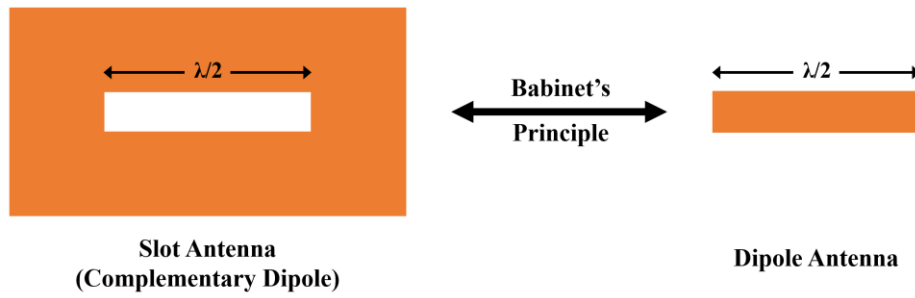


Fig. 6.1. Dipole antenna (right) and its complementary slot Antenna (left).

6.1.2. The Proposed CBSA Structure

A unit cell, consisting of an air groove surrounded by pins mounted on a solid wall on each side, is shown in Fig. 6.2. To design a CBSA based on the pin-form texture that proposed in Chapter 5, the X-band (8-12 GHz) is chosen. The width of the groove ($a = \lambda_g/2$) determines the lower cut-off frequency just similar to the conventional rectangular waveguides, while the pins height determines the upper frequency of the passband at which the pins height equals the half-wavelength of that frequency, as long as the period p is less than $\lambda/4$.

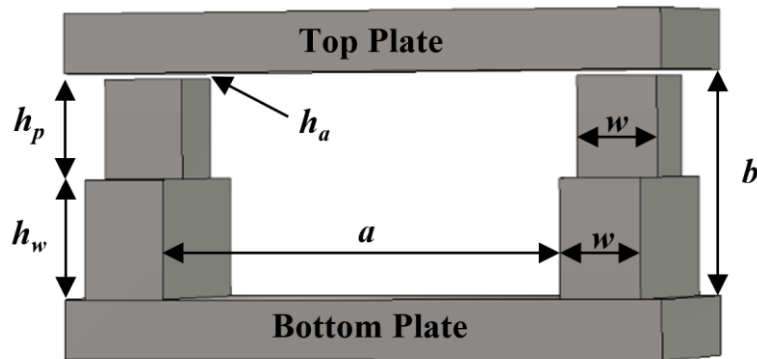


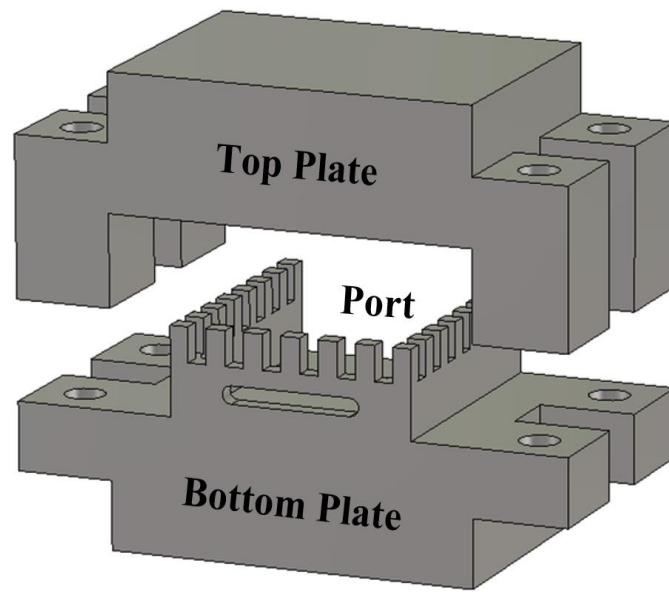
Fig. 6.2. A unit cell of the proposed gap waveguide structure including a groove between two of the proposed pin-form.

To demonstrate the usefulness of the proposed groove gap waveguide structure, Fig. 6.3 shows the designed CBSA. The designed CBSA consists of an air cavity (groove)

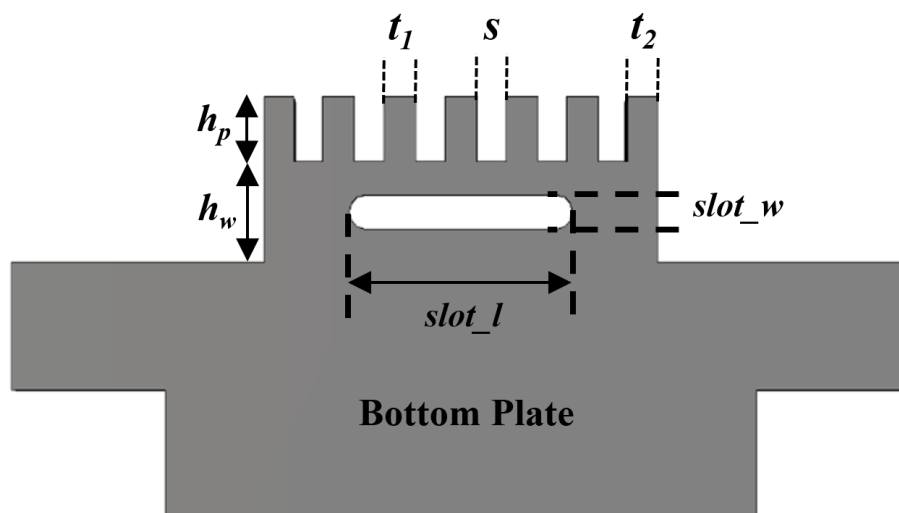
with a cross-section exactly the same as the cross-section of the standard WR-90 waveguide flange interface. This cavity is surrounded by one row of the proposed pin-form on each side and the lower and upper plates. In the simulations, a waveguide port with the same dimensions of the standard WR-90 waveguide flange is placed at one side of the cavity while a slot (aperture) is drilled through the solid metal wall at the opposite side as shown in Fig. 6.3. The slot length is chosen to be approximately $\lambda_{10\text{ GHz}}/2$ and the slot width is less than $\lambda_{10\text{ GHz}}/10$, where $\lambda_{10\text{ GHz}}$ is the wavelength at the resonant frequency of the CBSA at 10 GHz. The thickness of the slot is the same as the metal wall. Having the advantage of the proposed pin form that it is possible to design a groove gap waveguide structure with cross-section dimensions as the same as the standard waveguide adapters, there is no need to design a transition. In Fig. 6.3a, the upper plate is raised to show details of the lower plate. The dimensions of the proposed structure and the slot are shown in Fig. 6.3b. It is noteworthy that the boundary conditions of the structure are chosen to be open (with space) from all sides. The optimised parameters of the proposed CBSA are shown in Table 6.1.

Table 6.1. The optimised parameters of the proposed CBSA (Unit: mm).

Parameter	Description	Value
<i>a</i>	groove width	22.86
<i>b</i>	groove height	10.16
<i>h_a</i>	air gap height	0.300
<i>h_p</i>	pin height	4.930
<i>h_w</i>	wall height	4.930
<i>w</i>	pin width	2.000
<i>p</i>	periodicity of pins	4.000
<i>s</i>	space between pins	2.000
<i>slot_l</i>	slot length	15.25
<i>slot_w</i>	slot width	2.000
<i>t₁</i>	pin thickness #1	2.170
<i>t₂</i>	pin thickness #2	2.000



(a)



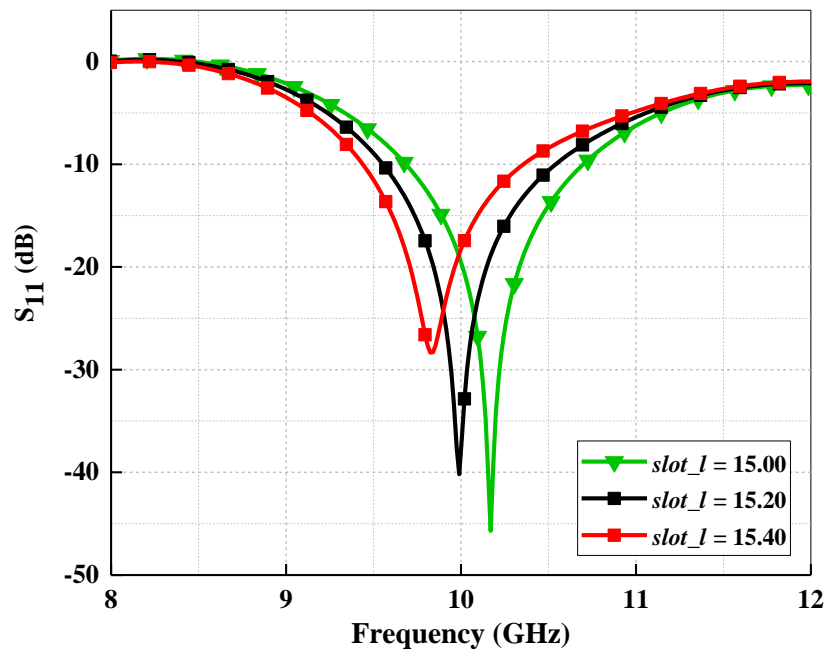
(b)

Fig. 6.3. The proposed CBSA. (a) 3D view. (b) Front view of the bottom plate with its dimensions (the upper lid is removed for clarity).

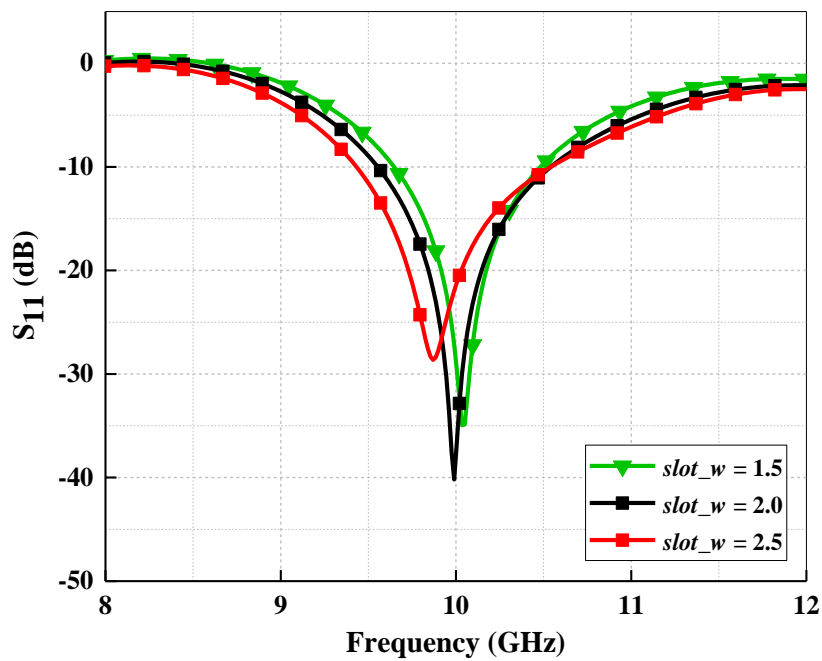
6.1.3. Simulations and Measurements

To demonstrate the influence of the slot dimensions on the frequency response of the proposed structure, a parametric study is carried out and shown in Fig. 6.4. It can be clearly noticed in Fig. 6.4(a) that a slight change in the slot length ($slot_l$) dramatically affects both reflection loss and resonant frequency of the device. It can be observed in Fig. 6.4(b) that the slot width ($slot_w$) will affect the bandwidth of the antenna. The whole structure of the optimised CBSA is shown in Fig. 6.3a. The metal used is brass. Fig. 6.5 depicts the fabricated CBSA prototype with the measurement setup, which is manufactured using CNC milling technology. The prototype CBSA is measured using an Anritsu 37369A vector network analyzer (VNA) with a standard WR-90 waveguide flange interface. A Thru-Reflect-Line (TRL) calibration was first performed to calibrate the VNA, the cables and the waveguide. The simulated and measured reflection coefficients of the proposed antenna are shown in Fig. 6.6. The measured $|S_{11}|$ of the proposed antenna is in good agreement with the simulated one. For better comparison, the measured $|S_{11}|$ is coincided with the simulated one. The measured resonant frequency is 0.2 GHz lower than the predicted one. Also, it can be noticed that the bandwidth of the measured $|S_{11}|$ is narrower than the simulated one. The mismatching between the simulated and measured results could be attributed to the manufacturing error. Nevertheless, it should be noted that the results were obtained after the first fabrication and no tuning was needed to achieve these measured results.

To further investigate the discrepancy, the CBSA structure is simulated again, taking into consideration the dimensions of the fabricated prototype. The blue curve in Fig. 6.6 represents the simulated performance of the post-fabrication antenna, showing the effect of manufacturing tolerance compared with the original response. Furthermore, the simulated 3D radiation pattern of the proposed antenna is shown in Fig. 6.7. The simulated and measured normalised 2D radiation patterns of the proposed cavity-backed slot antenna are shown in Fig. 6.8. It is apparent that the proposed CBSA has good agreement in radiation pattern between the simulation and measurements. In conventional gap waveguide structures, radiation can only be realised by slots created on the lower and upper plates, while with the proposed gap waveguide structure it can also be realised by slots on the side walls.

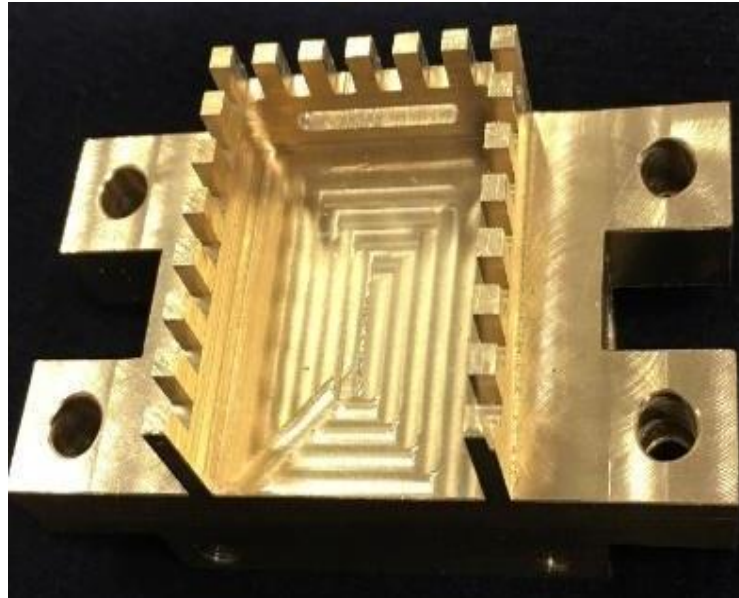


(a)

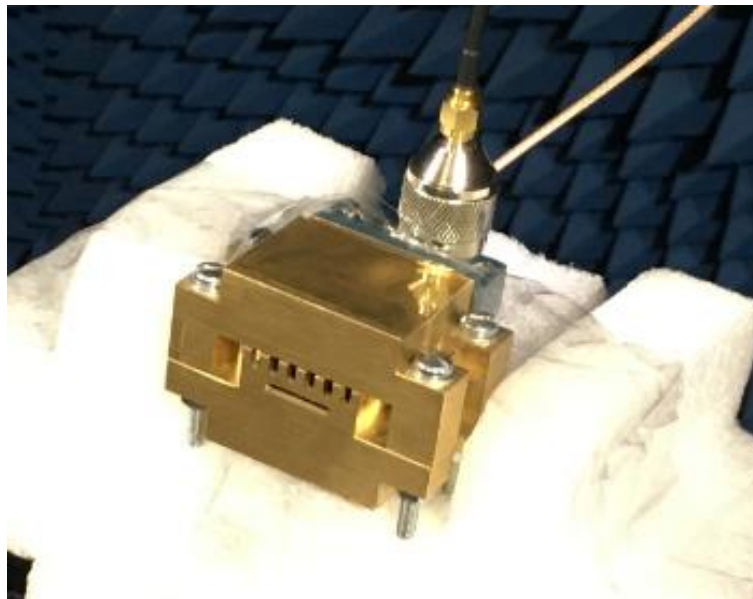


(b)

Fig. 6.4. Simulated reflection coefficient $|S_{11}|$ of the proposed cavity-backed slot antenna. (a) $slot_l$ effect. (b) $slot_w$ effect.



(a)



(b)

Fig. 6.5. A photograph of the proposed CBSA based on the new gap waveguide structure. (a) The bottom plate (the upper lid is removed for clarification). (b) The whole structure with the measurement setup.

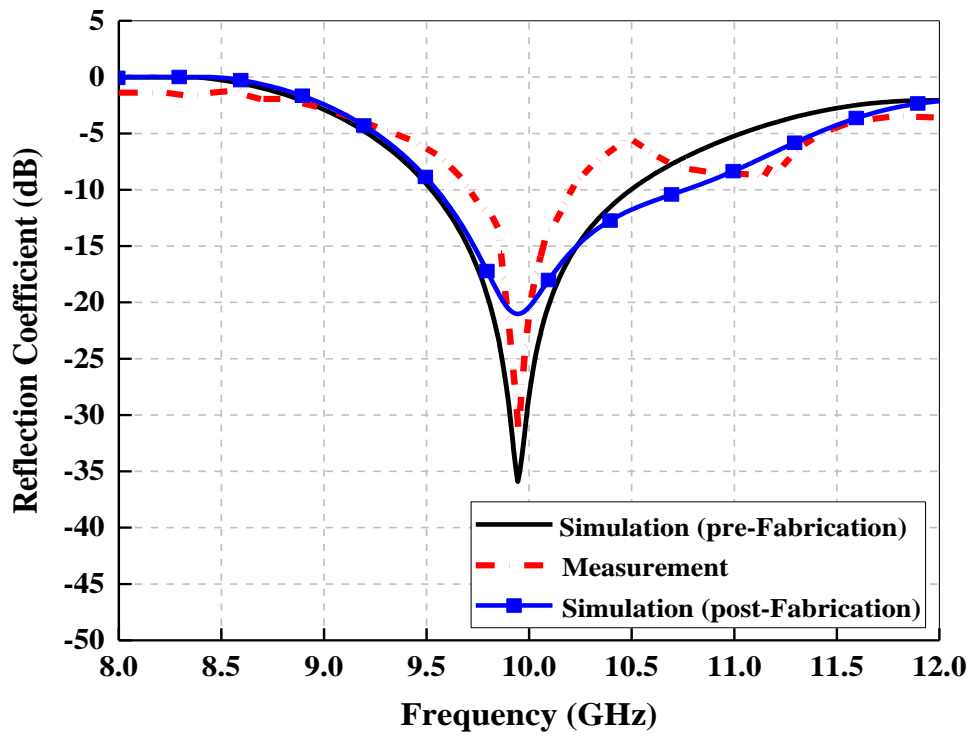


Fig. 6.6. Simulated (pre- and post-fabrication) and measured reflection coefficients of the proposed CBSA.

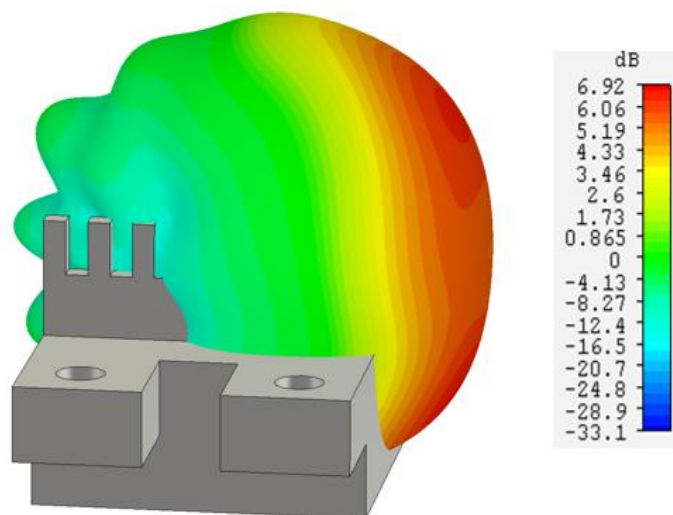


Fig. 6.7. The simulated 3D radiation pattern of the proposed CBSA at 9.74 GHz.

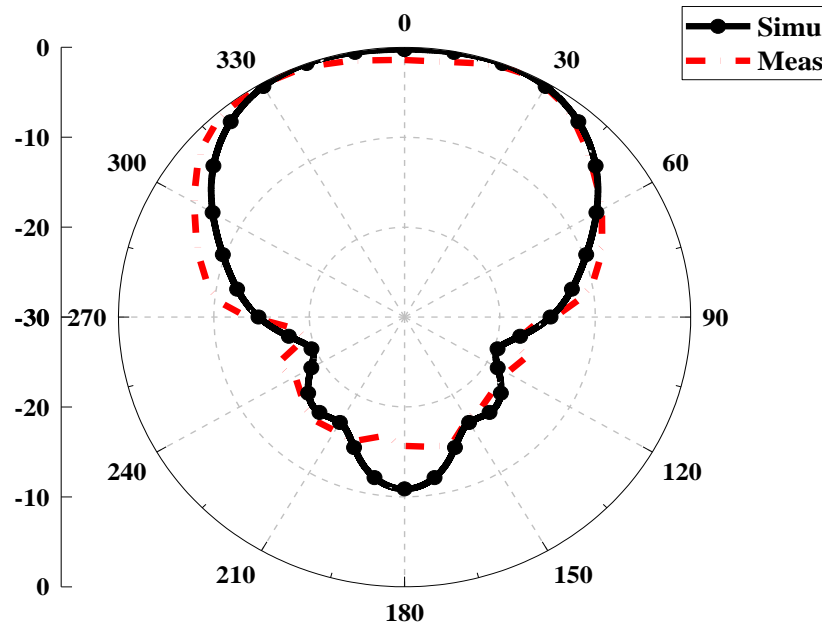


Fig. 6.8. Simulated and measured normalised 2D radiation patterns of the proposed CBSA at 9.74 GHz.

6.2. Cavity-Backed Slot Filtering Antenna (CBSFA)

6.2.1. A Brief Concept of CBSFA

The cavity-backed slot filtering antennas (CBSFA) were reported in the past few years [2], [3]. Comparing with other types of antennas, the CBSFAs have the advantages of low loss, high power-handling capacity and easiness of integration with other circuits. Using a conventional gap waveguide, a CBSFA can usually be achieved by etching a slot in either the upper plate or the lower plate. However, by using the proposed groove gap waveguide structure, this type of antennas can be achieved by etching a horizontal slot in the side- or end-wall (the proposed wall). So, now the location of the slot in gap waveguide slot antennas can be at any side of the antenna geometry instead of only the lower or upper plates as in the conventional gap waveguides. This will result in that the design of a multidirectional (so-called omnidirectional) antenna using gap waveguide structures. The slot leads to a leakage of the electromagnetic wave, forming the radiating element of the antenna. In this way, the radiating element and the

resonators of a filter can be seamlessly integrated without adding any extra circuits or increasing volume.

6.2.2. CBSFA Design

A filtering antenna (filtenna) is an antenna integrated with a filter. To achieve the cavity-backed slot filtering antenna, a counterpart bandpass filter is usually designed first as a reference with the required coupling coefficients and external quality factors. Then the last resonator is replaced by a slot antenna, which is designed to have a consistent external quality factor. As a common case, a band pass filter with Chebyshev responses is used. The steps for designing a filtering antenna can be summarised as following:

- (i) The specifications, including the order of the resonators n , centre frequency, ripple level in the band L_{Ar} and the fractional bandwidth of the bandpass filter are given first.
- (ii) According to the specifications, the required external quality factor Q_{ex} and the coupling coefficients between the resonators M_{ij} , where i and j are the indices of resonators, can be achieved by utilising the bandpass filter synthesis technology.
- (iii) Using a full-wave simulation, the required Q_{ex} and m_{ij} can be realised and the corresponding parameters among the resonators can be obtained.
- (iv) For a filtering antenna, calculate the external quality factor of the last resonator Q_{ex2} .
- (v) The desired filtering antenna with the frequency responses as the counterpart bandpass filter is then achieved.

A perspective view of the designed filtering antenna, built based on the new groove gap waveguide structure, is depicted in Fig. 6.9. The upper plate is raised to show details of the lower plate. Fig. 6.10 is a schematic of the proposed filtering antenna showing the dimensions of the whole structure. A cylinder (Q-cylinder) is placed on the bottom plate 1 mm away from the feeding port edge in the direction of propagation and at the centre between the lateral walls. By tuning the dimensions of this cylinder,

the external quality factor can be adjusted. To adjust the resonant frequency and bandwidth, two metal coupling cylinders are placed between the resonators. The specifications of the designed Ka-band 3rd-order Chebyshev bandpass filter bandpass filter with a passband equal-ripple $L_{Ar} = 0.1$ dB are as follows:

Centre frequency (f_0) = 30.5 GHz

Fractional bandwidth (FBW) = 6.3%

Return loss > 15 dB.

By using the design equations in Chapter 3 and tables in the literature [4] with the filter specifications, the values of the external quality factor and the coupling coefficients between the resonators M_{ij} are achieved to be: $Q_{ex1} = 16.37$ and $M_{12} = M_{23} = 0.058$.

The external quality factor of the last resonator of the proposed filtering antenna Q_{ex2} can be expressed by using the loaded quality factor Q_L and the unloaded quality factor Q_U [5],

$$\frac{1}{Q_{ex2}} = \frac{1}{Q_L} - \frac{1}{Q_U} \quad (6.1)$$

Using the method presented in [5], Q_L can be extracted from the reflection coefficients,

$$Q_L = \frac{f_0}{f_2 - f_1} \quad (6.2)$$

where f_0 is the resonant frequency of the loaded resonator at the minimum reflection coefficient S_{11}^{min} , f_1 and f_2 are the corresponding frequencies when $S_{11} = S_{11}^\phi$, where S_{11}^ϕ is defined as

$$S_{11}^\phi = 10 \log \frac{1 + 10^{S_{11}^{min}/10}}{2} \quad (6.3)$$

The unloaded quality factor Q_U can be calculated by using [5],

$$Q_U = Q_L(1 + k), \quad (6.4)$$

where k is the coupling coefficient between the excitation port and the last resonator of the filtering antenna which can be extracting using,

$$k = \frac{1 - 10^{S_{11}^{min}/20}}{1 + 10^{S_{11}^{min}/20}} \quad (6.5)$$

Similar to CBSA, the slot on the CBSFA is created at the centre of the solid wall under the pins at the end of the filtenna structure. The slot length is chosen to be 4.8 mm ($\sim \lambda_{\text{CBSFA}}/2$) and the slot width is 0.9 mm (less than $\lambda_{\text{CBSFA}}/10$), where λ_{CBSFA} is the wavelength of the resonant frequency of the CBSFA. The thickness of the slot is 1.5 mm which is slightly more than the lateral walls for matching purposes. The width and height of the cavity is kept similar to the width and height of the standard WR-28 waveguide feeding port. It is noteworthy that the boundary conditions of the structure are chosen to be open (with space) from all sides. All the optimised dimensions of the proposed CBSFA are shown in Table 6.2.

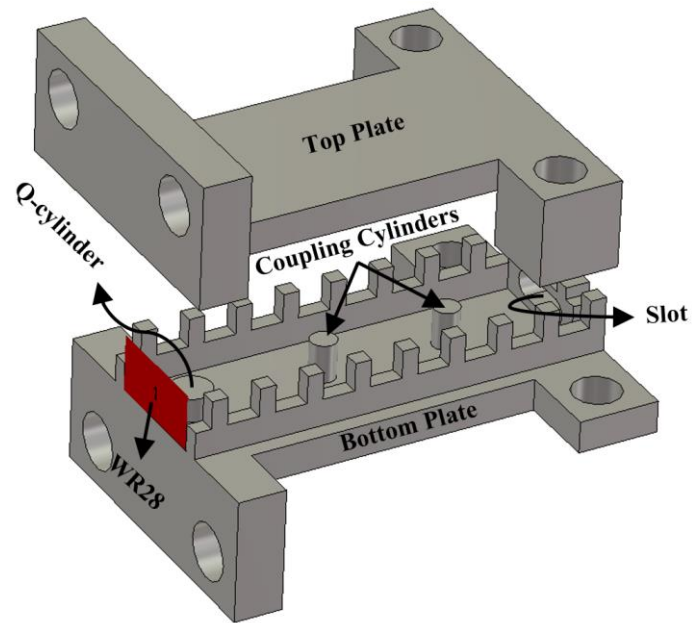
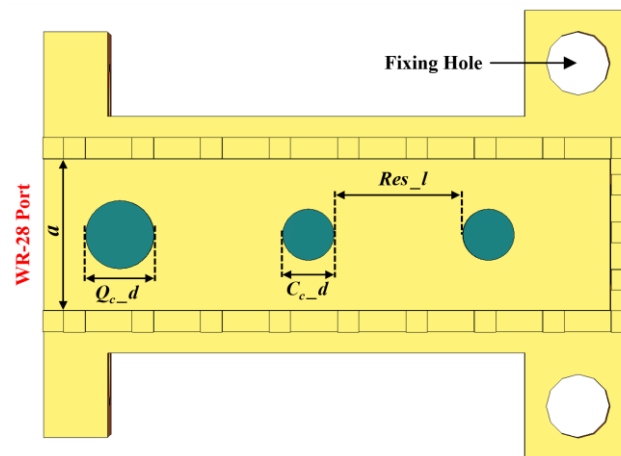


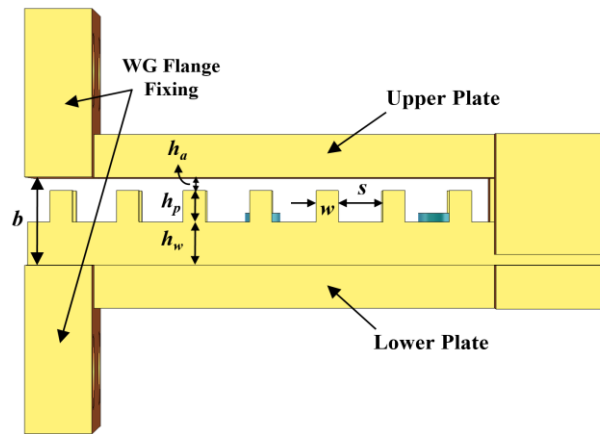
Fig. 6.9. The filtering antenna structure (The upper plate is lifted for clarity).

Table 6.2. The optimised parameters of the proposed CBSFA (Unit: mm).

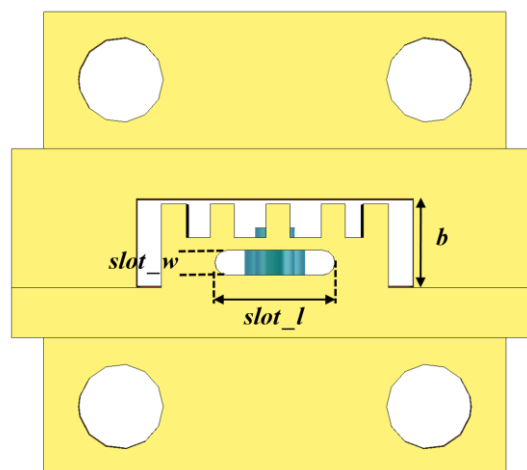
Parameter	Description	Value
a	groove width	7.112
b	groove height	3.556
h_a	air gap height	0.100
h_w	wall height	1.728
h_p	pin height	1.728
w	pin width	1.000
s	space between pins	2.000
$slot_l$	slot length	4.810
$slot_w$	slot width	0.900
C_c_d	coupling cylinder diameter	1.600
C_c_h	coupling cylinder height	2.400
Q_c_d	Q-cylinder diameter	2.500
Q_c_h	Q-cylinder height	1.500
Res_l	resonator length	6.270



(a)



(b)



(c)

Fig. 6.10. The schematic of the proposed filtering antenna. (a) Top view (The upper plate is removed for clarity). (b) Lateral view. (c) Front view showing the radiation slot.

6.2.3. CBSFA Results

A- Simulations

To demonstrate the importance of the antenna and filter combination, the reflection coefficient of the antenna with and without filter is plotted in Fig. 6.11. It can be seen that the selectivity of the antenna is much improved with the presence of the bandpass filter. Furthermore, the simulated 3D radiation patterns of the proposed filtering antenna at different frequencies are shown in Fig. 6.12. From the 3D radiation patterns, the filtering effect can be easily noticed when the radiation of the designed filtering antenna is examined at different frequencies, below, in and above the passband.

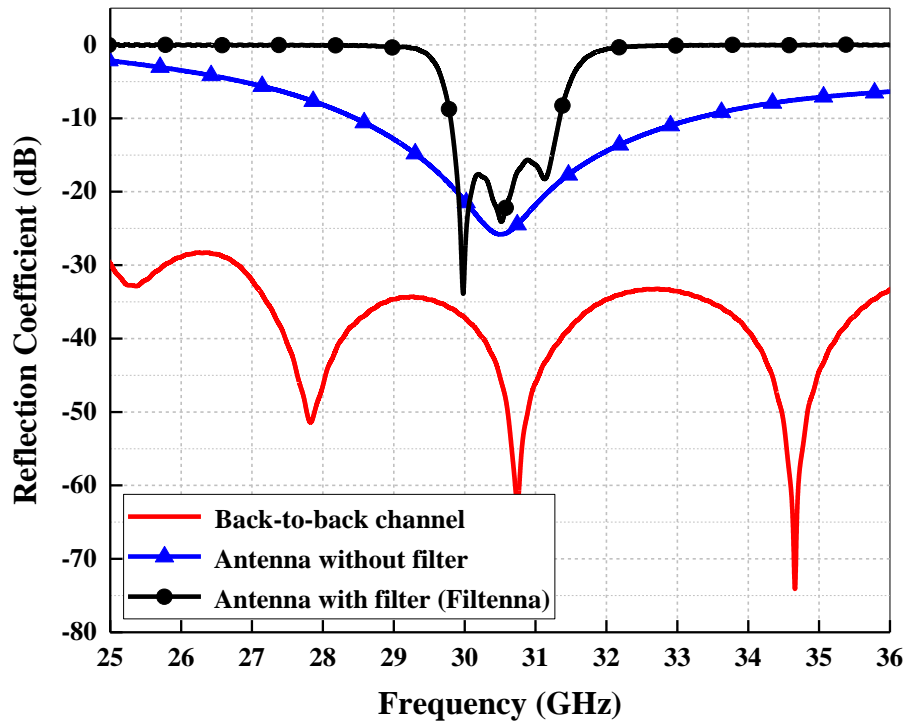


Fig. 6.11. The simulated reflection coefficients of the antenna with and without a filter.

B- Fabrication and Measurements

A photograph of the fabricated cavity-backed slot filtering antenna is shown in Fig. 6.13. The measurement setup of the fabricated CBSFA is shown in Fig. 6.14. The fabrication process is done based on CNC machining technology (the CNC machine

model is HAAS-TM1). The fabricated filtering antenna prototype is measured using an Anritsu 37369A vector network analyzer (VNA) with a standard WR-28 waveguide flange interface. With the new pin-form, no transition is needed to connect the filtenna to the standard waveguide adapters. WR-28 waveguide flange interface are used to measure the S-parameters and the radiation patterns. A Thru-Reflect-Line (TRL) calibration was first performed to calibrate the VNA, the cables and the waveguide adapters. The simulated and measured reflection coefficients of the proposed filtering antenna are shown in Fig. 6.15. The measured $|S_{11}|$ of the proposed filtering antenna is in good agreement with the simulated one.

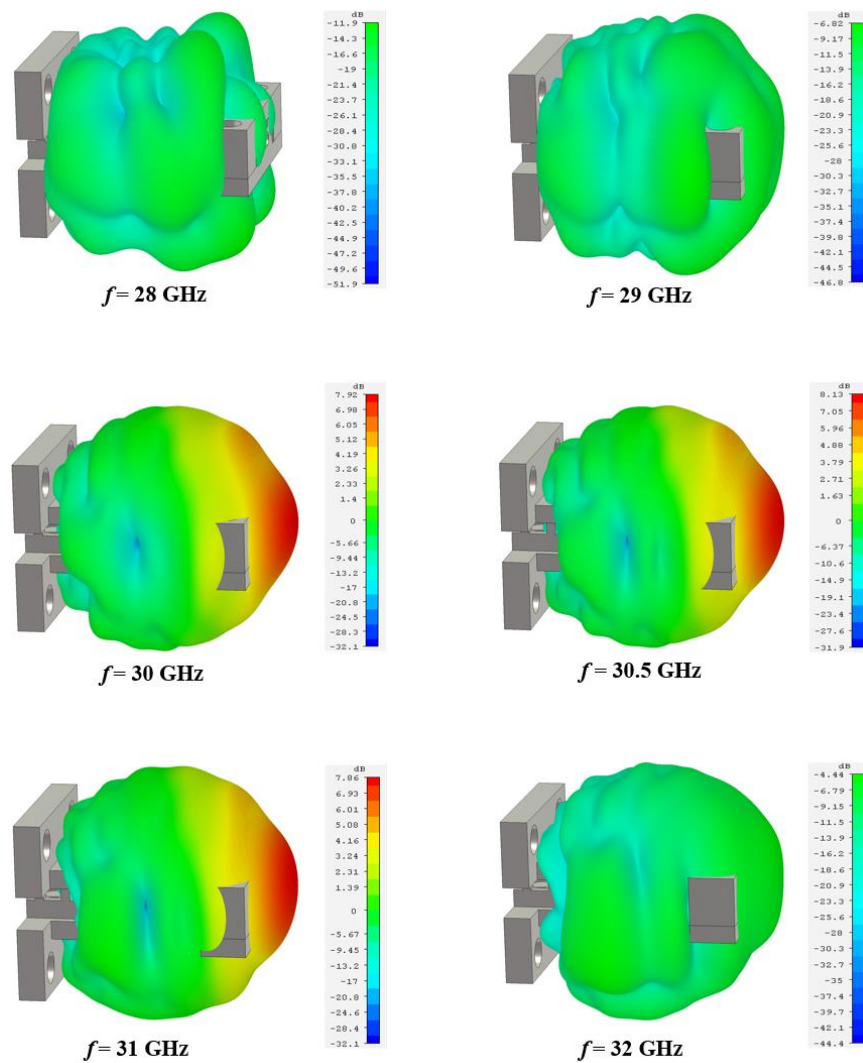
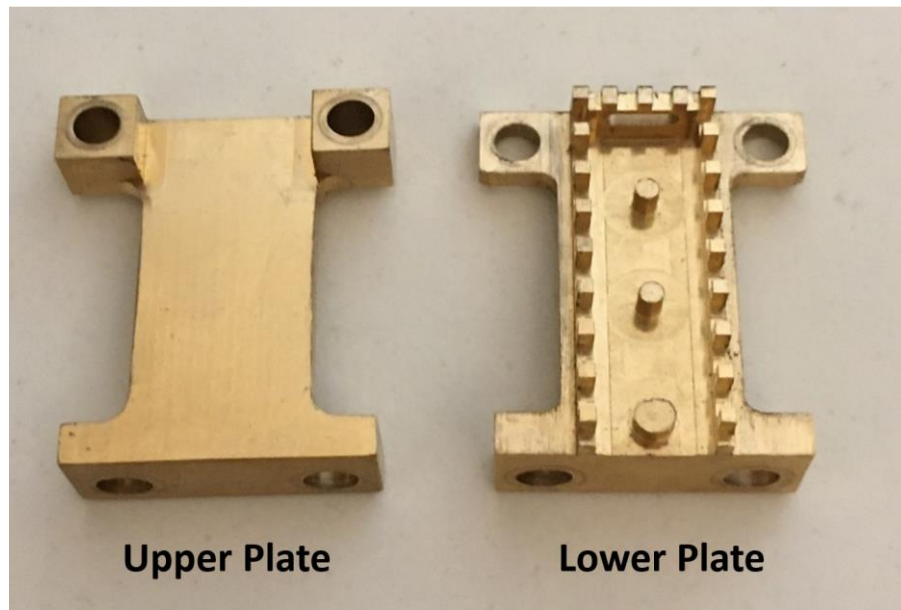
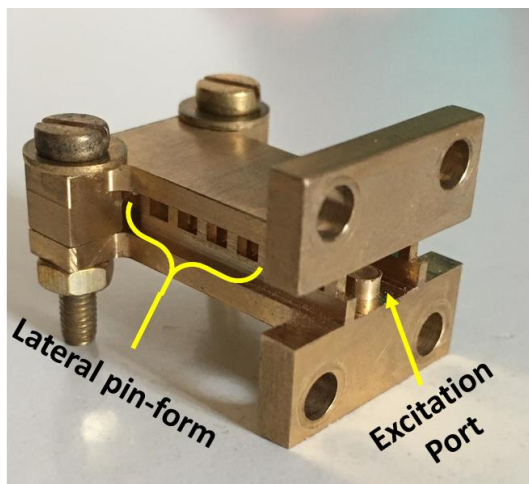


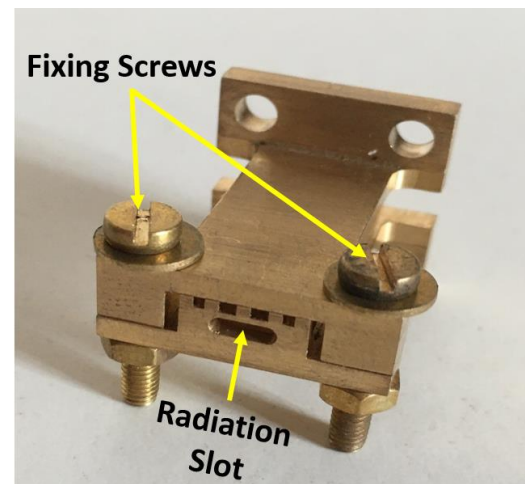
Fig. 6.12. Simulated 3D radiation patterns of the proposed filtering antenna at different frequencies.



(a)



(b)



(c)

Fig. 6.13. A photograph of the proposed CBSFA based on the new gap waveguide structure. (a) Separated plates. (b) Assembled CBSFA showing the excitation port. (c) Assembled CBSFA showing the radiation slot.

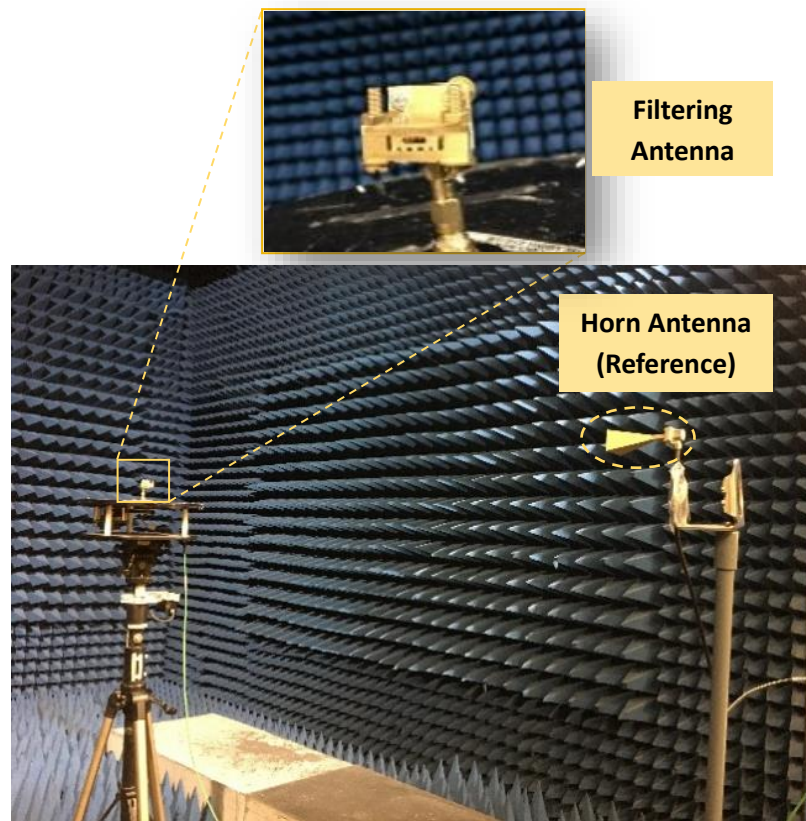


Fig. 6.14. A photograph of the measurement setup of the proposed CBSFA.

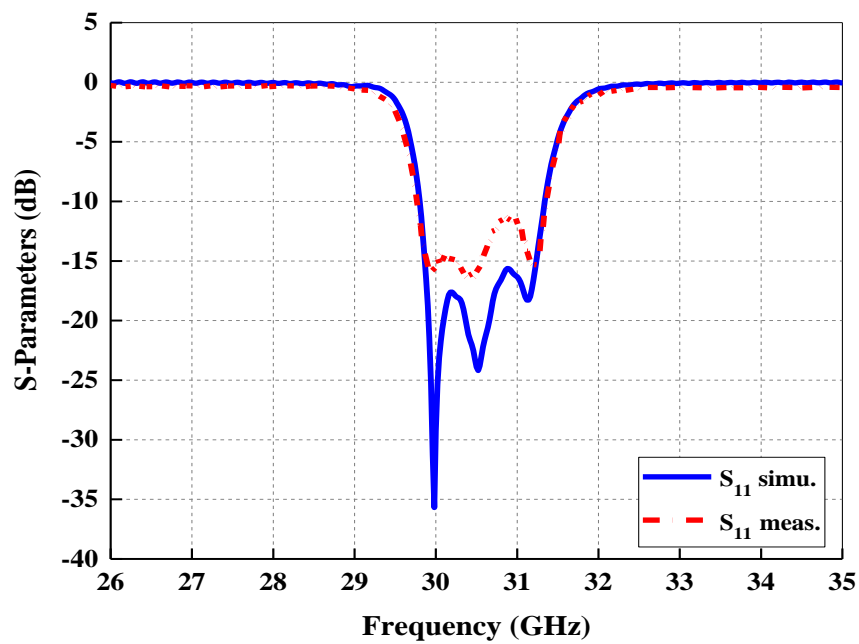


Fig. 6.15. Simulated and measured reflection coefficients of the CBSFA based on the proposed groove gap waveguide structure.

The simulated (with and without filter) and measured gains of the CBSFA are plotted in Fig. 6.16. From simulations, it can be noticed that over the passband (29.5 GHz – 31.5 GHz), an average gain of 8.5 dBi with a flat response out of the passband can be obtained for the slot antenna with the absence of filtering function. While with the filtering function, an average of 8 dBi with a steep roll-off around the passband can be achieved. The average measured gain of the CBSFA is 7.5 dBi with good suppression at stopband frequencies. There is a little impact on the gain performance with the existence of the filter, however, signals below and above the passband are effectively suppressed. The simulated and measured normalised 2D radiation patterns of the proposed cavity-backed slot filtering antenna at 31.5 GHz are shown in Fig. 6.17. It is apparent that the measured radiation pattern matches very well with the simulated one. This can support the validity of the newly proposed gap waveguide structure.

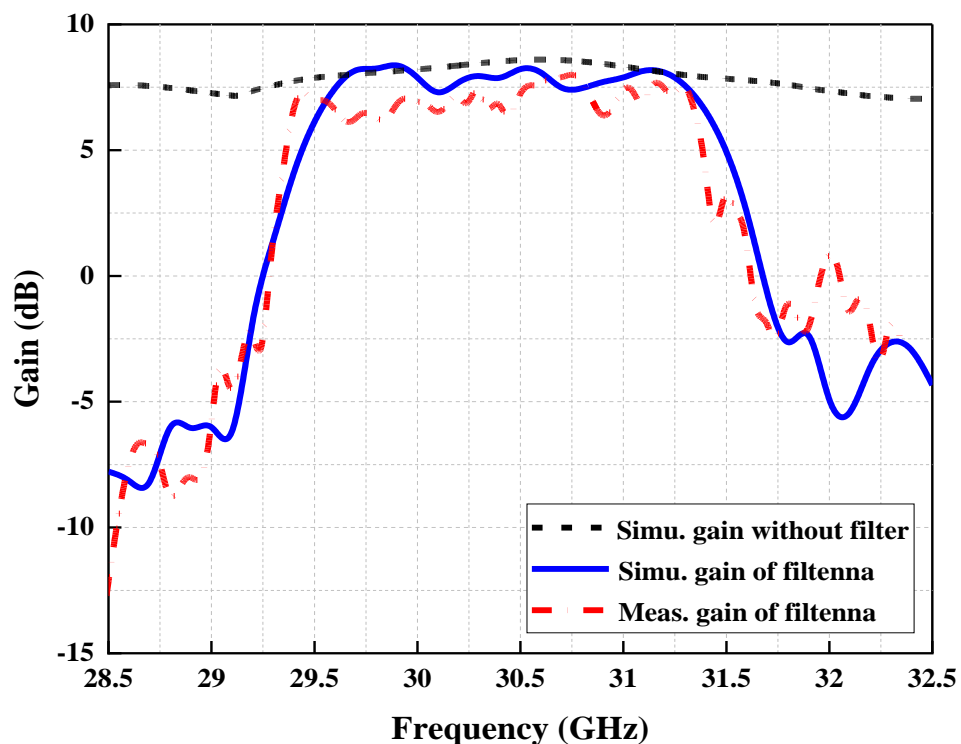
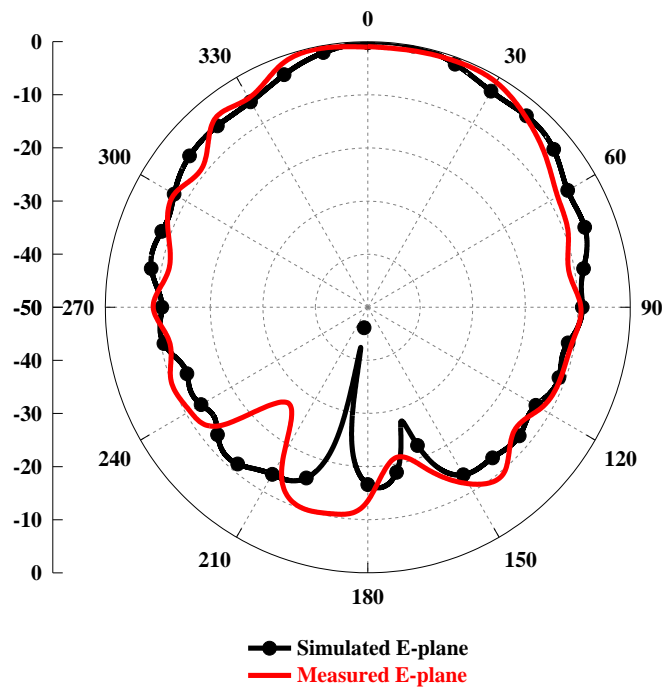
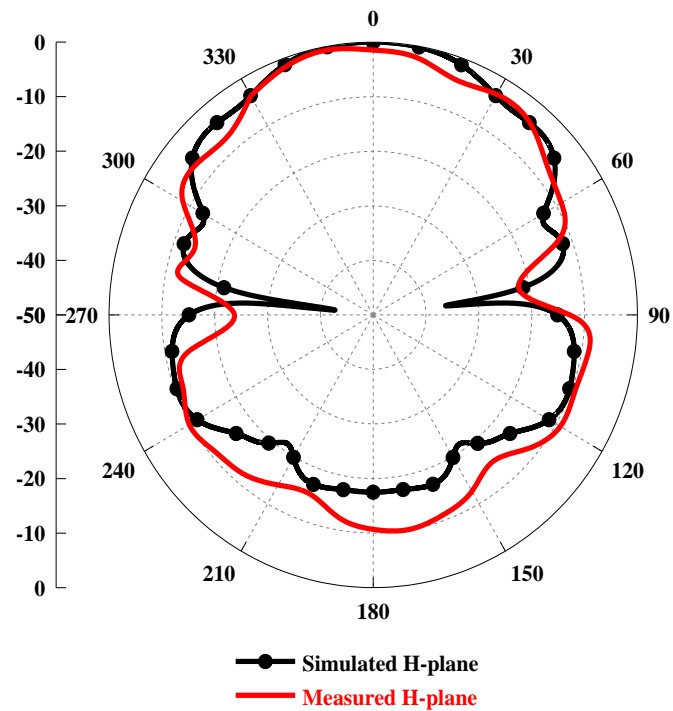


Fig. 6.16. Simulated (with and without filter) and measured gains of the proposed CBSFA.



(a)



(b)

Fig. 6.17. Simulated and measured normalised 2D radiation patterns of the proposed CBSFA at 31.5 GHz. (a) E-plane. (b) H-plane.

Finally, Table 6.3 compares the designed and fabricated gap waveguide cavity-backed slot filtering antenna with the state-of-the-art mmWave filtering antennas, designed based on different technologies. It can be seen that the proposed CBSFA has a comparable performance compared to the other filterennas. The proposed filtering antenna has the widest bandwidth among them. Although the gain in [8]-[10] is higher than that of the proposed filtering antenna, their antennas use either an array of slots or a horn-shaped antenna. However, the proposed antenna, with just one slot, can obtain an average measured gain of 7.5 dBi. In terms of size, the proposed filtering antenna is the smallest one when compared to those designed based on non-planar technologies, such as a conventional rectangular waveguide or gap waveguide.

Table 6.3. Performance summary of the state-of-the-art filtering antennas based on different technologies.

Ref.	Frequency (GHz)	Technology	Number of Resonators	BW ($S_{11} < -10$)	Gain (dBi)	Size ($\lambda_0 \times \lambda_0 \times \lambda_0$)
[6]	31.5	SIW	3	1.56%	6.75 (two slots)	1.51×1.47×0.10
[7]	29.25	SIW	3	1.2%	8.1 (1×4 array)	2.19×1.83×0.10
[8]	12.55	RWG	NA	4%	13.6 (2×3 array)	5.30×0.72×0.26
[9]	22	GW	3	5%	8.5-12 (horn antenna)	NA
[10]	29.21	GW	7	2.3%	31 (16×16 array)	17.53×17.53×1
This work	30.5	GW	3	6.3%	7.5 (single slot)	2.80×0.93×0.26

NA: not available.

6.3. Summary

The new gap waveguide structure proposed in Chapter 5 has been adopted to design a cavity-backed slot antenna and a cavity-backed slot filtering antenna. The designs and simulations of the proposed devices have been done with the aid of CST MICROWAVE STUDIO[®]. Both CBSA and CBSFA have been fabricated using CNC milling technology. The main contribution of the proposed designs in this chapter is that the half-height solid wall can be exploited to make a horizontal slot at the end of the cavity to be used for wave radiation which is not possible with the conventional gap waveguides. This is the first time that the sidewalls of gap waveguide structures can be used for slot radiation. The simulated and measured reflection coefficients, gains and radiation patterns of the proposed CBSA and CBSFA are in good agreement.

References

- [1] CST Microwave Studio. CST, Inc. [Online]. Available: <http://www.cst.com>.
- [2] H. Chu, C. Jin, W. J. Sun, J. X. Chen, Y. X. Guo, "Substrate-Integrated Millimeter-Wave Short Backfire antenna by a novel quad-slot cavity-backed feed," *IEEE Transactions on Components, Packaging and Manufacturing Technology*, vol. 5, pp. 1694-1699, 2015.
- [3] R. Lovato, and X. Gong, "A Third-Order High-Q SIW Filter antenna with Two cavities and one integrated slot antenna," *IEEE International Symposium on Antennas and Propagation (APSURSI)*, pp. 1219-1220, 2016.
- [4] J.-S. Hong, *Microstrip Filters for RF/Microwave Applications*, 2nd edition. Hoboken, N.J: Wiley, 2011.
- [5] R. J. Cameron, C. M.Kudsia, and R. R. Mansour, *Microwave Filters for Communication Systems: Fundamentals, Design, and Applications*. New York: Wiley, 2007, Ch. 11.
- [6] H. Chu, C. Jin, J. Chen and Y. Guo, "A 3-D Millimeter-Wave Filtering Antenna With High Selectivity and Low Cross-Polarisation," in *IEEE Transactions on Antennas and Propagation*, vol. 63, no. 5, pp. 2375-2380, May 2015.
- [7] H. Chu, J. Chen, S. Luo and Y. Guo, "A Millimeter-Wave Filtering Monopulse Antenna Array Based on Substrate Integrated Waveguide Technology," in *IEEE Transactions on Antennas and Propagation*, vol. 64, no. 1, pp. 316-321, Jan. 2016.
- [8] Z. Zheng, X. Fang, W. Wang, G. Huang, H. Zhang and X. Liang, "A Compact Waveguide Slot Filtering Antenna Based on Mushroom-Type Surface," in *IEEE Antennas and Wireless Propagation Letters*, vol. 19, no. 10, pp. 1823-1827, Oct. 2020.
- [9] M. Hamedani, H. Oraizi, A. Amini, D. Zarifi and A. U. Zaman, "Planar H-Plane Horn Antenna Based on Groove Gap Waveguide Technology," in *IEEE Antennas and Wireless Propagation Letters*, vol. 19, no. 2, pp. 302-306, Feb. 2020.
- [10] A. Vosoogh, M. S. Sorkherizi, A. U. Zaman, J. Yang and A. A. Kishk, "An Integrated Ka-Band Diplexer-Antenna Array Module Based on Gap Waveguide Technology With Simple Mechanical Assembly and No Electrical Contact Requirements," in *IEEE Transactions on Microwave Theory and Techniques*, vol. 66, no. 2, pp. 962-972, Feb. 2018.

Chapter 7. Conclusions and Future Work

7.1. Conclusions

Gap waveguide technology exhibits interesting properties as a new guiding structure that can be suitable to fill the existing gap between the planar printed transmission lines and the non-planar hollow waveguides in terms of loss and fabrication flexibility at high-frequency bands. The work presented in this thesis can be broadly grouped into four categories:

- (i) Exhibiting the advantages and features of using the metamaterial-based gap waveguide technology in the design of passive devices operating at the mmWave frequency bands when compared to the conventional planar and waveguide technologies.
- (ii) Adopting two different manufacturing technologies (computer numerical control machining and high-resolution metalised polymer jetting 3D printing) to fabricate a cross-coupled mmWave bandpass filter showing the difference between the two fabricated counterparts in terms of performance and mass. The metalised 3D printed filter exhibits lower loss and lighter weight when compared to the solid machined metal case.
- (iii) Proposing a new form of pins to constitute the sidewalls in gap waveguide structures to overcome the limitations of the traditional forms of pins. The unit-cell of the new pin-form consists of a pin located above a solid wall created on one parallel plate while keeping the other plate flat. With the proposed form, much more effective wave shielding at the operating band can be achieved compared to the traditional full-height pins. Another advantage is the bandwidth of the passband can be enhanced by moving the upper edge of the passband towards higher frequencies due to the use of shorter pins instead of full-height pins, with the same cross-section dimensions (width and height). Also, a good

matching between a groove gap waveguide structure and a standard waveguide port can be achieved without the need for a transition.

- (iv) The sidewalls of the new gap waveguide structure have been exploited for wave radiation by realising a horizontal radiation slot in the metal wall under the pins. Based on this idea, a cavity-backed slot antenna and a filtering antenna have been designed and tested giving good agreement with the predictions.

Each chapter is summarised as follows:

In Chapter 1, an overview of the mmWave frequency bands is given. The motivation and objectives of this thesis are also presented to provide the reader with the background needed to understand the work described in the rest of the thesis.

Chapter 2 has presented and discussed the state-of-the-art mmWave components design based on different technologies. Challenges of transmission lines at mmWave band have been addressed. Then, an overview of gap waveguide technology and its applications have been presented. Moreover, gap waveguide types and different pin forms have been analysed. Finally, the main manufacturing techniques of mmWave components have been addressed.

In Chapter 3, an overview of RF filter design by the insertion loss method has been described. A 5th-order Chebyshev BPF has been designed and its parameters have been computed based on the procedure of the insertion loss method. The schematic lumped-element circuit of the designed filter has been simulated with the aid of ADS software. The S-parameters of the simulated filter have been plotted. Because ideal lumped-element circuits are often unattainable at high frequencies, distributed elements have been used to represent the circuit components of the same filter. Series end-coupled resonators structures have been used in the design. Also, the theory of coupling matrix synthesis, cross-coupling and transmission zeros have been presented. Finally, the design formulae of a rectangular cavity resonator and a filtering antenna have been

stated.

In Chapter 4, a groove gap waveguide as a very attractive technology has been adopted to design a narrow and high-selectivity response BPF operating at the Ka-band. The designed filter is fabricated using two technologies: computer numerical control (CNC) machining technology and high-resolution metalised polymer jetting (PolyJet) 3D printing technology. The measured results of the 3D printed BPF are in excellent agreement with the simulations, without having any design iterations or post-fabrication tuning. The 35.65 GHz metalised 3D printed filter presents many advantages, when compared to other manufacturing technologies, in terms of mass, performance, development time and cost. The 3D printed BPF is expected to be employed for aerospace applications.

In Chapter 5, a novel pin-form of gap waveguide structure has been proposed. The proposed pin-form consists of a pin mounted on a solid wall. The S-parameters of two-port back-to-back channels based on the new pin-form gap waveguide have been investigated. The performance of the proposed structure is compared to that of the previous forms showing the advantages of the new form. It has been shown that, with the proposed pin-form, more effective wave shielding has been achieved, a wider passband bandwidth can be obtained by shifting the upper edge of the passband towards higher frequencies due to the use of shorter pins instead of full-height pins, with the same groove cross-section dimensions (width and height). Also, a good matching between a groove gap waveguide structure and a standard waveguide port can be achieved without the need for a transition.

In Chapter 6, the new gap waveguide structure proposed in Chapter 5 has been adopted to design a cavity-backed slot antenna and a cavity-backed slot filtering antenna by realising a horizontal radiation slot in the solid wall under the periodic pins. Both antennas have been fabricated using CNC machining technology. This is the first time that gap waveguide structures can be utilised for EM waves radiation via a slot realised at the sidewalls. The simulated and measured reflection coefficients, gains and radiation patterns of the proposed CBSA and CBSFA are in good agreement.

7.2. Key Contributions

- (i) Design of a compact size, light-weight and low-loss BPF operating at the mmWave spectrum with high selectivity by adding two transmission zeros before and after the passband. The designed filter has been fabricated using two different manufacturing technologies; CNC machining and high-resolution metalised polymer jetting 3D printing. The two fabricated counterparts have been compared in terms of performance and mass. The metalised 3D printed BPF exhibits lower loss and lighter weight (17 g) when compared to the solid metal case (112 g). Such low mass and low loss for BPFs operating at mmWave frequencies are of high importance for aerospace (unmanned drone, manned aircraft, satellite and interplanetary mission) applications.
- (ii) A novel form of pins in gap waveguide structures has been proposed. The unit-cell of the new pin-form consists of a pin located above a metal wall. With the proposed form, the wave shielding at the operating band will be more effective compared to the traditional full-height pins. Also, a good matching between a groove gap waveguide structure and a standard waveguide port can be achieved without the need for a transition. In addition, the bandwidth of the passband can be enhanced by moving the upper edge of the passband towards higher frequencies due to the use of shorter pins instead of full-height pins, with the same cross-section dimensions (width and height).
- (iii) The sidewalls of the new gap waveguide structure have been exploited for wave radiation by realising a horizontal radiation slot in the solid wall under the pins. Then, a cavity-backed slot antenna and a filtering antenna have been designed and tested giving excellent agreement with the predictions. Based on this idea, the wave radiation can be realised via slots in all sides of a gap waveguide structure rather than only the lower and upper plates.

7.3. Future Work

Based on the conclusion drawn above, various further work can be carried out. Using the proposed pin-form gap waveguide structure, the following work can be suggested:

- (i) Design of a cross-coupled BPF based on the new pin-form.
- (ii) The wide bandwidth of the new pin-form proposed in this thesis can be fully utilised by combining the new pin-form with other design techniques, such as ridge gap waveguides
- (iii) Several passive components such as power dividers, diplexers and couplers can be developed using the new pin-form as sidewalls.
- (iv) Omnidirectional antennas can be designed by realising slots in all sides of the proposed gap waveguide structure.
- (v) Based on the new gap waveguide structure investigated in Chapter 5, antenna array can be realised.

Also, the filtering antenna designed in this thesis can be developed by the following:

- (i) Realising of transmission zeros below and above the passband to increase the selectivity of the response and improve the suppression of the unwanted spectrum.
- (ii) Design a tuneable filtering antenna by using screws instead of the coupling cylinders used in this work.
- (iii) Improving its gain by realising all resonators radiation.

References

- [1] P.-S. Kildal, E. Alfonso, A. Valero-Nogueira, and E. Rajo-Iglesias, "Local metamaterial-based waveguides in gaps between parallel metal plates," *IEEE Antennas Wireless Propag. Lett.*, vol. 8, no. 4, pp. 84–87, Apr. 2009.
- [2] F. Fan, J. Yang, V. Vassilev and A. U. Zaman, "Bandwidth Investigation on Half-Height Pin in Ridge Gap Waveguide," in *IEEE Transactions on Microwave Theory and Techniques*, vol. 66, no. 1, pp. 100-108, Jan. 2018.
- [3] E. Rajo-Iglesias and P.-S. Kildal, "Numerical studies of bandwidth of parallel-plate cut-off realised by a bed of nails, corrugations and mushroom-type electromagnetic bandgap for use in gap waveguides," *IET Microw., Antennas Propag.*, vol. 5, no. 3, pp. 282–289, Feb. 2011.
- [4] A. U. Zaman, V. Vassilev, P.-S. Kildal, and A. Kishk, "Increasing parallel plate stop-band in gap waveguides using inverted pyramid-shaped nails for slot array application above 60 GHz," in *Proc. 5th Eur. Conf. Antennas Propag. (EuCAP)*, Rome, Italy, Apr. 2011, pp. 2254–2257.
- [5] S. I. Shams and A. A. Kishk, "Double cone ultra wide band unit cell in ridge gap waveguides," in *Proc. IEEE Antennas Propag. Soc. Int. Symp. (APSURSI)*, Jul. 2014, pp. 1768–1769.
- [6] Dongquan Sun, Xiang Chen, Jing-Ya Deng, Li-Xin Guo, Wanzhao Cui, Kang Yin, Zhenhua Chen, Changfei Yao, Feng Huang, "Gap Waveguide With Interdigital-Pin Bed of Nails for High-Frequency Applications," in *IEEE Transactions on Microwave Theory and Techniques*, vol. 67, no. 7, pp. 2640-2648, July 2019.

Appendices

Appendix A

The capacitances C_s of the lumped capacitors and the characteristic admittances J_s of the inverters of Fig. 3.9. can be calculated using the following explicit formulas, which are obtained by curve fitting for return loss $L_R = -20$ dB:

$$C_1(\Omega_a) = 1.22147 - 0.35543 \cdot \Omega_a + 0.18337 \cdot \Omega_a^2 - 0.0447 \cdot \Omega_a^3 + 0.00425 \cdot \Omega_a^4 \quad (\text{A-1})$$

$$C_2(\Omega_a) = 7.22106 - 9.48678 \cdot \Omega_a + 5.89032 \cdot \Omega_a^2 - 1.65776 \cdot \Omega_a^3 + 0.17723 \cdot \Omega_a^4 \quad (\text{A-2})$$

$$J_1(\Omega_a) = -4.30192 + 6.26745 \cdot \Omega_a - 3.67345 \cdot \Omega_a^2 + 0.9936 \cdot \Omega_a^3 - 0.10317 \cdot \Omega_a^4 \quad (\text{A-3})$$

$$J_2(\Omega_a) = 8.17573 - 11.36315 \cdot \Omega_a + 6.96223 \cdot \Omega_a^2 - 1.94244 \cdot \Omega_a^3 + 0.20636 \cdot \Omega_a^4 \quad (\text{A-4})$$

where Ω_a is the frequency locations of a pair of transmission zeros.